

Electrical Characterization of Polymeric DC Mini-Cables
by means of
Space Charge & Conduction Current
Measurements

Ioannis Alexandros Tsekmes

Supervisor: Dr. ir. Peter H.F. Morshuis

Daily Supervisor: Ir. Dennis van der Born

AUGUST 2012
HIGH VOLTAGE TECHNOLOGY AND MANAGEMENT

Τὸ εὖ γίνεσθαι μὲν παρὰ μικρόν,

οὐ μὴν μικρὸν εἶναι.

Ζήνων ο Στωικός, 336 – 264 π.Χ

To my parents

Abstract

The world's first commercial High Voltage Direct Current (*HVDC*) transmission link was built in 1954 between the Swedish mainland and the island of Gotland. At that time, it was proved that HVDC transmission is technically feasible. Since then, HVDC cable systems have been used worldwide in electrical energy transportation. Most HVDC installations in use around the world today, use paper-insulated, oil-filled type cables.

Extruded dielectric cables with cross-linked polyethylene (*XLPE*) has long been the preferred solution in HVAC applications due to a combination of low material and processing costs, reliability and appropriate mechanical and electrical properties. However, polymeric HVDC cables suffer greatly from space charge accumulation during dc voltage application and from 'low' depletion rate of accumulated space charge when the external field is removed. As a result, considerable modifications of the electric field distribution with respect to the geometric Laplacian field occur, especially in case of voltage polarity inversion. This may cause insulation degradation and premature breakdown.

Manufacturers are trying to tackle the problems related to space charge phenomena by introducing additives to the insulation or semicon layers. The development of new polymeric materials with improved performance under dc electrical stress requires a thorough investigation of the properties governing charge injection, transport and trapping. Particularly mobility and trap depth distribution are very useful to describe and compare the behavior of different materials from the view point of charge dynamics and field modification.

In this thesis, different polymeric mini-cables are examined under DC stresses with regard to their space charge dynamics. Two different types of XLPE insulation and four types of semi-conductive layers compose eight different combinations of mini-cables.

The specimens are subjected to space charge measurements and conduction current measurements in order for their electric field thresholds to be determined. The threshold for space charge trapping is an important parameter for the design of insulation systems subjected to dc electrical fields. If the applied electric field exceeds the threshold, charge injected from the electrodes can accumulate in traps located at the interface with electrodes and in the insulation bulk.

Furthermore, depolarization characteristics obtained at high electric fields and temperatures, are used in order to further investigate the performance of the mini-cables with respect to their apparent trap-controlled mobilities and trap depths, including the space charge distribution along the trap levels.

The main goal of this thesis is to evaluate how the composition of insulation and semi-conductive layers affects the space charge dynamics in polymeric mini-cables.

Table of Contents

1. Introduction	1
1.1 The dynamic role of HVDC in transmission systems	1
1.2 HVDC cables	2
1.3 Space charge phenomena	2
1.4 Polymeric cables in HVDC applications	3
1.5 Polyethylene based cables	3
1.6 Thesis outline	4
2. Background Theory	5
2.1 Space charge accumulation	5
2.1.1 Basic features	5
2.1.2 Macroscopic view	5
2.1.3 Microscopic view	9
2.2 Trapped space charge accumulation threshold	15
2.3 Dielectric polarization	18
2.4 Temperature dependence	20
2.5 Semicon - insulation interface	20
2.6 Charge packets	21
2.7 Mobility and trap depth	22
3. Experimental Methods	27
3.1 Test specimens	27
3.1.1 Cables	27
3.1.2 Semicon plaques	29
3.2 Space charge measurements	29
3.2.1 PEA for flat specimens	29
3.2.2 PEA for cables	33
3.3 Conduction current measurements on plaques	40
3.4 Conduction current measurements on cables	41
4. Experimental Results of Space Charge Measurements	44
4.1 Space charge measurements at positive polarity	44

4.1.1 Cable 11543-2	44
4.1.2 Cable 11544-2	48
4.1.3 Cable 11543-1	51
4.1.4 Cable 11544-3	54
4.1.5 Results obtained during an earlier project	57
4.1.6 Cable comparison & discussion	58
4.2 Space charge measurements at negative polarity.....	61
4.3 Mobility and trap depth estimation.....	64
4.3.1 Apparent trap – controlled mobility	64
4.3.2 Trap depth.....	66
5. Experimental Results of Conduction Current Measurements	70
5.1 Conduction current measurements on semicon plaques.....	70
5.2 Conduction current measurements on cables.....	71
5.2.1 Cable 11544-4	71
5.2.2 Cable 11543-3	75
5.2.3 Cable 11543-4	79
5.3 Discussion.....	83
6. Conclusions & Recommendations	84
6.1 Conclusions	84
6.2 Recommendations	87
Appendix I - Signal Processing.....	89
Appendix II - Technical Specifications of the PEA Setup.....	96
Appendix III - Technical Specifications of the CCM Setup for Plaques	101
Appendix IV - Technical Specifications of the CCM Setup for Cables	103
Bibliography	105
Acknowledgments.....	107

1. Introduction

1.1 The dynamic role of HVDC in transmission systems

High voltage direct current (*HVDC*) technology has characteristics which makes it especially attractive for certain transmission applications. HVDC transmission is widely recognized as being advantageous for long-distance, bulk power delivery, asynchronous interconnections and long submarine cable crossings.

The number of HVDC projects committed or under consideration globally has increased in recent years reflecting a renewed interest in this mature technology. New converter designs have broadened the potential range of HVDC transmission to include applications for underground, offshore, economic replacement of reliability-must-run generation, and voltage stabilization.

HVDC techniques are used in the power grid in cases where high voltage alternating current (*HVAC*) techniques simply cannot be used or have large disadvantages. If long distances have to be bridged, HVAC cables can no longer be used due to the high capacitive currents. From a certain length of cable on, the capacitive current is so large compared to the current that has to be transmitted, that it is no longer feasible to use AC voltage. This break-even point depends on many factors, but at present lies around 30 km for submarine cables and around 500 km for overhead lines.

Other important advantages, that the use of HVDC in transmission can offer, are listed below.

- Connecting power grids that operate at different frequencies
- Connecting power grids that operate with different control procedures
- Increasing the transmission capacity and the possibilities for energy exchange
- Higher power transfers are possible over longer distances using fewer lines with HVDC transmission than with HVAC transmission.
- The control of reactive power, which supports the network stability and the power quality (when voltage source converters *VSC* are used)
- HVDC cable systems are considered environmentally friendly, because of their low visual and noise impact
- Using HVDC cables in a bipolar configuration, practically no magnetic field is produced
- Relatively short time for constructing a new link

However, the electric field distribution at DC voltage differs greatly from that at AC voltage. The field distribution at DC is determined by the conductivity σ of the insulation which is not constant and depends strongly on the temperature and the electric field. Surface charges and space charges play an important role too. As a result, the intermediate fields are space, temperature and time dependent. This makes the determination of the electric field at DC voltage a far more complex matter than the equivalent case at AC voltage.

1.2 HVDC cables

Most of the HVDC cables are mass-impregnated or oil insulated. Through the years, the power transported by the DC links and their rated voltages have increased, the cable systems have become longer, the AC/DC conversion technology has changed, but mass impregnated and oil-filled insulation have been, in practice, the only type of insulation to be used up to 1999.

The type of mass-impregnated paper insulated cable is mainly used in long sea crossings. This type of cable needs no oil feeding and has a proven reliability. The first HVDC cable in the world was a cable of this type and is known as the Gotland cable. It connects the Gotland island with the Swedish mainland and it was constructed in 1954.

The oil-filled cable is also paper-insulated, but impregnated with thin oil and has a proven reliability as well. It has a higher transport capacity due to its higher continuous electrical design stress and higher operating temperature. However, the disadvantage of this cable is the need for oil feeding once every 10 to 20 kilometers. This makes it less interesting for long water crossings. The only cable of this type in service so far connects Denmark with Germany (400kV, 600MW, 175km).

The main issue, which needed to be resolved for the development of the HVDC polymeric cables, is the control of the space charge phenomena which affect the reliability of the connection. Nowadays, this concern has been addressed, but only partially solved. As a consequence, mass-impregnated paper is still the dominating technology for HVDC cable insulation.

Recently, some innovative HVDC cable projects making use of polymeric cable insulation have been completed [26, 27]. However, the polarity of the DC voltage must be kept fixed and then the inversion of the power flow has to be done by inverting the current direction. This limits the application of the polymeric cable systems to HVDC links using IGBT-based converters (VSC).

1.3 Space charge phenomena

One of the intrinsic properties of the DC cable insulation is the accumulation of charges. Insulating materials allow a weak electrical conduction. This weak flow of charge within the insulation may not be uniform, because of a local non-homogeneity of the material. When an inequality occurs between the flow of charges into a region and the flow of charges out of that region, charge accumulates in that region.

In an AC situation, the flow of charges inverts its direction too quickly to allow a significant growth of space charge at the insulation inhomogeneities, at least for conventional insulating materials. This means that the space charge field can be neglected.

However, under a DC stressing condition, the flow of charge maintains the same direction. This allows a build-up of charge, which, in general, significantly affects the electric field distribution inside the insulation.

Accumulated charges can be released by the insulation when the external field is removed and the insulation is short-circuited. However, this process can last quite a long time, depending on the insulation type and temperature. In general, charge depletion takes much longer for polymeric insulated cables than for mass-impregnated or oil-filled insulated cables.

A consequence of this phenomenon is that the accumulated charges will be kept within the insulation also when the external DC voltage is removed or when the value of the external DC voltage changes. The inversion of the voltage polarity in HVDC cables is a practical example of such a situation. In this case, the insulation experiences the sum of the space charge field and the field induced by the DC voltage which direction has been inverted. This generally leads to a maximum field near the inner conductor of the cable.

1.4 Polymeric cables in HVDC applications

Extruded dielectric cables with cross-linked polyethylene insulation have been used for underground transmission and distribution of power using HVAC transmission. Extruded XLPE has long been the preferred insulation material due to a combination of low material and processing costs, reliability and appropriate electrical and mechanical properties. However, it has been mentioned that most current HVDC installations in use around the world today use paper-insulated, oil filled-type cables.

The reasons for using paper-insulated, oil filled-type cables are mainly two. Firstly, the adoption of XLPE for dc applications is not possible by simple translation from ac technology. Secondly, the demand for using HVDC cables has in the past been very low, mostly in underwater installations, so that the use of polyethylene in HVDC became attractive to cable manufacturers only when the number of HVDC projects increased sufficiently to make the development costs recoverable.

It is now widely believed that the extruded HVDC cables offer significant advantages over the traditional paper insulated cable types. A higher conductor temperature can be used, giving a more compact cable for the same power rating. Lighter moisture barriers can be used, giving a lighter cable. Joining of extruded cables is much simpler and requires less skill. Finally, the use of extruded cables avoids the significant long-term environmental hazards associated with oil leaks.

1.5 Polyethylene based cables

Polyethylenes vary in molecular weight and degree of branching, with the highest branching occurring in low-density polyethylene *LDPE*. Other polyethylene families are unbranched or high-density polyethylene *HDPE* and short-branched linear low density polyethylene *LLDPE*. The polyethylene most commonly used for HV insulation purposes is cross-linked polyethylene *XLPE*, which is LDPE cross-linked with an organic peroxide, typically dicumyl peroxide. XLPE offers good electrical characteristics, ease of processing and acceptable cost, and has therefore been a popular extruded dielectric material.

In the production of XLPE, methane, acetophenone and cumyl alcohol are among the by-products of the decomposition of dicumyl peroxide. Since methane is explosive, the XLPE insulation of cables is vented. For instance, it is heated to 70°C in a fan-forced oven, to remove most of the methane and other by-products before the next stage of manufacturing is commenced. The amount of dicumyl peroxide initially added to the base polyethylene is also kept to a minimum for the same reason.

The mechanical properties of XLPE are such that, when used as insulation in a power cable, it can tolerate a conductor temperature of 90°C almost indefinitely, 130°C for up to 36 hours during emergencies and 250°C for a few seconds during short-circuit. It undergoes a phase change from a ductile semicrystalline solid to a noncrystalline elastomer in the temperature range 90-110°C and the associated expansion is an important factor in the design of cable joints and terminations.

Space charge may accumulate in a solid dielectric when a dc voltage is applied across it. The electric field distribution is distorted and if the space charge density is sufficiently high, the local field strength may exceed the breakdown strength of the dielectric, leading to a failure. Polymer structure and degree of crystallinity can influence the dielectric strength and space charge formation. The amorphous regions in polyethylene are the preferred trapping locations of charge-carrying species.

In the area of polymer insulators additive technology is used in order to improve their overall performance. Most strategies to date involve an extension of the role of existing polyethylene additives. Insulating grade XLPE used in HVAC cables typically contains additives, such as stabilizers (i.e. antioxidants), cross-linking agents and other compounds that increase the ability of the material to withstand oxidation, electrical and thermo-mechanical stresses. Lubricating additives, unsaturated compounds to increase cross-linking density and scorch retarding agents may also be added. Additives traditionally used for HVAC cables can be selectively used in various combinations to produce XLPE insulation for HVDC cables with reduced space charge accumulation.

Currently, accumulation of space charge limits the use of polymeric insulated HVDC cables to transmission systems that do not undergo polarity reversals and have a limited voltage range. The use of polymeric insulation for HVDC cables is highly desirable from a commercial perspective, and so there is a need for further research to gain a more complete understanding of processes involved in space charge accumulation.

1.6 Thesis outline

The aim of the here described research is to electrically characterize different polymeric mini-cables with regard to their space charge behavior under HVDC. More specifically, the space charge dynamics of these mini-cables is investigated by means of space charge and conduction current measurements. The mini-cables under investigation are based on different types of insulation and semi-conductive materials and the goal is to evaluate the performance of each combination when it is subjected to HVDC fields.

In chapter 2, the basic background theory related to space charge phenomena is presented. In the following chapter, the experimental methods used for the space charge and conduction current measurements are described in detail.

In chapter 4, the experimental results with regard to the space charge measurements are presented and discussed. The space charge accumulation thresholds at positive and negative polarity are presented in the first part of the chapter. Next, a comparison between all the specimens follows in order to evaluate the performance of each mini-cable with respect to its electric field threshold. Finally, the results of apparent trap-controlled mobilities and trap depths are displayed and discussed in the last part of the chapter including the space charge distribution along the trap levels.

The experimental results of the conduction current measurements on three mini-cables are quoted in chapter 5. The purpose of these measurements is to verify the results of the space charge measurements with regard to the electric field thresholds of the mini-cables with the use of another technique. The two measuring techniques should give close, if not identical, results.

Chapter 6 contains the conclusions drawn from the measurements and some recommendations for future research.

2. Background Theory

In this chapter, the background theory of the main processes whose parameters are measured by means of space charge and conduction current measurements is explained. An overview of space charge accumulation is given in section 2.1. In section 2.2, the concept of electric field threshold for space charge accumulation is discussed. Section 2.3 contains the effect of dielectric polarization which occurs when a dielectric is subjected to a DC electric field. The effect of temperature and the role of semi-conductive layers are explained in section 2.4 and 2.5 respectively. The space charge behavior at high electric fields related to the generation and movement of charge packets is presented in section 2.6. Finally, section 2.7 contains the basic theory behind the estimation of apparent trap-controlled mobility, trap depth values and distribution by using depolarization characteristics.

2.1 Space charge accumulation

The major phenomenon of space charge accumulation which complicates the design procedure under DC stress is discussed in this section. Space charge is examined both from a macroscopic and a microscopic point of view [1],[4],[5].

2.1.1 Basic features

The existence of space charge causes two major problems:

- i. Space charge distorts any electrical field present according to Poisson's equation.

$$\vec{\nabla} \cdot \vec{E} = \frac{\rho}{\epsilon_0 \epsilon_r} \quad (2.1)$$

- ii. Energy is required to separate charged particles of different polarity. This energy is stored in the system and may be used to damage or deform the material locally.

$$W_e = \frac{\epsilon_0 \epsilon_r E^2}{2} \quad (2.2)$$

2.1.2 Macroscopic view

From a macroscopic point of view, space charge accumulates when the current density J is divergent. Therefore, when the flow of charged particles into a region of space differs from the flow out of that region, a net charge builds up in time in this region [5]. Places and circumstances that can lead to a divergence of current density are listed below.

- Electrode-dielectric interface
- Dielectric – dielectric interface
- In the presence of a temperature gradient
- In case of gross inhomogeneities
- In case of morphological inhomogeneities

Electrode – dielectric interface

The flow of charged particles through the interface is determined by the charge injection/extraction mechanisms and their field and temperature dependence. On the other hand, the flow of charged particles through the dielectric is governed by the charge transport mechanism of the dielectric and its field and temperature dependence. Therefore, the build-up of space charge depends on the difference:

$$J_{inj}(E;T) - J_{tran}(E;T) = \Delta J_{interface} \quad (2.3)$$

Where J_{inj} is the injection current density and J_{tran} is the current density through the dielectric. Three cases can be distinguished which are described below.

1. $J_{inj}(E;T) = J_{tran}(E;T)$

In this case the interface is called Ohmic and no space charge is accumulated as the amount of charges injected/extracted from the electrodes is just enough to replace the charges that are removed from/towards the interface by transport.

2. $J_{inj}(E;T) < J_{tran}(E;T)$

In this case the electrode interface cannot convey the charges as fast as the dielectric can conduct them. Therefore, positive hetero-charge will build up in front of the cathode and negative hetero-charge in front of the anode. The hetero-charge increases the electric field in front of the electrode and hence the injection current while reducing the bulk field and the transport current. Eventually, a steady state situation is achieved when the two currents coincide.

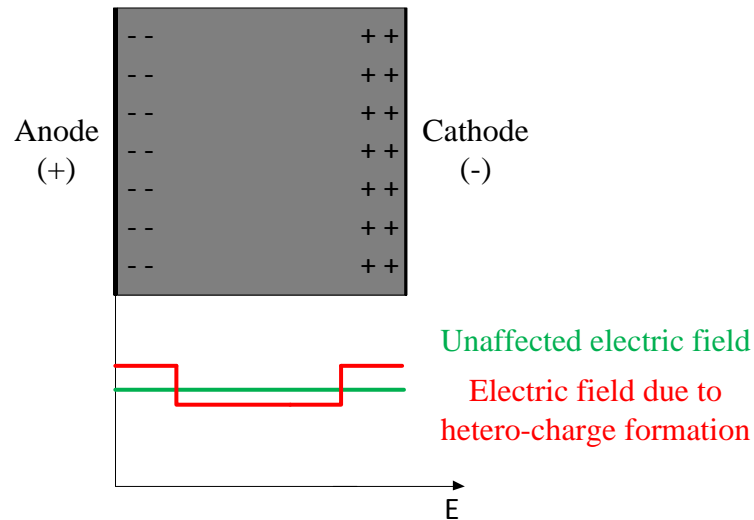


Figure 2.1 – Effect of hetero-charge on the electric field

3. $J_{inj}(E;T) > J_{tran}(E;T)$

In this case the electrodes yield more charges than the dielectric can handle. Therefore, negative homo-charge builds up in front of the cathode and positive homo-charge in front of the anode. The homo-charge decreases the electric field in front of the electrode and hence the injection current while increasing the bulk field and the transport current. Eventually, a steady state situation is achieved when the two currents coincide.

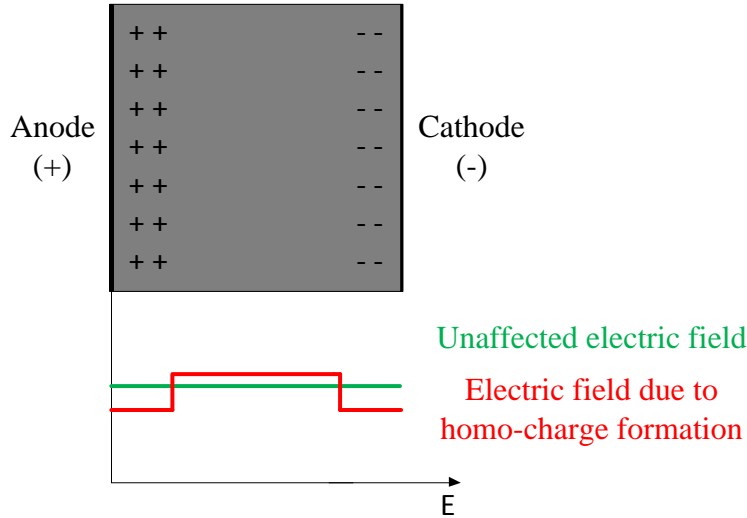


Figure 2.2 – Effect of homo-charge on the electric field

Dielectric – dielectric interface

Space charge accumulation at the interface of two different dielectrics is described by the Maxwell – Wagner theory. A hypothetical capacitive configuration is used to describe the phenomena at the interface between two different dielectrics which is called Maxwell capacitor. The latter consists of two parallel electrodes separated by two dielectric slabs A,B of thickness d_a and d_b respectively. The Maxwell capacitor is presented in figure 2.3.

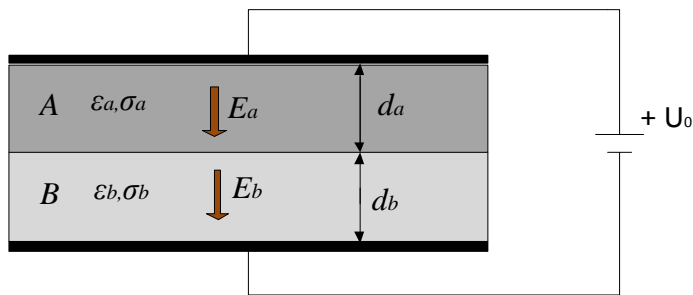


Figure 2.3 – Maxwell capacitor

At time $t=0$, a DC voltage U_0 is applied. Equation 2.4 combines the laws of Maxwell, Ohm and continuity.

$$\nabla \cdot \sigma E + \frac{d}{dt} \nabla \cdot \varepsilon E = 0 \quad (2.4)$$

In a homogeneous electric field E acting in one direction, equation 2.4 results in equation 2.5.

$$(\sigma_a E_a - \sigma_b E_b) + \frac{d}{dt} (\varepsilon_a E_a - \varepsilon_b E_b) = 0 \quad (2.5)$$

Where $\varepsilon_a, \varepsilon_b$ denote the permittivities of the two materials, σ_a, σ_b denote the conductivities and E_a, E_b are the electric field components in the two materials.

The voltage between the electrodes is given by equation 2.6.

$$d_a E_a + d_b E_b = U_0 \quad (2.6)$$

By using equation 2.6 and eliminating the term E_b , the solution of the differential equation 2.5 is given by equation 2.7.

$$E_a = \frac{\sigma_b U_0}{d_b \sigma_a + d_a \sigma_b} \left(1 - \exp\left(\frac{-t}{\tau}\right) \right) + \frac{\varepsilon_b U_0}{d_b \varepsilon_a + d_a \varepsilon_b} \exp\left(\frac{-t}{\tau}\right) \quad (2.7)$$

Where τ is the time constant and it is calculated according to equation 2.8.

$$\tau = \frac{d_b \varepsilon_a + d_a \varepsilon_b}{d_b \sigma_a + d_a \sigma_b} \quad (2.8)$$

The growth of the surface charge κ at the interface is calculated with the use of equation 2.9.

$$\kappa = \frac{\sigma_b \varepsilon_a - \sigma_a \varepsilon_b}{d_b \sigma_a + d_a \sigma_b} U_0 \left(1 - \exp\left(\frac{-t}{\tau}\right) \right) \quad (2.9)$$

The difference in permittivities and conductivities between the two materials leads to a discontinuity in the electric field at the interface. As a result, a difference in conduction current density occurs which results in the formation of space charge at the interface.

Temperature gradient

A deviation from the geometric Laplacian electric field can occur when a cable is supplied by a DC voltage and the insulation is subjected to a temperature gradient caused by heating losses originating from the current in the conductor. Because the electrical conductivity of any insulating material depends exponentially on temperature, a temperature gradient generates a conductivity gradient and thus the permittivity to conductivity ratio ε/σ varies as well. Therefore, space charge ρ is generated in the dielectric according to equation 2.10 [8].

$$\rho = J \cdot \nabla \left(\frac{\varepsilon}{\sigma} \right) \quad (2.10)$$

Where J is the steady dc current density flowing through the insulation, ε is the permittivity of the insulation and σ is the conductivity of the insulation.

The electric field profile at steady state can be significantly different from that derived by considering only the cylindrical geometry of the cable insulation. If the accumulated space charge ρ is sufficiently large, the electric field at the sheath of the cable can become higher than the field near to the conductor. This phenomenon is known as field inversion.

Gross inhomogeneity

Most of the insulating materials contain fillers with inevitably different conductivities and permittivities to that of the host material. The presence of those fillers introduces numerous interfaces between the host material and the fillers. As a result, space charge accumulates at these interfaces due to the fact that the quotient ε/σ differs between the two materials.

Morphological inhomogeneity

In polymers such as polyethylene, crystalline parts and amorphous parts can be observed. The different conduction properties between these regions can lead to charge accumulation at the boundary between crystalline and amorphous regions.

2.1.3 Microscopic view

From a microscopic point of view, three important parameters are related to space charge accumulation in polymers [4].

- Trapping of charge carriers
- Injection and extraction of charge carriers
- Conduction

Energy band model

At this point it is essential to mention the difference between insulators, semi-conductors and conductors. Their different behavior can be explained by using the atom model of Niels Bohr. According to that, a number of electrons move in separate orbits around the nucleus of an atom. Not every orbit is possible; a limited number of orbits which are situated at discrete distances from the nucleus are available. An electron may leap from one orbit to another; it cannot move in between, every orbit represents a distinct energy level.

There are two important energy bands, the valence band and the conduction band which are shown in figure 2.4. In the valence band the electrons are firmly coupled to the atom. The upper band is the conduction band. Electrons in this band can easily leap from one atom to another. Between these two bands lies a forbidden area, the band gap. No electrons can occur in this band gap. An electron from the valence band can reach the conduction band only if it obtains sufficient energy (thermal or otherwise) to pass the forbidden band gap in one single leap. The same consideration is also valid for holes.

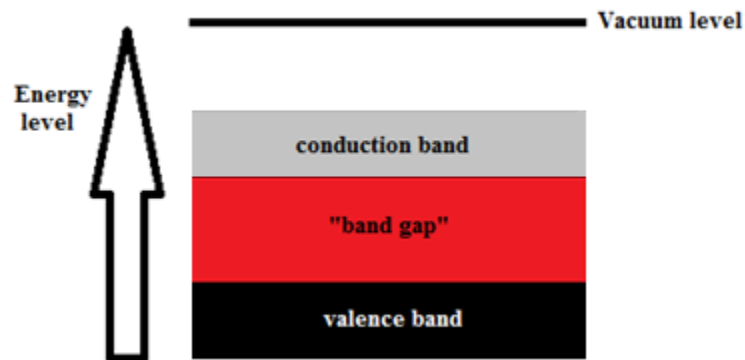


Figure 2.4 – Energy band model of Niels Bohr

Therefore, the conductivity of a material depends on the size of the band gap. If this gap is large it is extremely improbable that an electron can pass the gap and add to the conductivity. The width of this gap is expressed in electron volts eV . The band gap for an insulator is larger than $2eV$, for a semi-conductor is between 0.2 and $1eV$ and finally for a conductor is less than $0.2eV$.

Structure of polyethylene

Polyethylene consists of long-chain molecules of CH_2 -groups. Sometimes side chains occur which disturb the regular shape of the macro molecules. These regions are shown in figure 2.5. The main chains have a length of thousands to tens of thousands CH_2 -groups. These chains run partly parallel to themselves or to other chains. The parallel regions form the crystalline part of the polymer.

However, for another part of their length, the chains follow an arbitrary path and create amorphous regions. In these regions, additives such as impurities and anti-oxidants are accumulated. This is an important factor for the formation of space charge [4].

The amorphous regions play an important role in determining the electrical properties of polyethylene and it is thought that charge transport occurs mostly within them [8]. However, electron and hole transport through band structure may exist along the length of polymer chains where a regular chain conformation is maintained [1].

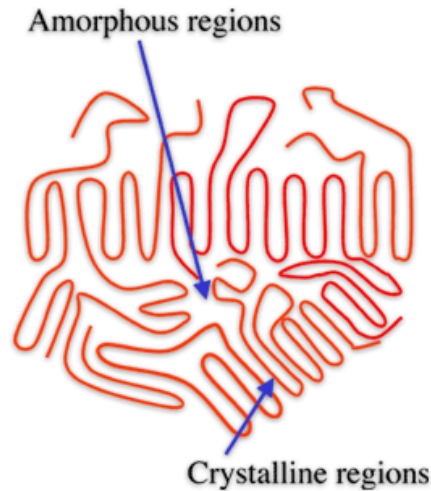


Figure 2.5 – Molecular structure of Polyethylene

Trapping of charge carriers

Incompletely bound atoms at crystal defects give rise to dangling bonds which can be satisfied by either the removal or donation of an electron (or both) and thus behave as states within the band gap. However, these energy states are not extended throughout the crystal, they only exist in the vicinity of chemical or structural defects (often in amorphous regions). Electrons and holes entering these localized states are therefore not available for conduction and may have to acquire considerable energy before they can leave. These states are called traps. A trap for electrons is called acceptor and a trap for holes, donor.

Donors have energy levels immediately above the top of the valence band and acceptors have energy levels immediately below the bottom of the conduction band.

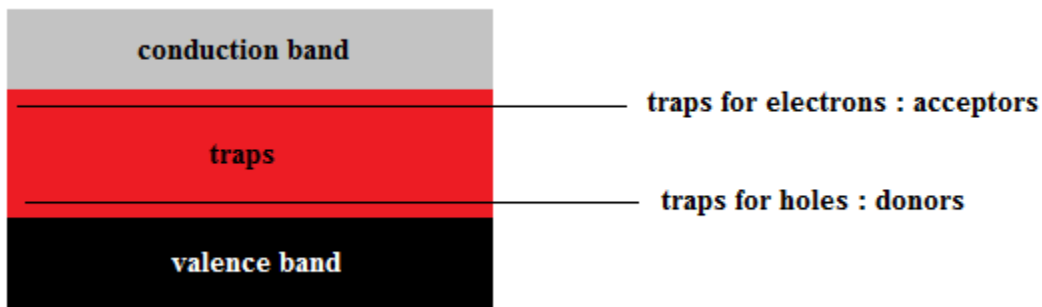


Figure 2.6 – Energy levels of electrons and traps

Furthermore, traps may take the form of sites where the field from an electron or hole can reorientate the local structure thereby creating a potential well from which escape may be difficult. The depth of a trap is defined as the energy that a charge carrier needs in order to be liberated. These are called self-traps.

Self-trapped charge is a form of space charge in which a region of an insulation contains localized charge of one polarity which is not compensated by an equal concentration of opposite polarity charge [1]. This causes local field enhancement due to Poisson's equation.

$$\nabla E = \frac{\rho_c}{\varepsilon} \quad (2.11)$$

Where ρ_c is the charge density (C/m^3) and ε is the permittivity. Self-traps can be deep and keep charges for a considerable time, up to many hours or even days.

Electrons can escape from localized states given sufficient energy and drift to other localized states under the influence of the local electric field. However, conduction in the band gap by this method is very slow since carriers spend most of their time in traps and very little travelling between them (trap-limited conduction).

The occurrence of these traps is related to the additives in polymers, which tend to concentrate in the amorphous regions. These additives consist of anti-oxidants which are added to the material to counteract thermal aging, residues of the chemical processes during production such as crosslinking by-products and finally, impurities which cannot be prevented in any material. Small differences in additives can have large effects in the number of traps, so that the ability to store space charge is greatly affected by the type and concentration of additives.

Injection and extraction of charge carriers

The conduction and the emission of charges in polyethylene are mainly performed by electrons, not by ions [4]. Injection of electrons at the cathode and extraction of electrons at the anode are the main mechanism for the emission of charges in polyethylene.

In order for a charge to leave the metal and enter the insulation, a potential barrier has to be passed. The height of this barrier depends on the interface properties. Figure 2.7 presents this potential barrier.

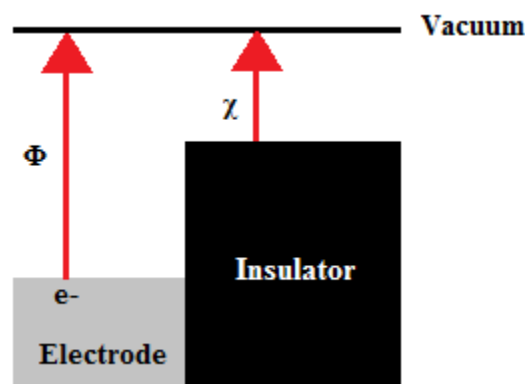


Figure 2.7 – Barrier at the interface between electrode and dielectric

The required energy for electrons is given by equation 2.12.

$$W = \Phi - \chi \quad (2.12)$$

Where Φ is the work function of the metal and χ is the electron affinity of the insulator.

Two main processes of charge injection are considered. The first one is the Schottky injection and the other one is the Fowler-Nordheim injection.

The Schottky process is valid for “low” fields up to $\sim 100\text{kV/mm}$. Due to the applied electric field the potential barrier is reduced and an electron can travel across the barrier. The Schottky injection current density depends on temperature T and electric field E according to equation 2.13.

$$J = AT^2 \exp \left[-\frac{\Phi - e \sqrt{\frac{eE}{4\pi\epsilon_0\epsilon_r}}}{kT} \right] \quad (2.13)$$

Where A is a constant, T is the temperature and Φ is the total barrier height.

On the other hand, the Fowler – Nordheim injection is valid for “high” fields above $\sim 100\text{kV/mm}$. In this case the barrier becomes very thin, less than 1nm at 1000kV/mm . Therefore, electrons can pass through narrow potential barriers despite having insufficient energy to surmount them, this is known as tunneling. The injection current density, according to equation 2.14, depends strongly on electric field E and there is no or small temperature T dependence.

$$J = BE^2 \exp \left[\frac{-C\varphi^{\frac{3}{2}}}{E} \right] \quad (2.14)$$

Where B and C are constants and $\varphi = \Phi - E_{fermi}$.

Conduction

Conduction occurs when charge carriers move in response to an electric field. However, in many dielectrics charge carriers spend most of their time in traps and they cannot move even if an electric field is applied [5].

Electrons can travel very quickly between traps with velocity approximately 10^5 m/s. On the other hand, an electron spends more time trapped than travelling between traps. For “shallow” traps, the trapping time is short. For instance, for traps with depth smaller than 0.5eV , the trapping time at 20°C is less than $1\mu\text{s}$. However, in traps of 1eV depth, electrons can spend more than an hour. The mobility of these electrons is effectively reduced by the traps. This is called trap-limited mobility or trap-limited conduction.

If an insulator already contains charge, then it is likely to be deeply trapped. This is known as space charge and can result in the increase of the mobility of other charges.

Poole – Frenkel mechanism

In this case, barriers which are localizing carriers within the dielectric are lowered by the applied electric field in contrast to the Schottky effect where the electrode-insulator barrier is lowered. As a result there is an increase in the conduction. This is called Poole - Frenkel effect and according to that, the conduction current density is given by equation 2.15.

$$J = \sigma_0 E \exp \left[-\frac{e\Phi - \beta\sqrt{E}}{2kT} \right] \quad (2.15)$$

Resonance tunneling

As it is mentioned above, conduction mainly takes place in the amorphous regions of polymeric materials where defects occur in the crystal structure. In order for the conduction of the amorphous parts of the molecular chains to be explained, the theory of hopping is devised. There are many dislocations in the chain, where an electron can be trapped. The potential barrier between two traps is so high that an electron cannot pass this barrier. However, from the point of view of quantum mechanics, the position of an electron can also be regarded as the probability that an electron is located on the other side of the barrier. This probability depends on the distance between traps. As this distance is small, the probability differs from zero, so that an electron can sometimes appear on the other side of the barrier. This is called resonance tunneling, as it can be said that the electron digs a tunnel through the potential barrier.

However, a pure tunneling process is valid only at zero temperature ($T=0K$) because at higher temperatures the exponential reduction of the electron wavefunction with distance limits the range over which it can be effective and also the principle of energy conservation restricts the participating sites to those having the same energy level [1]. Therefore, what actually takes place at higher temperatures is a thermally assisted tunneling from site to site. According to that, thermal promotion at one site raises the electron to a level which is equi-energetic with that of an empty neighboring site. Tunneling between the two sites is allowed at this energy level and there will be a finite probability that the electron resides at the previously empty site.

Space charge limited conduction *SCLC*

A power law dependence of the current density J on the electric field E has been found for electrical conduction in insulating polymers [33]. Therefore, equation 2.16 can be used for describing this statement.

$$J = aE^n \quad (2.16)$$

Various conduction mechanisms are characterized by different values of n . The case in which n equals 1 is known as Ohmic conduction and carrier concentration and mobility are field independent.

Space charge limited conduction *SCLC* occurs when the conduction is the result of the injection of excess carriers from an Ohmic contact into a material of very low mobility. In case that traps are present in the dielectric, some of the carriers become trapped and do not contribute to the conduction. As a result, only a proportion of the charges contribute to the conduction. At a sufficiently high voltage the charge carrier number density being injected is approximately equal to the number density of traps. In this case the traps

must be considered deep instead of shallow. When all the traps are filled the so-called trap-filled limit is reached and the number of electrons available for conduction increases which results in the rapid raise of the current density. The *SCLC* current density is given by equation 2.17.

$$J = \frac{9}{8} \frac{\varepsilon \mu V^2}{L^3} \quad (2.17)$$

Where ε is the relative permittivity, μ is the carrier mobility, V the applied voltage and L is the sample thickness.

O'Dwyer [3] has shown that combining the effects of a non-Ohmic contact (i.e. Schottky barrier) with the effects of space charge results in a current density given by equation 2.16 where the exponent n is equal or larger than 2.

2.2 Trapped space charge accumulation threshold

The concept of electrical threshold for insulating materials has been considered in literature over the years. It is defined as the value of the electric field above which space charge accumulates. Estimation of dc electric field threshold can be achieved either by dc charging measurements or space charge profile observation. Both methods should give very close threshold values.

The presence of space charge modifies the internal field distribution in a dielectric. In a parallel plate configuration the electric field is uniform when the total space charge is zero. A linear relationship exists between the current and the applied voltage (Ohmic behavior). In this case, the charge contributed by the mobile carriers is compensated by an equal amount of counter charge, and the net charge density is zero. An increase in the voltage causes the accumulation of some amount of space charge (both mobile and trapped), so that a non-linear relationship is established between current and voltage. Ohmic behavior and space charge are mutually incompatible [17].

A life model which describes the mechanism of insulation degradation due to the presence of space charges, is based on the assumption that even if the applied electric field is not large enough to inject hot electrons which are able to break inter and/or intra-molecular bonds, the trapped charges are responsible for local storage of electromechanical and electrostatic energy which may favor degradation reactions via a process of lowering an activation energy barrier. This occurs above a level of electric field, which changes with material and technology, and it is called threshold for trapped space charge accumulation.

It has been proposed in recent literature that the threshold for electrical aging under dc field may be close to the threshold above which space charge becomes trapped in the insulation [17]. Therefore, the meaning and investigation of such a threshold can acquire fundamental importance in electrical insulation characterization, since working at electric stresses below the threshold means extremely long lives with regard to electrical aging and thus high reliability in service, provided that there are no other significant stresses acting on the insulation.

The direct way to examine the formation of space charge into insulation is resorting to techniques able to display space charge concentration along the insulation thickness. In this work the pulsed electro-acoustic method *PEA* is used for this purpose.

The determination of the electrical threshold requires an electric field E - average space charge density ρ characteristic, in order to single out the electric field above which space charges become steadily and noticeably resident in insulation and increase with field. Therefore, measurements at different voltage levels are required. A typical form of the E - ρ characteristic of an insulation is shown in figure 2.8.

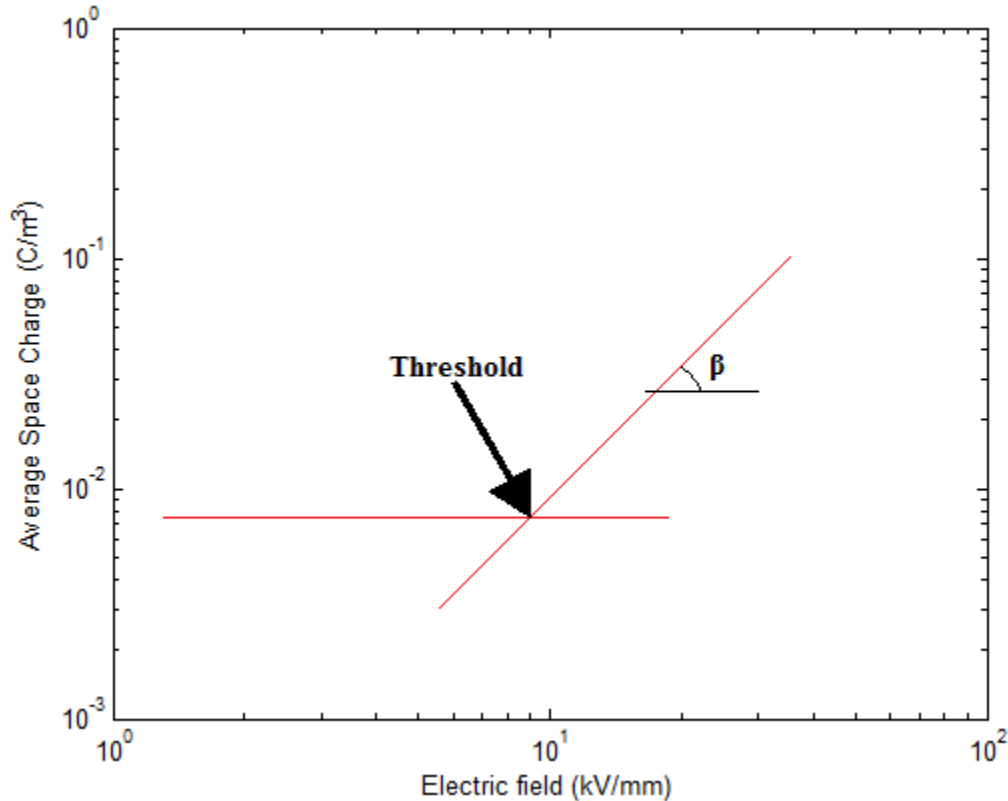


Figure 2.8 – E- ρ characteristic of an insulating material

The slope β of the E - ρ characteristic represents the rate of charge accumulation as function of the applied electric field.

According to the space-charge limited current theory, dc charging currents measured at different values of electric field can provide voltage- steady-state current characteristics which reveal the transition from a low-field regime where Ohm's law prevails (represented by a straight line with slope approximately equal to 1 in a log-log coordinate system) to a high-field behavior, determined by the establishment of steady trapped space charges. In the latter condition, the conduction model is described by a power law, providing a straight line in log-log coordinates with slope equal or larger than 2.

When the logarithm of steady-state values of current or current density (I or J) are considered and plotted vs. the logarithm of applied voltage or field (V or E), the transition from the low-field regime to the high-field behavior is evident and the value of the electric field at which the transition occurs can be roughly estimated. Therefore, the change of the J - E characteristic from linear to supra linear is accompanied by the onset of space charge. This kind of behavior is presented in figure 2.9 and in figure 2.10.

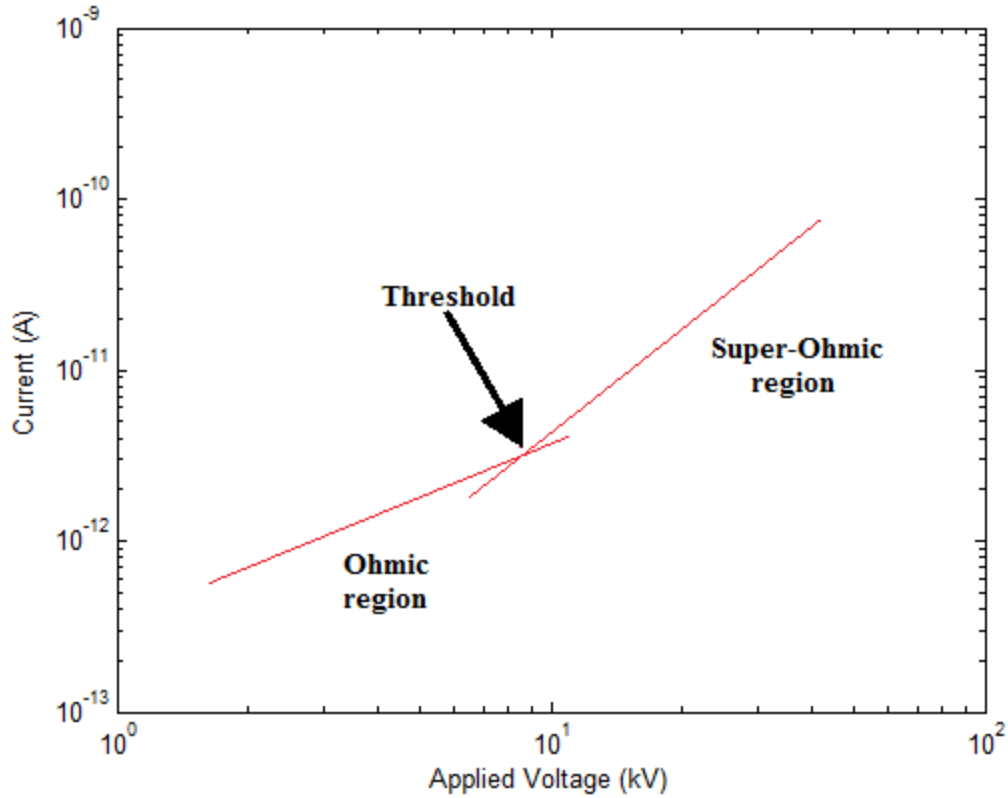


Figure 2.9 – V-I characteristic of an insulator

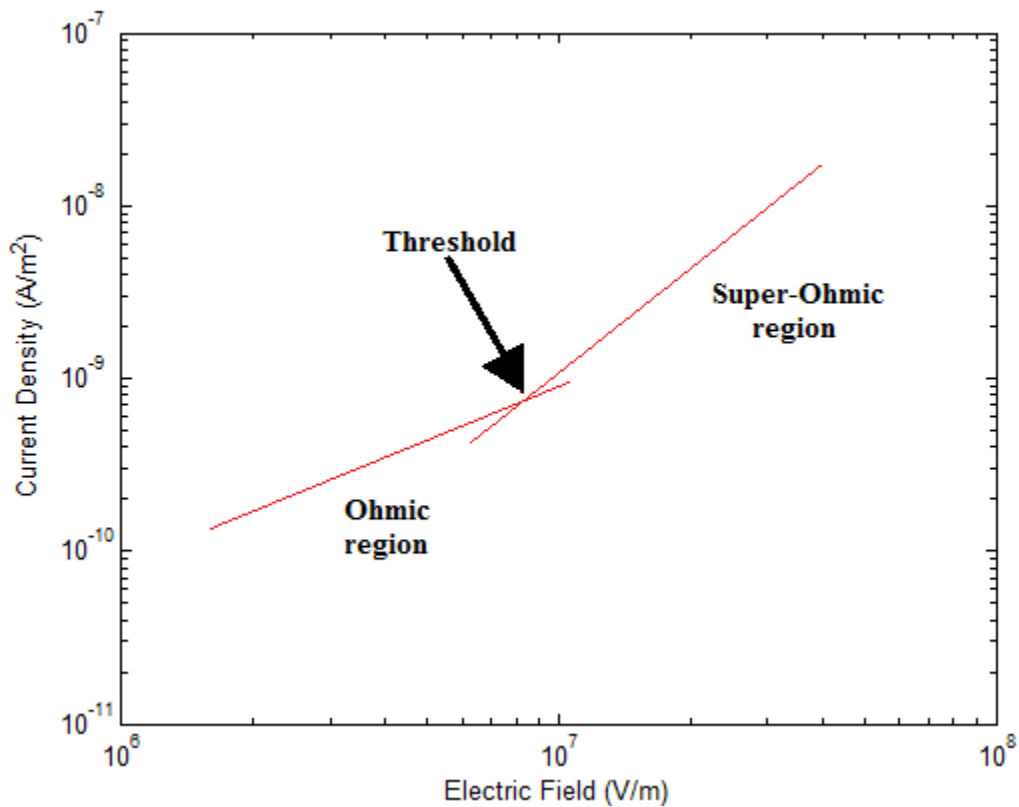


Figure 2.10 – E-J characteristic of an insulator

2.3 Dielectric polarization

When switching on a DC voltage U , the dielectric is stressed as if it were an AC voltage. A capacitive current i_c flows through the dielectric which is given by equation 2.18.

$$i_c = C \frac{dU}{dt} \quad (2.18)$$

After this, the current falls back to a small steady-state leakage current. But before this occurs, a transient phenomenon takes place which is called polarization current. This current decreases slowly and it can take several hours before it reaches a steady-state value. This kind of behavior is presented in figure 2.11.

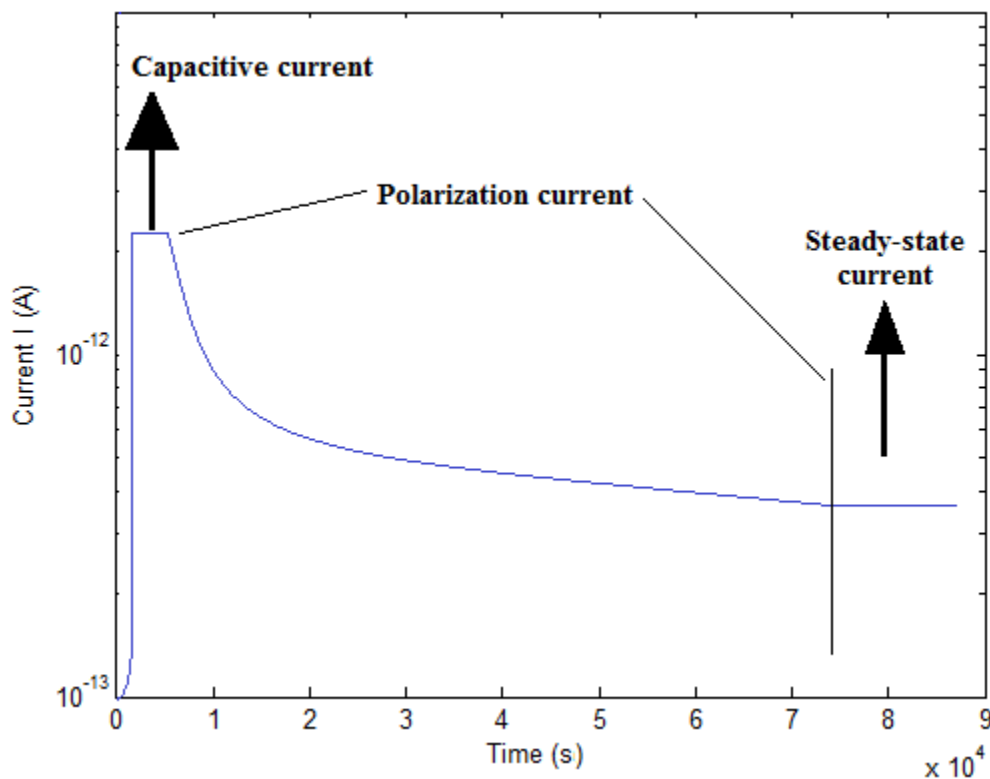


Figure 2.11 – t-I characteristic of a dielectric after voltage application

Every kind of dielectric consists, at an atomic level, of negative and positive charges balancing each other on the microscopic and macroscopic scale (if no unipolar charge was deposited within the material by well known charging effects). Macroscopically, some localized bipolar space charge may be present, but even then, an overall charge neutrality exists.

As soon as a dielectric is exposed to an electric field (generated by a voltage across electrodes embedded in the insulation), the positive and negative charges become oriented and form different kind of dipoles even on atomic scales. A local charge imbalance is thus induced within the neutral species as the centers of gravity for the equal amounts of positive and negative charges $\pm q$ become separated by a finite distance d , thus creating a dipole with a dipole moment $\vec{p} = q\vec{d}$ which is related to the local or microscopic electric field E acting in close vicinity to the charges. The dipole moment can also be written as $\vec{p} = \alpha\vec{E}$, where α is the polarizability of the dielectric. As the distance will be different for different species as well as their number of dipoles per unit volume, the polarizability is also different. Due to chemical interactions between dissimilar atoms forming molecules, many molecules will have a stable distance d between the charge centers, thus forming permanent dipoles, which are usually randomly oriented and distributed within the material, as long as no external field is applied [32].

Polarization arises from a finite displacement of charges in a steady electric field and this is to be contrasted with the complementary physical phenomenon of electrical conduction which arises from a finite average velocity of motion of charges in a steady electric field.

Dipoles are polarizing species which are incapable of leading to a continuing conduction current in a static electric field, since the charges in question cannot be completely separated or dissociated under normal conditions. A dipole could only become dissociated in a field that would be sufficiently large to break the strong bonding forces of the neutral dipolar molecule and this is not normally possible in solids and liquids where various forms of electrical breakdown take place at much lower fields.

The main mechanisms that produce macroscopic polarization are listed below.

- **Electronic polarization** is effective in every atom or molecule as the center of gravity of the electrons surrounding the positive atomic cores will be displaced by the electric field. This effect is extremely fast and thus, effective up to optical frequencies.
- **Ionic polarization** refers to materials containing molecules forming ions that are not separated by low electric fields or low working temperatures. A process which is effective up to infrared frequencies.
- **Dipolar polarization** refers to materials with permanent dipole moments with orientations statistically distributed to the action of thermal energy. Under the influence of an electric field the dipoles will be oriented only partially, so again, a linear dependence of polarization and electric field exists. An effect which is effective up to infrared frequencies.
- **Interfacial polarization** is predominantly effective in insulating materials composed of different dielectrics. The mismatch of the product of permittivity times resistivity for the different dielectrics causes, under the influence of an electric field, movable positive and negative charges to become deposited on the micro- or macro-interfaces of the different materials, also forming some kinds of dipoles. This phenomenon is often very 'slow' and general active in the power frequency range and below.
- **Space charge**, trapped charge polarizes the surrounding medium. It is a very 'slow' process, below the power frequency.

2.4 Temperature dependence

As it is mentioned in section 2.2, below a given electric field (the threshold for space-charge accumulation), the same amount of injected charge from one electrode is extracted by the other electrode and no space charge remains trapped in the bulk of the insulation (Ohmic behavior). As soon as the field exceeds the threshold, the electrodes are not able to extract the increasing amount of injected charge, which finally accumulates in the insulation bulk.

The dynamics of space charge injection and accumulation depends significantly on temperature as charge injection and transport are mostly thermally activated mechanisms. The threshold field shows negative temperature dependence. Therefore, an increase in temperature results in a decrease of the threshold field.

Furthermore, DC conductivity is much dependent on temperature and electric field. An increase in temperature leads to an increase in steady-state conduction current density.

2.5 Semicon - insulation interface

As the conductor and the earth screen surface are relatively rough with protrusions and sharp points, the application of a semicon layer can result in a uniform electric stress distribution over the rough metal surfaces. The inner semicon ensures a tight contact between the insulation and the cable conductor, avoiding cavities that may lead to partial discharges. Similarly, the outer semicon ensures a tight contact between the insulation and the earth screen.

Both semicon layers are chemically bonded with the cable insulation. This is obtained by the triple extrusion production process and the following cross-linking process. The smoothness of the semicon-dielectric interface is very critical with regard to the performance of the cable, as protrusions of the semicon into the insulation can lead to local field enhancements.

Interfaces can constitute weak points of the insulation, at which space charge can be accumulated and/or injected and electric fields can be enhanced. As it has been mentioned in section 2.1.3, for fields up to 100kV/mm, the Schottky law is used to describe the injection mechanism according to equation 2.19.

$$J = AT^2 \exp\left(-\frac{\Delta W - \beta_s \sqrt{E}}{kT}\right) \quad (2.19)$$

Where J is the conduction current density, A is a constant of the material, T is the absolute temperature, k is Boltzmann's constant, ΔW is the activation energy and E the electric field. Finally, $\beta_s = \sqrt{\frac{e^3}{4\pi\epsilon}}$.

The properties of the electrode-insulation and thus semicon-insulation interface will considerably affect the activation energy ΔW and therefore, the extent of injected and accumulated space charge.

A previous investigation [24] has revealed that semi-conductive materials seem to have a large influence on charge injection and removal at the electrodes. Therefore, this particular interface plays a major role in space charge injection/accumulation in the insulation bulk.

2.6 Charge packets

Charge packets are a feature related to charge injection and transport which has been observed in solid polymeric insulation. The phenomenon known as a ‘charge packet’ is a pulse of net charge that remains in the form of a pulse as it crosses the insulation. Charge packets are activated generally by high dc fields, with inception values depending on material, temperature and mechanical stress. Contaminants present in a material decrease the charge inception field. They constitute an important aging factor, concerning dc electrical stress, due to large magnification of the electrical field inside the insulation associated with packet movement. Charge packets have typically a mobility in the range of 10^{-14} to 10^{-12} $\text{m}^2/(\text{Vs})$ and they are considered as “slow” packets in contrast to the “fast” packets having a mobility ranging from 10^{-10} to 10^{-9} $\text{m}^2/(\text{Vs})$.

The generation of slow charge packets requires a local production rate of charge that exhibits a form of hysteresis. A low generation rate switches to a high rate when a given local field is exceeded, and reduces back to a low rate as the local field is reduced to the generated charge. In the absence of such hysteresis the charge is generated continuously and cannot form a pulse. Although, a number of different theories has been proposed, currently none of these theories is able to describe the large generality of cases of slow charge packets. The common point is that high electrical fields are required to activate packets and the presence of contaminants can drastically reduce this field.

Due to fast space charge acquisition systems, it has been observed that hetero-charge formation can occur very rapidly in thin polymeric materials, within a fraction of a second or a few seconds. Very fast charge packets or pulses, characterized by high repetition rate and small charge magnitude have been observed. This high mobility of fast charge packets cannot be obtained considering the conventional packet theories. The mobility of these charge packets depends significantly on temperature, their average mobility increases with temperature.

This rapid appearance of hetero-charge might be explained through the separation of ionic species due to the presence of contaminants and/or crosslinking by-products in the insulation bulk. Also, hetero-charge accumulation could be associated with injection, when the rate of charge trapping is low compared to the transit time of the charge and extraction is slow compared to the rate of arrival of charge. In this case a hetero-charge region would build up at the counter electrode, with a width that increases with time but without any observable change in the bulk of the material.

Positive and negative space charge pulses of small charge magnitude and high repetition rate have been observed crossing 1mm thick specimen of nanostructured epoxy resin during space charge tests [19]. These tests carried out with the use of an ultra-fast space charge acquisition system. The shape of each pulse did not change while crossing the insulation, even for a distance greater than 1mm, while the opposite occurs for slow packets. This leads to the speculation that charge pulses propagate as charged solitary waves rather than independent charge carriers as in slow packets. The packet therefore behaves as a single charged entity, which has been termed in physics as a soliton. The latter is a wave in which the forces that would cause it to break up have been countered by a non-linear binding mechanism. In addition, it seems that, contrary to slow packets, traps cannot be involved in such phenomenon, due to the inherent low mobility that even shallow traps can cause.

Semicon layers between insulation and electrode can significantly modify charge injection and extraction features. Relevant investigation has revealed that hetero-charge build-up can be observable only if a semi-conductive layer is present between insulation and metal electrode. Tests performed on flat specimens having semicon layer only on one side showed that no hetero-charge was observed close to the electrode not in contact with the semicon [21]. It seems that semicon material can partially block the extraction of injected charge from the counter electrode.

It has been observed that charge packets cross an insulation without any detectible change in material properties [10]. Packets due to ionization fronts and compression boundaries, leaves the material unchanged after passage and thus should not cause aging themselves. Therefore, any aging effects that occur should be due to the modification of field distribution as the packets move.

2.7 Mobility and trap depth

Mobility

Charge accumulation constitutes a major problem for HVDC cable insulation materials. These materials should not only store limited amounts of charges when voltage is applied but also deplete charge rapidly as voltage is switched off or inverted. Therefore, this kind of behavior would enable a fast material relaxation in the absence of voltage and prevent or limit the formation of hetero-charge distributions close to the electrodes when voltage polarity is inverted.

Mobility and trap depth in polymeric DC insulation are important parameters from a DC design perspective as their value range can affect conduction and trapping mechanisms of charges in polymeric materials. Therefore, these quantities can be used to describe or even compare the behavior of materials from the viewpoint of charge dynamics and field modification.

Charge transport quantities seem to be sensitive to material degradation and evidences were found of mobility decrease and trap depth increase for thermally and/or electrically aged polyethylene-based-materials [20]. This phenomenon can be attributed to the fact that during aging process additional and deeper traps are formed resulting in mobility decrease and trap depth increase.

Mobility can be estimated from the ratio between charge packet velocity and applied electric field when charge packets cross the insulation thickness. This procedure requires the application of high electric fields, as at lower fields the space charge dynamic is very low, if not negligible.

$$\mu = \frac{s}{E} \quad (2.20)$$

Where s is the packet charge velocity and E is the mean electric field.

However, this is a rough approximation and it relies heavily on the assumption that charge transfer is unipolar and that charge recombination processes in the material are negligible. Also, field amplification is not taken into account.

Furthermore, mobility can be estimated by using the space charge limited current *SCLC* theory. Therefore, a first approximation of mobility can be determined from the results of conduction current measurements above the electric field threshold according to equation 2.21.

$$\mu = \frac{8Jd^3}{9V^2\varepsilon} \quad (2.21)$$

Where J is the current density, V is the potential, ε is the electric permittivity and d is the thickness of the sample.

However, this expression should be applied to the steady-state measurements of the charging current at different poling fields and it is expected to provide information related to the free or shallow trapped charges.

Finally, depolarization characteristic from space charge measurements can be used in order to achieve an estimation of the range of apparent trap-controlled mobility and trap depth distribution. The polarization – depolarization procedure consists of the application of a poling field for a given time, so charge is trapped in the insulation. Then the voltage is removed and the electrodes are grounded for a certain time period. If it is assumed that the recombination between opposite charges can be neglected then the charge is depleted via the electrodes within a time period related to the depths of the charge traps and to the transit time between the traps. If the transit time is negligible with respect to the time spent within the traps, mobility and trap-depth calculations can be carried out through proper processing of the depolarization characteristic. This particular type of mobility is defined as apparent trap-controlled mobility as it depends only on the time that charges spend within traps and it can be described as the mobility of charges trapped at different states due to chemical-physical features.

The average magnitude of the volume density of the charge accumulated in the specimen at time t of depolarization can be calculated from the space charge profiles by using equation 2.22.

$$q = \frac{1}{r_{out} - r_{in}} \int_{r_{in}}^{r_{out}} |q(r)| dr \quad (2.22)$$

However, in order to derive information about apparent trap-controlled mobility from equation 2.22, two main considerations should be taken into account. First of all, charge acquisition during depolarization begins 30 seconds after voltage removal. This delay is due to the fact that the HVDC generator has to discharge after turning off the voltage and the oscilloscope has an initialization time in order to suppress the noise by averaging over 1000 sweeps. Since, the initial transient is omitted for apparent trap-controlled mobility evaluation; the derivation of the mobility of the free or shallow trapped charges is not possible.

Secondly, the use of depolarization characteristic in order for the apparent trap-controlled mobility to be estimated, takes into account average values of space charge density (equation 2.22). Therefore, there is no distinction between positive and negative charges and the estimation of mobility holds essentially for unipolar distributions.

The relationship for apparent trap-controlled mobility is derived in [20] and it is given by equation 2.23.

$$\mu(t) = \frac{2\varepsilon}{q^2(t)} \frac{dq}{dt} \quad (2.23)$$

Where q is the mean density of the total measured charge and ε is the electric permittivity.

Apparent trap-controlled mobility varies with time, since it is related to progressive emptying of deeper and deeper traps as depolarization time elapses. On the contrary, mobility, estimated from the space charge limited current (equation 2.21), it is not a function of time as it is related to the free or shallow trapped charges.

Equation 2.23 related to the estimation of apparent trap-controlled mobility is considerably approximated [20]. However, it can provide a useful quantity for evaluating different materials.

Trap depth estimation

The model for trap depth evaluation which is used in this particular work is derived in [13] and it is applied to the depolarization characteristic. For the derivation of this model three situations are considered. Firstly, the equilibrium of trapping – detrapping between trap levels due to thermal excitation. Then, the effect of the external applied electric field on space charge accumulation and finally, the discharging procedure when the voltage is removed and the electrodes are grounded.

In the proposed model, there are m number of available energy levels (trap levels). Potential energy decreases from level 1 to level m . $N(i)$ stands for the maximum number density of charges trapped in each energy level and it is assumed to be constant for $i=1,2,\dots,m$. Furthermore, $n(i)$ is the number density of charges trapped in the i th level. The level 1 corresponds to the energy state of free charges.

i. Equilibrium distribution when no electric field is applied, zero net charge

If an uncharged material is considered, some of the trap sites are occupied. The charge is continually exchanged between different levels. Therefore, a charge from level i can be thermally excited to the highest level 1, from which it can fall back to any unoccupied trap of the lower levels. The rate of charge exchange is given by equation 2.24.

$$\frac{d(n_1)}{dt} = n_2(t) \frac{N_1 - n_1(t)}{N_1} v \exp\left[\frac{U_2 - U_1}{kT}\right] - n_1(t) \frac{N_2 - n_2(t)}{N_2} v \quad (2.24)$$

+ Promotion from level i to 1

– Demotion to level i from 1

Where $v=kT/h$ is the attempt frequency and h is the Planck constant, U_2-U_1 is the activation energy between levels 2 and 1. Finally, the relative trap density available at level i is given by equation 2.25.

$$\frac{N_1 - n_1(t)}{N_1} \quad (2.25)$$

The first term of equation 2.24 determines the rate of promotion of charge from level 2 to level 1 and the second term describes the rate of demotion to level 2 from level 1.

As the rate at which charge is promoted to the top level is equal to the rate at which it falls back into the lower levels ($dn_i/dt = 0$), no space charge builds up.

The depolarization characteristic can be used to estimate the coefficients a_i and b_i . It is noteworthy that the energies U_i' and U_1' differ from the energies U_i and U_1 due to the effect of local field on the energy barrier. Therefore, the measured values U_i' and U_1' are lower than the actual values as the local electric field decreases the energy barrier for charge detrapping. As a result, $\Delta U_i'$ represents the energy barrier for charge detrapping decreased by the local electric field.

The corresponding unaffected energy levels ΔU_i could be derived by subtracting a suitable expression for the field dependence from $\Delta U_i'$ (i.e. a correction term based on the Poole-Frenkel law). However, the effectiveness of such a correction is questionable and the analysis will be limited to $\Delta U_i'$ values.

The depolarization characteristic is divided into an appropriate number of segments; each of them corresponds to a trap level. The number of segments depends on the steepness of the depolarization characteristic.

3. Experimental Methods

In this chapter, a description of the specimens under examination is given in section 3.1. All the setups used for evaluating the performance of the test objects are described in the rest of the chapter. In section 3.2 the PEA methods for space charge measurements on plaques and cables are presented. A description of the setups for conduction current measurements on plaques and cables is given in section 3.3 and 3.4 respectively.

3.1 Test specimens

3.1.1 Cables

Experimental investigations were performed on 8 different polymeric mini-cables composed of different combinations of insulation and semi-conductive layers.

A mini-cable is essentially a scaled down test model of a DC power cable consisting of an inner conductor, an inner semi-conductive layer, the dielectric and an outer semi-conductive layer. A schematic representation of a mini-cable produced by a triple extrusion process is shown in figure 3.1. The extrusion process results in a chemical bond at the semicon-insulation interfaces through a crosslinking process. The result is a chemical interface between the insulation and the semicon in the mini-cable which is similar to those found in a full scale DC power cable.

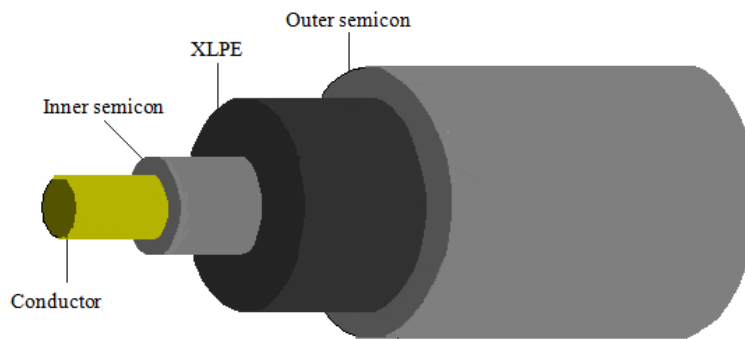


Figure 3.1 – Schematic representation of a mini-cable

Two types of insulation are used. Type I which consists of crosslinked polyethylene *PE* with less than 0.5 wt.% styrenic charge trapping agent and type II composed of crosslinked polyethylene *PE* with less than 1 wt.% carbon black.

Styrenic charge trapping agent is added to the insulation in order to create more shallow traps and not deep traps. The purpose of adding carbon black is to increase the overall conductivity.

As far as the semi-conductive layers are concerned, 4 different types are used. Type C, E and D which are composed of ethylene copolymer with polar comonomer but each type contains different amount of carbon black. The fourth type, F, consists of copolymer blend of reduced polarity with a certain amount of carbon black. The carbon black content of each semicon is given in table 3.1.

Table 3.1 – Composition of the different semicon types

Semicon Type	Composition	Carbon content
C	ethylene copolymer with polar comonomer	‘low’
E	ethylene copolymer with polar comonomer	‘medium’
D	ethylene copolymer with polar comonomer	‘high’
F	copolymer blend of reduced polarity	‘medium’

The cables under examination are presented in table 3.2 and their dimensions in table 3.3.

Table 3.2 – Composition of the cables under examination

Cable	Type of insulation	Type of semicon
11543-1	I	F
11543-2	I	E
11543-3	I	C
11543-4	I	D
11544-1	II	D
11544-2	II	E
11544-3	II	F
11544-4	II	C

Table 3.3 –Cable dimensions

Cable	Radius [mm]	Thickness [mm]
Conductor	0.815	-----
Inner semicon	1.320	0.505
Insulation <i>XLPE</i>	2.845	1.525
Outer semicon	3.605	0.760

The specimens used for space charge and conduction current measurements were initially free of space charge. Discharging of charged specimens were brought by short circuit and, if necessary, by heating the specimens at 80°C for a sufficient period of time.

3.1.2 Semicon plaques

The different semicon types which are used in the cable production are also provided in the form of plaques. Each semicon plaque is a square of 20x20mm with thickness approximately equal to 0.65mm.

Conduction current measurements were carried out on these plaques in order to determine their conductivity. The results are presented in section 5.1.

3.2 Space charge measurements

Space charge inside an insulator distorts the electric field and can cause significant field enhancements. Therefore, the magnitude and location of the space charge in a dielectric is a matter of major importance. In earlier days, destructive methods to measure space charge were used such as field mills and capacitive probes [4]. These methods are, in fact, surface charge measurements as the test object has to be cut into slices in order to arrive at the site of the charge.

The disadvantage of destroying the sample has been overcome by the use of a new generation of space charge measurement methods. All these methods use a common principle. An externally applied physical quantity interacts with the charge inside the sample. The charge in its turn interacts with, or generates a second physical quantity that can be externally measured. The physical quantities differ per method and they can be pressure, temperature, electric voltage or current.

Nowadays, pulsed methods are widely used and the most popular method used to determine the charge profile in dielectrics is the acoustic pulsed method. If the acoustic wave is generated externally and propagating in the dielectric to profile the space charge, it is called the pressure wave propagation *PWP* method. If the acoustic wave is internally generated by the space charge and propagates through the dielectric with the space charge information, it is known as the pulsed electro-acoustic *PEA* method. In this work, the latter method is used.

3.2.1 PEA for flat specimens

A schematic representation of the PEA setup for flat specimens is displayed in figure 3.2. The PEA method for flat specimens is used in order to explain the basic operational principle behind this measuring technique [6],[9],[30].

In the Pulsed Electro-Acoustic *PEA* method, a pulsed voltage $U_p(t)$ is applied across a flat test object. The pulsed voltage can be superimposed on a DC voltage U_o . In order to achieve this, a decoupling capacitor C and a resistor R should be placed in series to the pulse source and the DC source respectively.

The applied DC voltage U_o results in the formation of surface charges on the electrodes and space charge in the material. During a measurement, a very short high voltage pulse $U_p(t)$ is applied which results in an electric field which acts on the surface charges on the electrodes and the space charges inside the material. Due to this field, the charges experience an electrostatic force. This force causes the charges to move slightly. This movement can initiate an acoustic wave at the charge location which travels through the sample and the earth electrode towards the piezoelectric sensor *PVDF*. Depending on the thickness of the sample, the amplitude of the pulse ranges between 0.1 and 4kV whereas the pulse width varies from 5 to 200ns. Also, it is worth noting that the earth electrode is much thicker than the HV electrode. In this way, the former has the function of delaying the acoustic wave until its arrival at the piezoelectric sensor.

The delay is necessary, because of the interference of the electromagnetic noise caused by the firing of the electrical pulse.

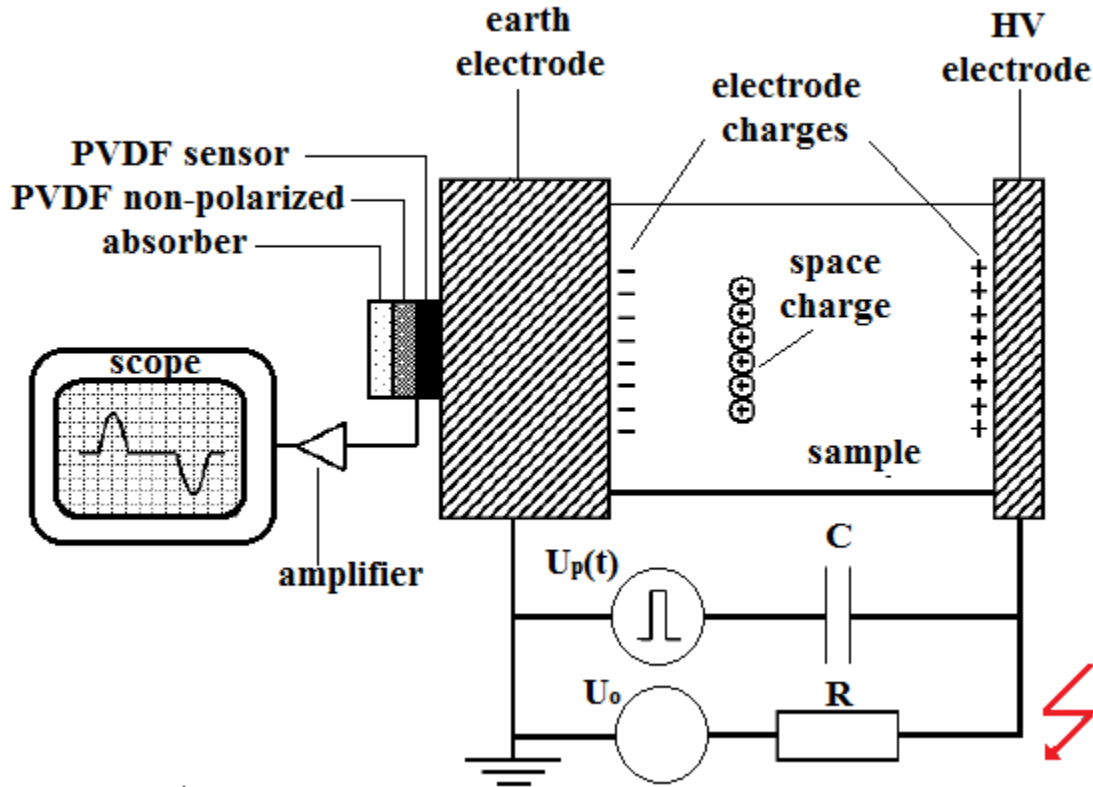


Figure 3.2 – Schematic representation of the PEA setup for flat specimens

The polyvinylidene fluoride *PVDF* sensor is a polymeric piezoelectric transducer with certain properties that make it suitable for detecting acoustic signals generated by space charge and converting them into voltage signals. The magnitude of the signal is proportional to the space charge density and the sign of the signal coincides with the sign of the space charge. That means that positive charges will cause a positive voltage and vice versa. Such kind of properties that favor the use of *PVDF* sensors are: high levels of piezo-activity, an extremely wide frequency range, a broad dynamic response and a low acoustic impedance. In order to avoid reflections of acoustic waves, a proper acoustic termination is required at the sensor. For this purpose, a material (*PVDF* non-polarized) with the same acoustic properties of the sensor is used in combination with a material (absorber) able to absorb the acoustic waves. The electrical signal provided by the sensor is amplified and fed into an oscilloscope, where it is displayed and stored.

Deconvolution

The amplified electrical signal detected at the scope does not directly represent the acoustic signal at the sensor. This is mainly due to the fact that the sensor itself has a certain capacitance which in combination with the input resistance of the amplifier acts as a high pass filter. Therefore, the higher frequencies are gained in favor of the lower frequencies. In order to correct the detected signal a deconvolution technique is adopted.

Attenuation and dispersion

Acoustic waves are attenuated and dispersed while travelling through lossy media. Therefore, the acoustic signal detected at the sensor does not directly correspond to the space charge distribution within the test specimen.

In a lossy medium, the amplitude of a pressure wave due to space charge decreases while the wave travels through the test object. Attenuation is a frequency dependent phenomenon which causes high frequency components to be more attenuated than lower frequencies. Therefore, the charge peak in the detected signal results not only smaller but also wider if compared to the peak that would be detected if the medium was ideal.

In a dispersive medium, the shape of a pressure wave due to space charge changes while the wave travels through the material. This is due to the fact that the speed of sound in a material is frequency dependent.

In figure 3.3, the effect of attenuation and dispersion is shown for acoustic signals originated at different locations of a test object. It is clear that the longer the distance that waves have to travel within the medium, the more attenuated and distorted the corresponding signals are. The attenuation and dispersion phenomena are frequency and position dependent.

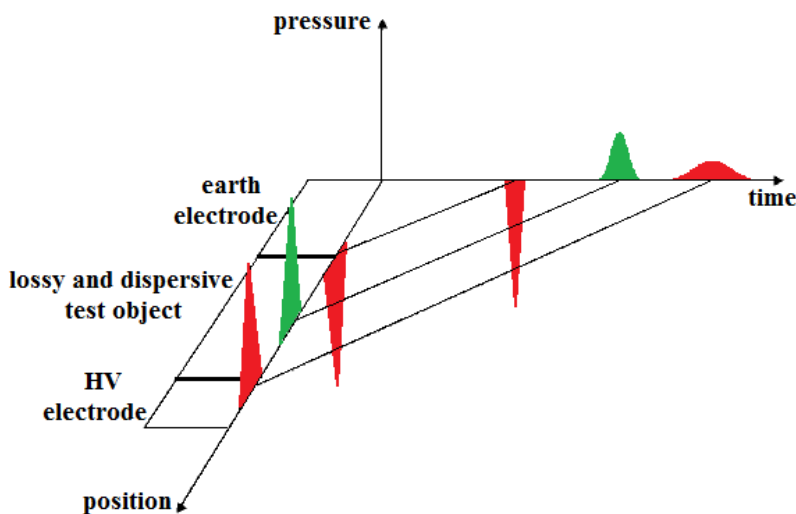


Figure 3.3 – Attenuation and dispersion of acoustic waves in PEA method

Calibration

Finally, calibration of the measuring system must be performed in order to convert the detected signal at the scope [mV] into a space charge density signal [C/m^3]. This procedure can be carried out on the basis of a known charge distribution at the earth electrode.

To convert a voltage signal $v(t)$ into a calibrated space charge profile $\rho(t)$, a calibration factor K_{cal} is defined according to equation 3.1.

$$K_{cal} = \frac{v_{pr}(t)}{\rho(t)} \quad (3.1)$$

Where $v_{pr}(t)$ is the processed signal after deconvolution, attenuation and dispersion correction.

In order for the calibration factor to be calculated, a certain DC voltage V is applied to an initially space charge free sample. The calibration factor can be calculated according to equation 3.2.

$$K_{cal} = \frac{\int_{x_1}^{x_2} v_{pr}(x) dx}{\sigma_e} \quad (3.2)$$

Where x_1 and x_2 denote the starting and the ending point of the earth electrode respectively, σ_e is the earth electrode surface charge density and for a known applied voltage V it can be calculated according to equation 3.3.

$$\sigma_e = \varepsilon_0 \varepsilon_r E_e = \varepsilon_0 \varepsilon_r \frac{V}{d} \quad (3.3)$$

Where d is the sample thickness and ε_r is the relative permittivity of the sample.

Once the calibration factor has been determined, the space charge profile can be obtained according to equation 3.1.

In order to verify that the calibration procedure is correctly done, the electric field distribution $E(x)$ across the sample can be calculated according to equation 3.4.

$$E(x) = \frac{1}{\varepsilon_0 \varepsilon_r} \int_0^d \rho(x) dx \quad (3.4)$$

Afterwards, the voltage distribution $V(x)$ across the sample can be calculated according to equation 3.5.

$$V(x) = - \int_0^d E(x) dx \quad (3.5)$$

Measurement procedure

Measurements can be performed in two different ways. The first case is voltage-on measurements where space charge within the test object is measured while a DC voltage is applied. The space charge present in the bulk of the insulation and the charges at the electrodes are detected. Electrode charges consist of two types of charges. The first type is a result of the presence of the DC voltage and the second type is induced by the space charge in the sample.

Furthermore, voltage-off measurements can be carried out where space charge is measured while the DC voltage is absent and the test object is short-circuited. The space charge present in the bulk of the insulation is detected. Charges at the electrodes are also detected but they are only induced by the space charge. These charges at the electrodes are called mirror charges.

3.2.2 PEA for cables

The operational principle of this method is the same with the *PEA* method for flat specimens. However, there are some differences between the two methods. In this work the *PEA* method for cables is used as the tested objects are cylindrical mini-cables. Their construction consists of a conductor, an inner semi-conductive layer, an insulation layer of XLPE and finally, an outer semi-conductive layer. A cross section of such a mini-cable is presented in figure 3.4.

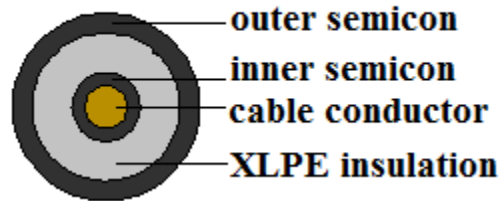


Figure 3.4 – Cross section of a mini-cable under examination

A schematic representation of the *PEA* setup used for space charge measurements on cables is displayed in figure 3.5. The technical specifications of all the components of the setup are given in Appendix II.

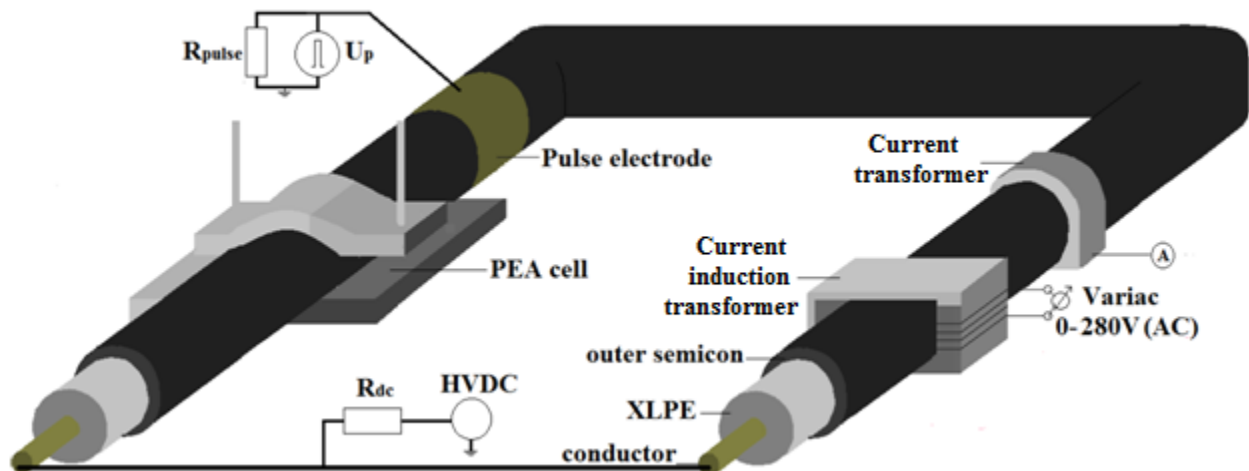


Figure 3.5 – Schematic representation of the *PEA* setup for cables

A DC voltage is applied between the cable conductor and the earthed outer semi-conductive layer via a resistor. This voltage causes a DC electric field and in its turn results in the formation of space charge in the bulk of the insulation. The use of the resistor R_{dc} is essential in order to limit the maximum current drawn from the DC supply and to decouple the power supply. The value of the resistance is $30\text{M}\Omega$.

Pulsed voltage

In this work the pulsed voltage is applied to the outer semi-conductive layer with the use of a pulse electrode wrapped around the cable. The pulse electrode is made from copper tape. In this case, the pulse is applied between the pulse electrode and earth. Therefore, the PEA cell is at earth potential. This fact enables the equipment for measuring the output signal to be directly connected to the PEA cell without the use of an electrical isolation system between the measuring equipment and the PEA cell. Furthermore, a decoupling capacitor is not necessary as the cable itself acts as a decoupling capacitor.

The generation of the pulses is performed with the use of a HVDC power supply connected to a switching device which switches the high DC voltage. The output of the switching device is connected to the pulse electrode with the use of a cable. The characteristic impedance Z_{line} of the cable is 50Ω . Therefore, the cable is properly terminated by means of the resistor R_{pulse} and its value equals 50Ω as well.

The pulse has a very short rise time and a narrow width. Typical values are 2-20ns and 20-200ns for pulse rise time and pulse width respectively. The amplitude of the pulse is in the range of 0.5 to 5kV. Therefore, stray inductances L_s present at the test cable can cause the generation of fly-back voltages. This effect can distort the pulse shape. Moreover, the outer semi-conductive layer has a finite resistance R_{sem} between the pulse electrode and the earth electrode which can cause a mismatch in the termination of the pulse cable.

In order to reduce the distortion caused by the effects mentioned above, a low inductance damping resistor R_d is placed in series between the termination of the pulse cable and the pulse electrode. The value of this resistor equals 155Ω . Figure 3.6 shows the equivalent circuit.

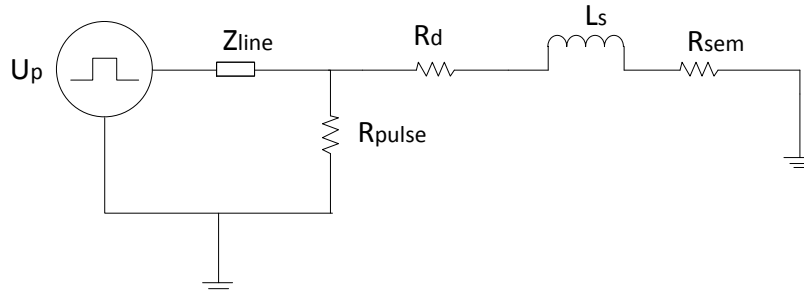


Figure 3.6 – Equivalent circuit of the pulsed voltage

The amplitude of the pulsed voltage ranges from 3.5 to 4kV. The rise time of the pulse is 10ns and the pulse width Δt is 80ns. Therefore, the spatial resolution r equals $160\mu\text{m}$ according to equation 3.6.

$$r = \Delta t * v \quad (3.6)$$

Where v [m/s] denotes the acoustic wave velocity in XLPE insulation.

PEA cell

Different types of PEA systems have been developed for space charge measurements on cables. The main difference between them is in the shape of the earth electrode. The earth electrode can be curved in order for the outer semi-conductive layer of the cable to fit in. In this case, the sensor and the acoustic termination have a curved geometry as well. The second arrangement includes a flat earth electrode, a flat sensor and a flat acoustic termination.

In this work a flat PEA cell configuration is used. A flat earth electrode can ensure a better acoustic contact at the electrode-sensor interface and also, cables of different sizes can fit into the setup. However, in the flat-electrode configuration, the piezoelectric sensor is relatively narrow. Then, the capacitance of the sensor is smaller than that of the sensor used in the curved-electrode configuration. A low sensor capacitance may lead to a distorted signal if the input impedance of the amplifier is low. Figure 3.7 shows a cross section of the PEA cell.

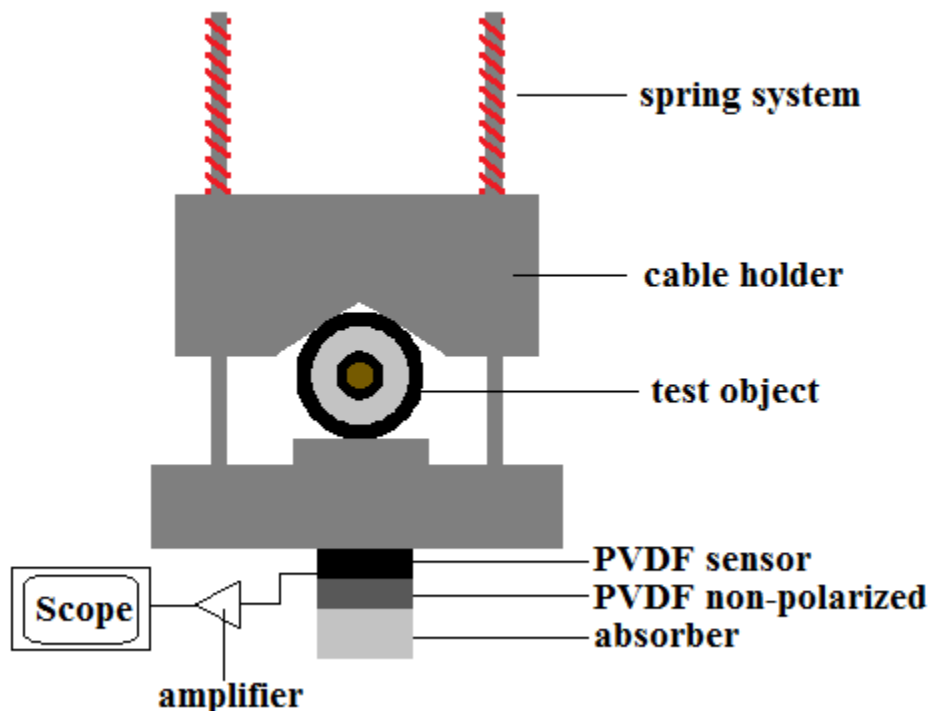


Figure 3.7 – Cross section of the PEA cell

The outer semi-conductive layer is to be attached to the measuring electrode of the PEA cell. The acoustic impedance of the semi-conductive layer is similar to that of the cable insulation. Therefore, no reflections of acoustic waves occur at the semicon-insulation interface. The cable holder guarantees a good contact between the outer semi-conductive layer and the measuring electrode. Furthermore, in order to improve even more the acoustic contact between the cable and the measuring electrode, silicone oil is applied to this particular interface before applying pressure to the cable holder.

The piezoelectric sensor consists of a polyvinylidene fluoride *PVDF* foil of 25 μm thickness. The used amplifier has an input impedance of 1.5k Ω in order to overcome the low capacitance of the piezoelectric sensor. However, this high input impedance causes higher noise level. The gain of the amplifier is 70dB and the bandwidth ranges from 0.1 to 100MHz.

Heating system

Tests at higher temperatures than room temperature are carried out with the use of an induced current heating technique composed of an AC current induction transformer. In this way, an AC current is induced in the inner conductor of the cable and flows in a closed loop as the ends of the cable are connected to each other. Therefore, the cable is heated up due to resistive losses. A temperature gradient is present between the inner conductor and the outer semi-conductive layer of the cable. The temperature at the inner conductor is higher than the temperature at the outer semicon.

The tested cable plays the role of the secondary winding of the current induction transformer. The primary winding of the current induction transformer is connected to a variable autotransformer. Therefore, the primary current is adjusted and the current which flows through the tested cable can be regulated in order for the desired temperature to be reached.

The temperature is always monitored both at the inner conductor and the outer semi-conductive layer with the use of thermocouple sensors. However, as the inner conductor is under high voltage, the temperature sensors cannot be connected to it. Therefore, a dummy loop with the same length and characteristics as the tested cable is used. This dummy loop is not connected to high voltage and the thermocouple sensors are placed at this cable. Two sensors are attached to the outer semi-conductive material of the mini-cable and two more are inserted between the conductor and the inner semi-conductive layer.

In order to ensure that the temperatures of both cables (tested cable and dummy cable) are equal, the currents flowing through the two cables are always monitored. This is achieved with the use of two current transformers in combination with two ammeters. These two currents should always be equal.

The measurements at 20 $^{\circ}\text{C}$ were performed without the use of the heating system as the ambient temperature in the laboratory was approximately 20 $^{\circ}\text{C}$ ($\pm 1^{\circ}\text{C}$). Therefore, there was no temperature gradient across the insulation and isothermal conditions were considered. However, the measurements at 40 $^{\circ}\text{C}$ and 60 $^{\circ}\text{C}$ were carried out with the use of the heating system. In the case of 40 $^{\circ}\text{C}$, there was a temperature difference between the inner and the outer semicon of approximately 5 $^{\circ}\text{C}$. In the case of 60 $^{\circ}\text{C}$ the temperature difference was nearly 10 $^{\circ}\text{C}$. This temperature gradient leads to a conductivity gradient which could affect the threshold for space charge accumulation, as it is mentioned in section 2.1.2.

Signal processing

As in the case of *PEA* for flat specimens, the amplified electrical signal detected at the scope does not directly represent the space charge distribution in the sample. The signal should be processed in an appropriate way in order to obtain the space charge profile in the insulation. Deconvolution, attenuation and dispersion correction can be performed in the same way as in the *PEA* method for flat specimens.

However, due to the cylindrical geometry of cables, the electric field distribution is not homogeneous but divergent. Therefore, the divergence of the pulsed field and of the acoustic waves has to be taken into consideration.

The correction procedure includes deconvolution, divergence correction, attenuation and dispersion correction and finally, calibration. All these processes are discussed in detail in Appendix I.

Accuracy of the measurements

The accuracy of the PEA measurements is subjected to an uncertainty of approximately 15%. This is due to a systematic error in the calibration procedure and a statistical error due to the presence of noise in the output signal.

The systematic error in the calibration process depends on the dimensions of the tested object, the speed of sound inside the insulation, the calibration DC voltage and the area of the signal peak at the earth electrode. The systematic error is approximately 12%.

The presence of noise in the signal results in a statistical error. Sources of noise are considered to be the sensor-amplifier connection, the amplifier and the cables which bring the signal into the oscilloscope. The signal is saved at the scope by averaging 1000 sweeps. This technique results in the reduction of the noise level by a factor 32. The statistical error is approximately 3%.

Finally, electromagnetic disturbances generated by the firing of the pulse affect the detected signal. However, these disturbances are constant and can be removed by saving the initial signal before starting a measurement. Then, this signal is subtracted from the detected signal.

Measurement procedure

As in case of flat specimens, voltage-on and voltage-off measurements can be carried out for space charge measurements on cables as well.

During voltage-on measurements the space charge accumulation in the tested object is recorded while a DC voltage is applied. The process of space charge accumulation in an insulation is called polarization process. In this case, space charge present in the bulk of the insulation and the charges at the electrodes are detected. Electrode charges consist of two types of charges. The first type is a result of the presence of the DC voltage and the second type is induced by the space charge in the sample (mirror charges). A typical processed waveform of such a measurement is displayed in figure 3.8.

In this work, the polarization duration was two hours at each poling field. At least three hours of relaxation are required in order for the accumulated space charge to be depleted before starting a new measurement. The polarization characteristics were used in order to obtain the electric field – average space charge density ($E-\rho$) characteristics. The latter were used for the determination of the electric field thresholds of the cables as it is explained in section 2.2.

Furthermore, voltage-off measurements can be carried out where space charge is measured while the DC voltage is absent and the test object is short-circuited. The space charge present in the bulk of the insulation and the mirror charges at the electrodes are detected. Figure 3.9 represents a relative processed waveform obtained during a voltage-off measurement.

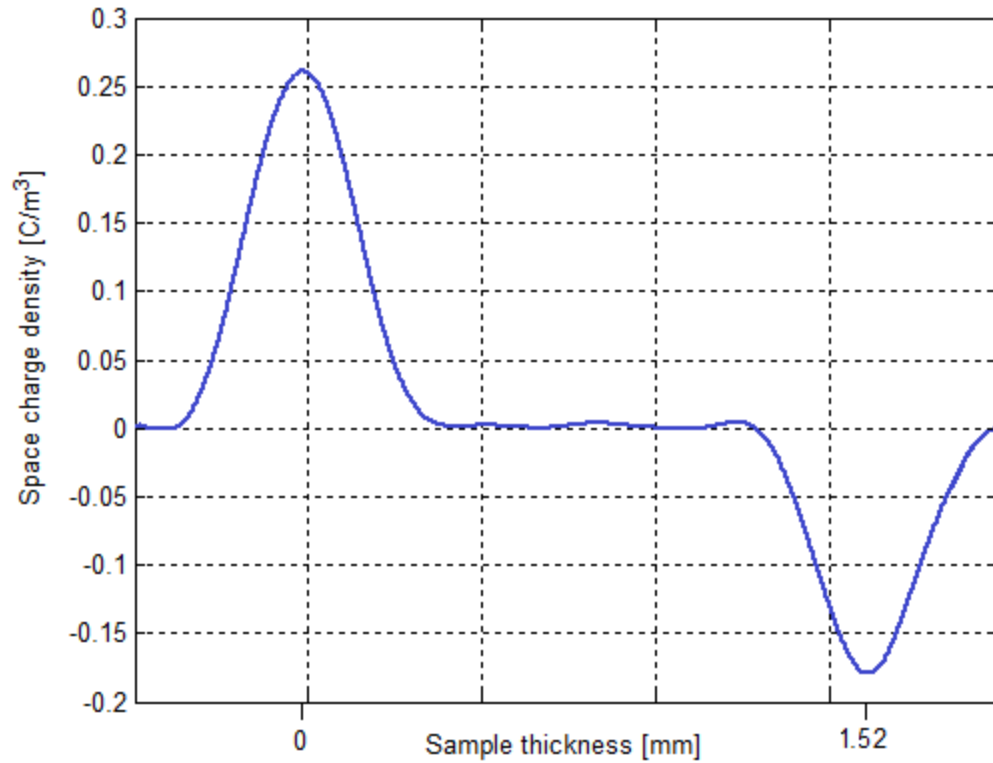


Figure 3.8 – Processed signal of a voltage-on measurement

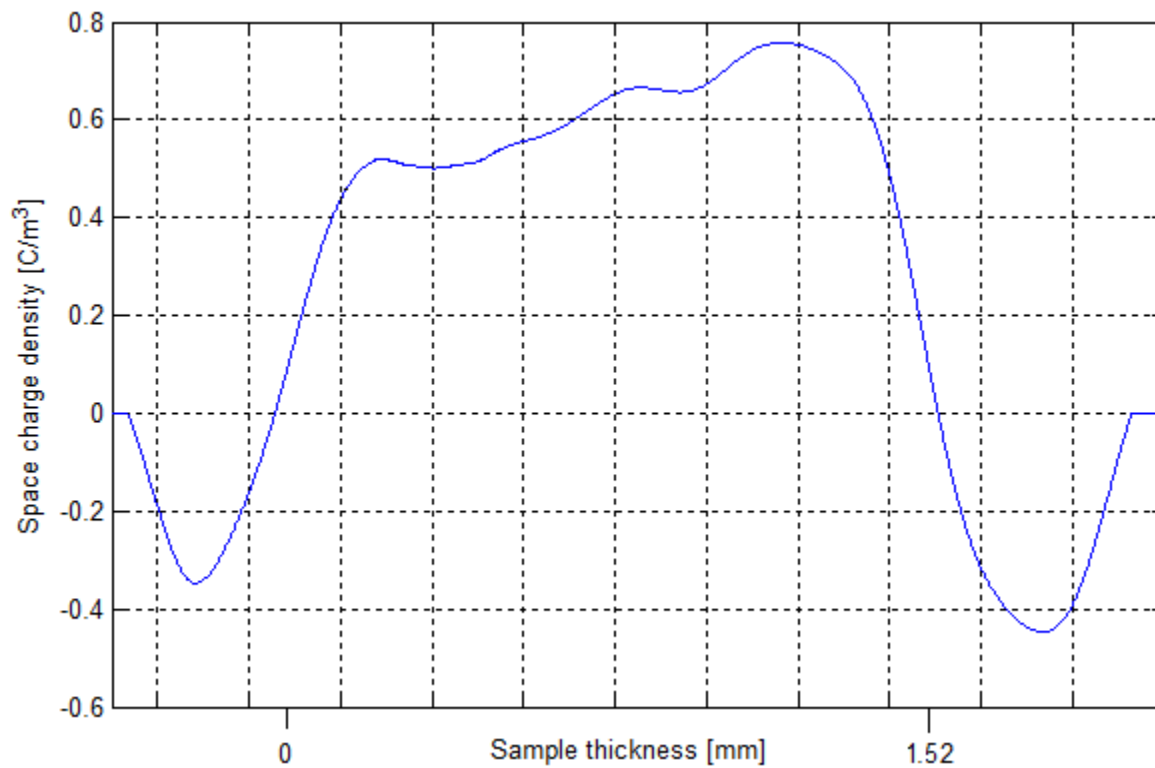


Figure 3.9– Processed signal of a voltage-off measurement

Before starting a voltage-off measurement, the tested object is polarized for a certain time period. The polarization duration in this work was three hours. Afterwards, the applied DC voltage is removed and the tested object is short-circuited. As a result, the space charge which has been accumulated during the polarization time starts depleting with a certain rate. This particular process is called depolarization process. In this work, the depolarization duration was three hours. The depolarization characteristics were used for the determination of the apparent trap-controlled mobility and the values of the trap depths.

During polarization or depolarization, the average space charge density $\rho_{avg}(t)$ in the sample is calculated with respect to the elapsed time according to equation 3.7.

$$\rho_{avg}(t) = \frac{1}{r_{out} - r_{in}} \int_{r_{in}}^{r_{out}} |\rho(r)| dr \quad (3.7)$$

A typical waveform which corresponds to a voltage-on measurement within two hours of polarization is given in figure 3.10.

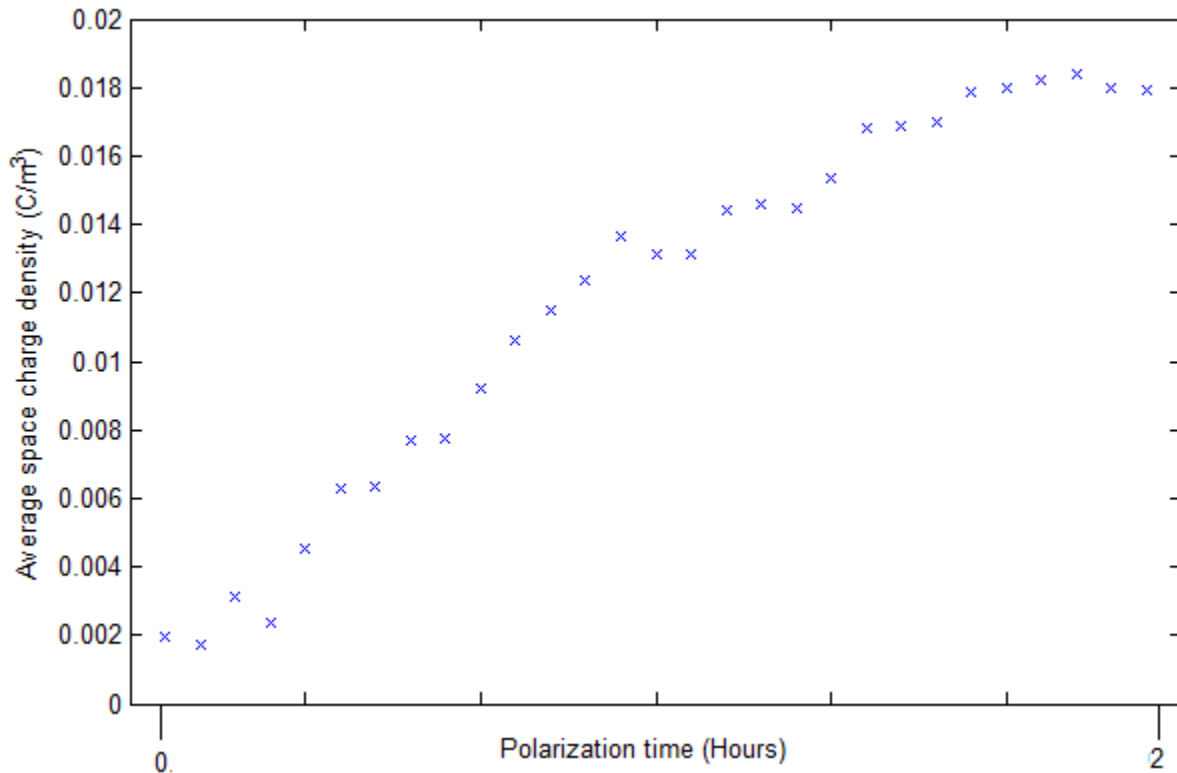


Figure 3.10– Average space charge density during a voltage-on measurement

3.3 Conduction current measurements on plaques

A schematic representation of the setup which is used for conduction current measurements on plaques is displayed in figure 3.11. The technical specifications of all the components of the setup are given in Appendix III.

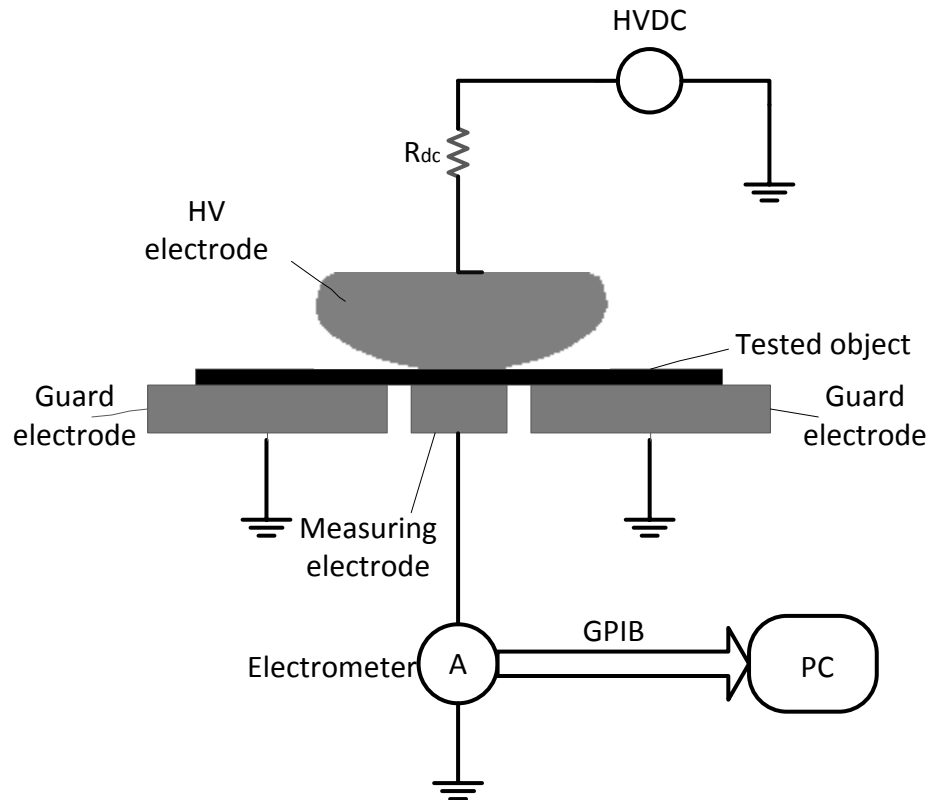


Figure 3.11 - Schematic representation of the setup for conduction current measurements on plaques

During a conduction current measurement, a DC voltage is applied across the sample and current flows through the material. When the transient phenomenon of polarization processes (section 2.3) is finished, the current reaches a steady state value which is called conduction current. The required time for the conduction current to reach a steady state value depends on the kind of the material, the applied electric field and the temperature. An insulating material requires much longer polarization time than a semi-conductive material as the conductivity of the latter is much higher. Also, at relatively high electric fields and temperatures a steady state value is reached sooner.

The DC voltage is supplied to the tested object via a Rogowski-profiled electrode made from aluminum. In order to protect the sensitive electrometer from overcurrents, a resistance R_{dc} is connected in series with the DC supply. The value of the resistance is $627\text{M}\Omega$. Also, in order to avoid currents which flow along the surface of the tested object, a grounded guard electrode is placed around the measuring electrode. In this way, surface currents cannot reach the measuring electrode.

Finally, the electrometer is connected to a computer via a GPIB interface in order for the data to be displayed and stored. The total measuring setup is placed in an EMC shielded cage in order to avoid electromagnetic disturbance.

Measurement procedure

Once the conduction current I at a certain poling field E is determined, the conduction current density J can be calculated according to equation 3.8.

$$J = \frac{I}{A_{meas_electr}} \quad (3.8)$$

Where A_{meas_electr} is the area of the measuring electrode.

So, the conductivity σ of the insulation can be determined with the use of equation 3.9.

$$\sigma = \frac{J}{E} \quad (3.9)$$

Accuracy of the measurements

The accuracy of the conduction current measurements is subjected to an uncertainty of approximately 12%. This is due to the uncertainty in the applied DC voltage and the thickness of the tested object which is about 12%. Also, there is a statistical error of 2% due to noise in the measured current.

3.4 Conduction current measurements on cables

A schematic representation of the setup used for conduction current measurements on cables is presented in figure 3.12. The technical specifications of all the components of the setup are given in Appendix IV.

The voltage is applied with the use of a dc generator and it is connected to the cable conductor via a protecting resistance and an aluminum spherical electrode. The value of the resistor is equal to 627M Ω and it is used in order to protect the electrometer from overcurrents. The spherical electrode is used in order to avoid corona discharges.

Two grounded guard electrodes are used in order to prevent surface currents which can reach the measuring electrode. These electrodes are made from copper tape and they are wrapped around the cable. The measuring electrode is made from copper tape as well.

A coaxial cable connects the measuring electrode to the electrometer. The latter is connected to a computer via a GPIB interface in order for the data to be recorded.

It is worth noting that the measured currents are at low levels (in pA range or lower) and therefore noise currents generated in the cable or from other sources can affect the results. Currents generated by triboelectric effects are a primary cause of noise currents. These currents are generated at the junction between a conductor and an insulator due to friction. Free electrons rub off the conductor and create imbalance that causes the current flow. In order to minimize these effects, all the connections should be kept short, away from temperature changes which would create thermal expansion forces. Furthermore, the measuring coaxial cable of the electrometer and the tested cable should be kept as still as possible by tying them to a non-vibrating surface.

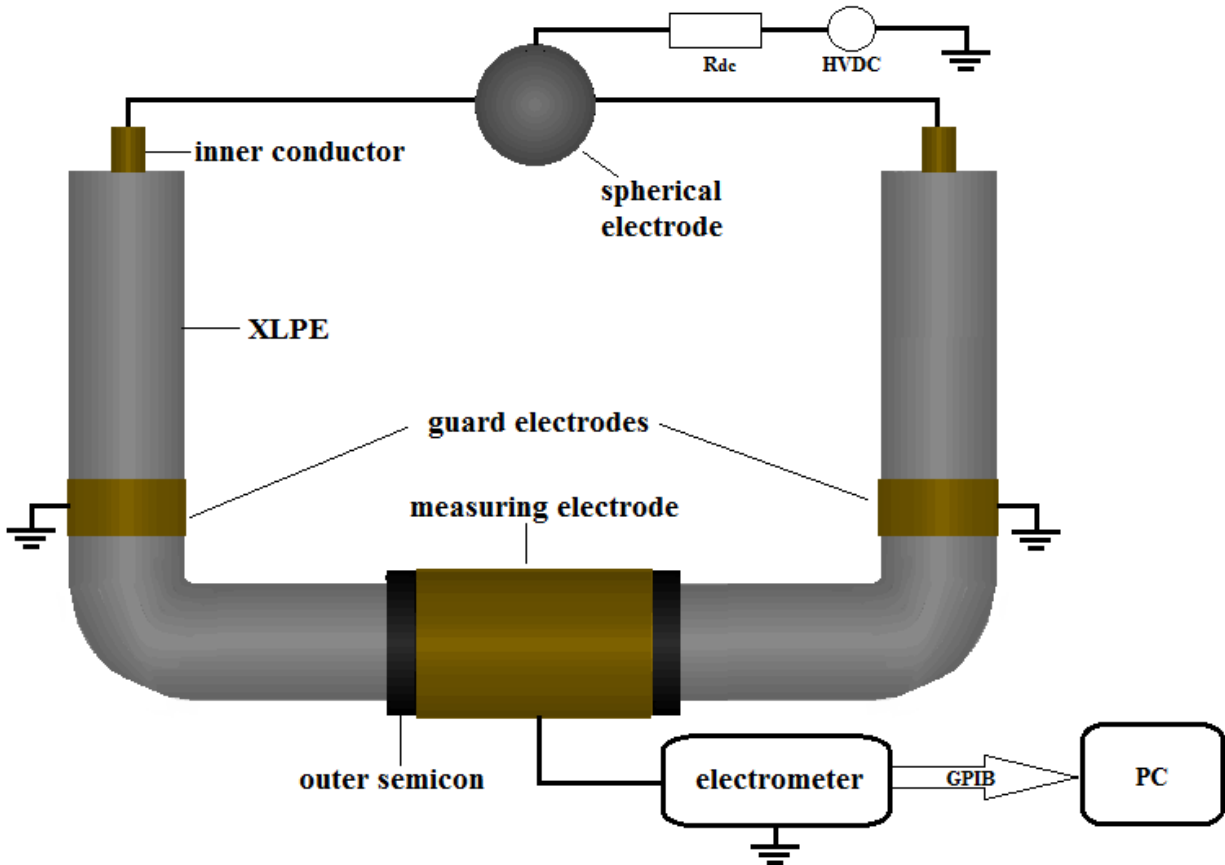


Figure 3.12 - Schematic representation of the setup for conduction current measurements on cables

Measurements at higher temperatures are carried out with the aid of an oven. The tested object is placed in a suitable furnace which can heat the cable up to 80°C . No temperature gradient is present in the cable. The whole measuring setup is placed in an EMC shielded cage in order to avoid external electromagnetic disturbance.

Measurement procedure

The measuring procedure is the same as in the case of conduction current measurements on plaques. A voltage is applied to the sample and current flows through the cable insulation. The current reaches a steady state value when all polarization processes are finished. A typical waveform is presented in figure 3.13. At 40°C and 60°C the steady state value of the current is reached in a shorter time period than in case of room temperature.

At room temperature and at low electric fields (below 5kV/mm) the conduction current can be too low and significantly affected by noise currents. In this case, the conduction current is estimated with the use of the extrapolation technique. Thus, a fitting line described by a power law is used in order to estimate the steady-state value of the current.

After determining the conduction current I at a certain poling field E , the conduction current density J can be calculated according to equation 3.10.

$$J = \frac{I}{A_{meas_electr}} \quad (3.10)$$

Where A_{meas_electr} is the area of the measuring electrode and it is given by equation 3.11.

$$A_{meas_electr} = 2\pi r_{out} l \quad (3.11)$$

Where r_{out} is the outer cable radius and l is the length of the cable. The conductivity σ of the insulation can be calculated with the use of equation 3.12.

$$\sigma = \frac{J}{E} \quad (3.12)$$

Accuracy of the measurements

The accuracy of the conduction current measurements on cables is subjected to an uncertainty of approximately 14%. This is due to the uncertainty in the applied DC voltage and due to the presence of noise currents. The latter play a significant role as the conduction current is at low levels. In some cases (low applied electric fields at room temperature) the conduction current can be comparable to the noise currents.

Apart from triboelectric effects, noise currents are caused by thermoelectric voltages. These voltages are generated when different conductors made of dissimilar materials are joined together.

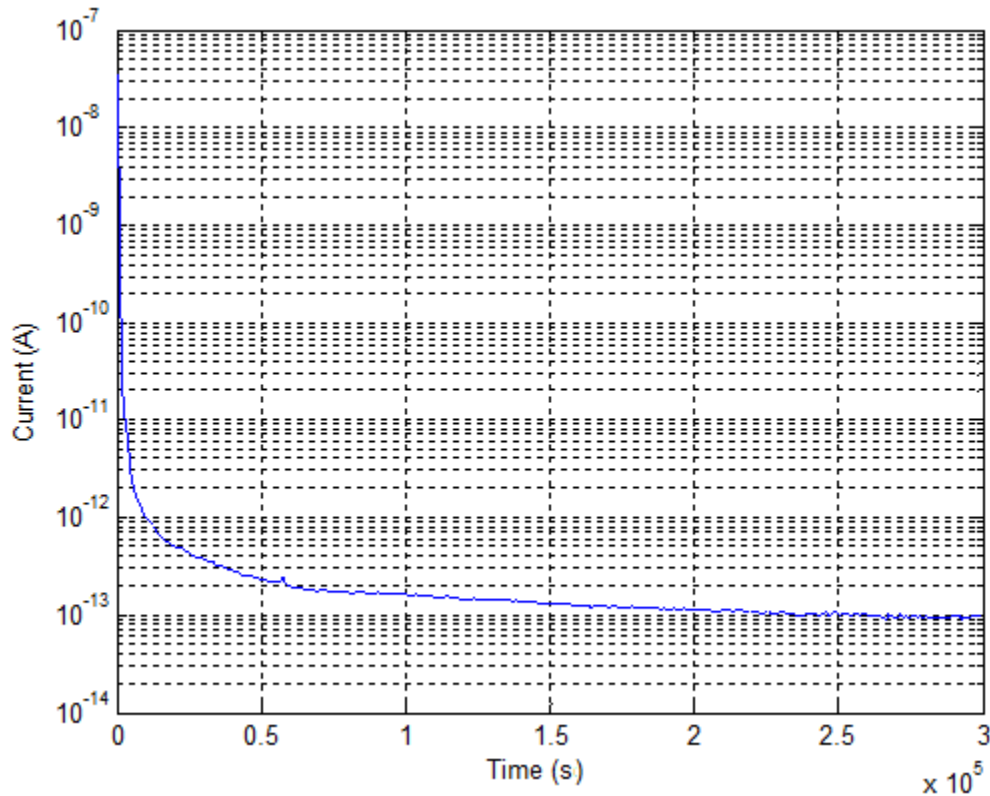


Figure 3.13 – Typical waveform of a conduction current measurement @ 20 °C

4. Experimental Results of Space Charge Measurements

In this chapter, the results of the space charge measurements are presented and discussed. Section 4.1 contains the results of the space charge measurements at positive polarity including a comparison between all the cables. In section 4.2, a cable is examined under negative polarity and the relevant results are presented. Section 4.3 includes the evaluation of the apparent trap-controlled mobility, trap depths and space charge distribution along the trap levels for all the cables.

4.1 Space charge measurements at positive polarity

In this work, the space charge accumulation threshold for four different cables under positive voltage was examined by means of the pulsed electro-acoustic *PEA* method. The polarity of the applied voltage refers to the polarity of the cable conductor.

The threshold for space charge accumulation is determined by carrying out a number of measurements at different poling fields ranging from 1.5kV/mm to 20kV/mm and at three different temperatures, 20°C, 40°C and 60°C.

The average space charge densities accumulated at higher poling fields (i.e. 30kV/mm and 60kV/mm) were obtained during an earlier project carried out at TU Delft.

4.1.1 Cable 11543-2

Space charge accumulation threshold

This cable is composed of insulation type I (cross-linked polyethylene with less than 0.5 wt.% “styrenic” charge trapping agent) and two semicon layers of type E (ethylene copolymer with polar comonomer, “medium” carbon black loading). The obtained E- ρ characteristics at 20°C, 40°C and 60°C are displayed in figures 4.1, 4.2 and 4.3 respectively.

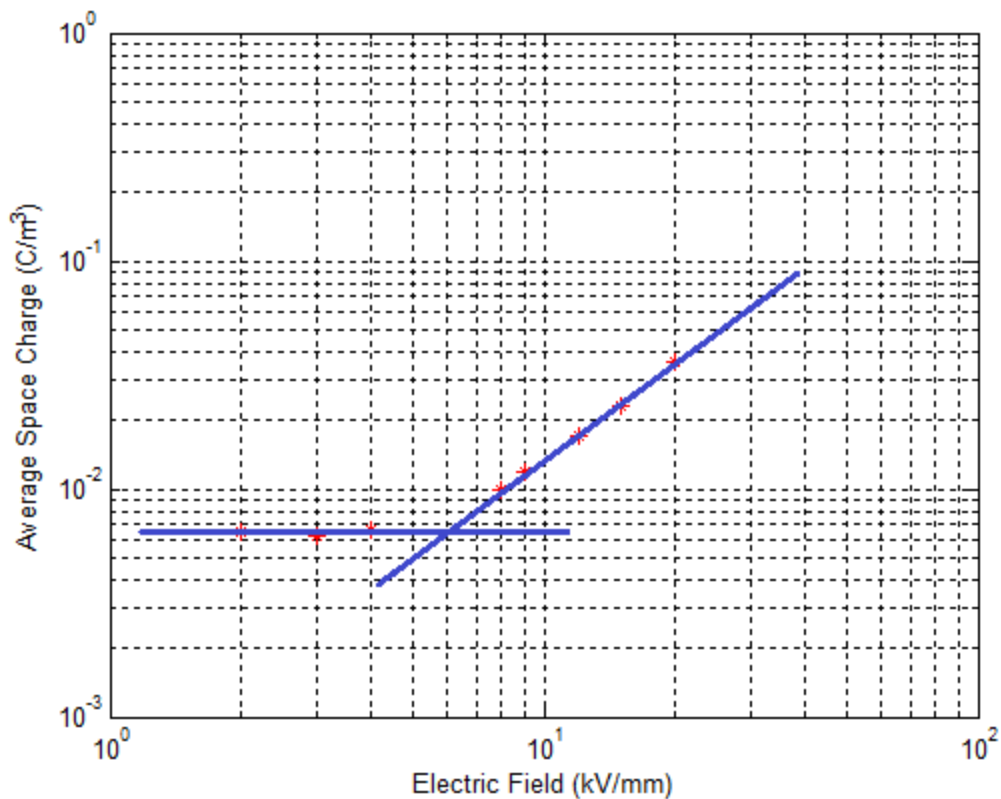


Figure 4.1 – E-ρ characteristic of cable 11543-2 @20°C

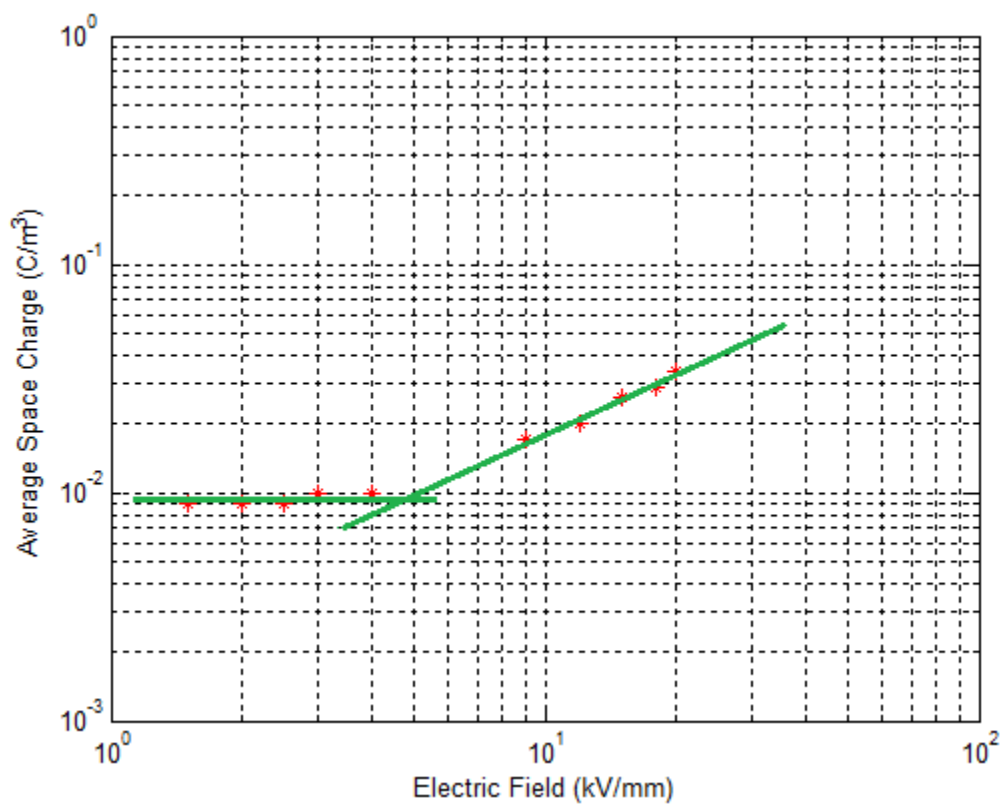


Figure 4.2 – E-ρ characteristic of cable 11543-2 @40°C

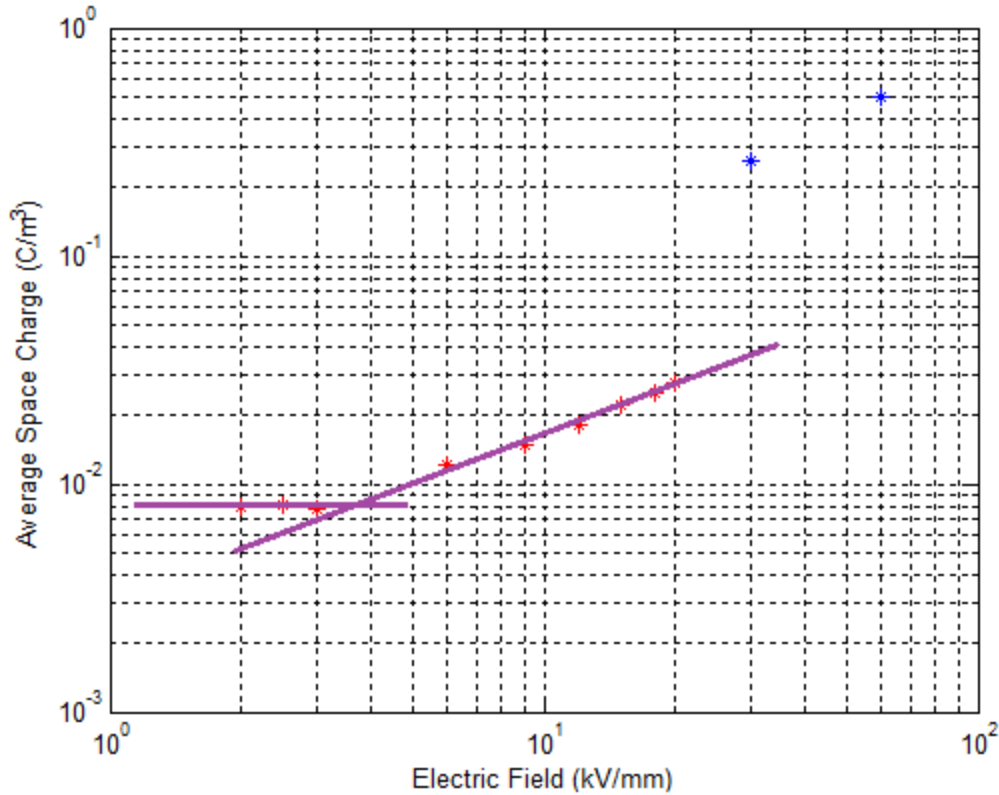


Figure 4.3 - E- ρ characteristic of cable 11543-2 @60°C

The point at which the slope of the E- ρ characteristic changes, determines the electric field above which space charge starts accumulating. At 20°C the electric threshold field is found to be at 6kV/mm. At 40°C and 60°C the threshold for space charge accumulation is determined at 4.5kV/mm and 3.5kV/mm respectively.

In figure 4.3, it can be observed that the average space charge densities at 30kV/mm and 60kV/mm are higher than expected according to the fitting line. Fast moving charge packets could cause this difference. They activated generally by high dc fields and the basic theory behind this process is presented in section 2.6 of this thesis.

Temperature effect on the fitting line slope

The slope of the fitting line above threshold determines the dependence of the space charge density on the applied electric field. The slopes at the three different temperatures are presented in table 4.1.

Table 4.1 – Fitting line slopes at different temperatures for cable 11543-2

Temperature	20°C	40°C	60°C
Slope	1.37	0.91	0.62
Angle	53.8°	42.2°	31.7°

The steepest fitting line is observed at room temperature. The slope of the fitting line decreases when temperature increases. Therefore, at a certain applied electric field more space charge is accumulated at room temperature than at higher temperatures. This particular behavior is observed in figure 4.4 and it could be attributed to the temperature dependence of injection, extraction and detrapping processes of charge carriers.

According to the Schottky injection process (equation 2.13), the Schottky injection current density depends positively on temperature. Thus, an increase in temperature, results in an increase in injection current density. Moreover, the rate of charge detrapping increases as temperature increases due to the higher thermal energy of the trapped charge carriers. Finally, the extraction process is assumed to have a positive temperature dependence as well.

Therefore, the fact that the slope of the fitting line decreases as temperature increases can be attributed to the hypothesis that when temperature increases, the injection rate increases at slower pace than the extraction and charge detrapping rate. However, at high temperatures, the injection rate is still higher than the detrapping and extraction rate. Otherwise, there will be no space charge formation in the insulation.

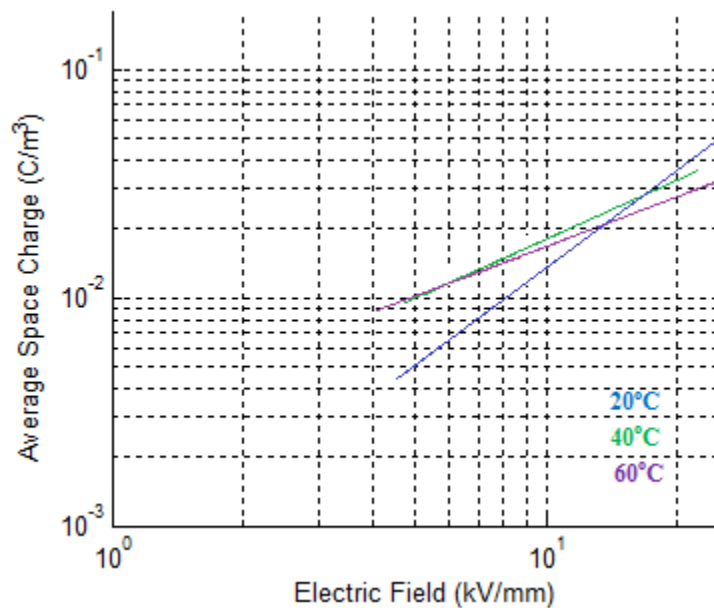


Figure 4.4 - Fitting line slopes above threshold at different temperatures for cable 11543-2

Threshold temperature dependence

The space charge accumulation threshold shows an exponential temperature dependence according to figure 4.5. Equation 4.1 describes the threshold temperature dependence of cable 11543-2.

$$E_{thr} = 0.0675 \exp \left[\frac{1314.5}{T} \right] \quad (4.1)$$

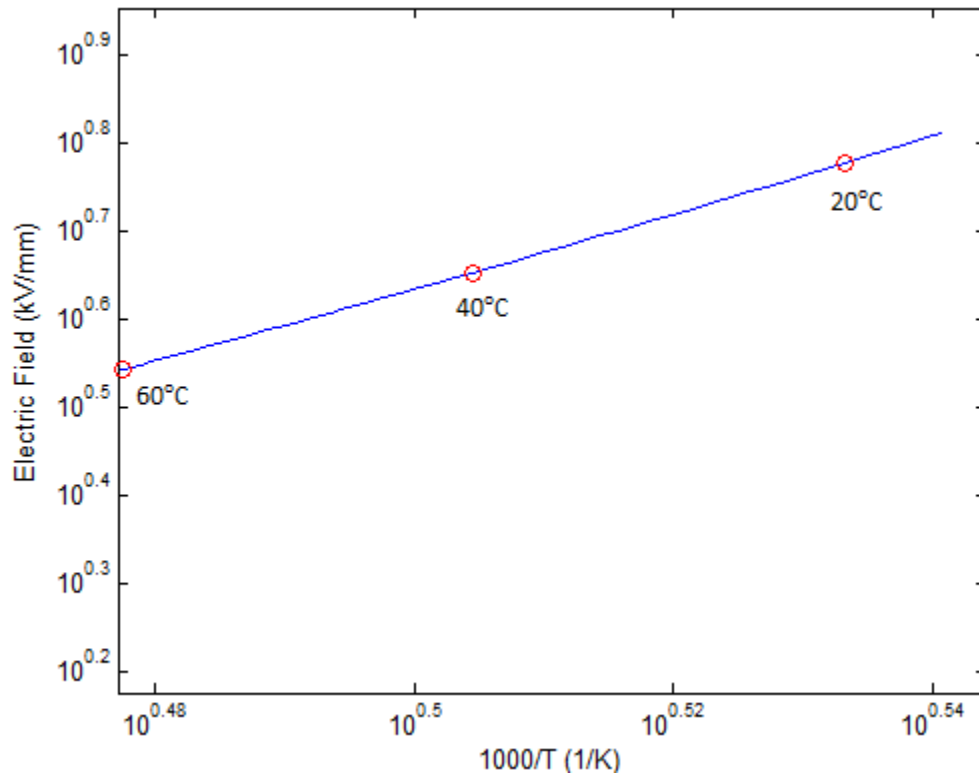


Figure 4.5 – Temperature dependence of electric threshold for cable 11543-2

4.1.2 Cable 11544-2

Space charge accumulation threshold

This cable is composed of insulation type II (cross-linked polyethylene with less than 1 wt.% carbon black) and two semicon layers of type E (ethylene copolymer with polar comonomer, “medium” carbon black loading). The obtained E- ρ characteristics at 20°C, 40°C and 60°C are displayed in figures 4.6, 4.7 and 4.8 respectively.

For this cable the electric field thresholds are the same as in the case of cable 11543-2. Therefore, at 20°C the threshold is determined at 6kV/mm. At 40°C and 60°C the thresholds are 4.5kV/mm and 3.5kV/mm respectively.

The only difference between the two cables is the type of insulation as both of them have the same type of semicon. This observation suggests that the threshold is significantly affected by the semicon type.

In figure 4.8, the observation that the data points at 30kV/mm and 60kV/mm are not included by the fitting line seems to be consistent. A possible existence of fast moving charge packets could explain this kind of behavior.

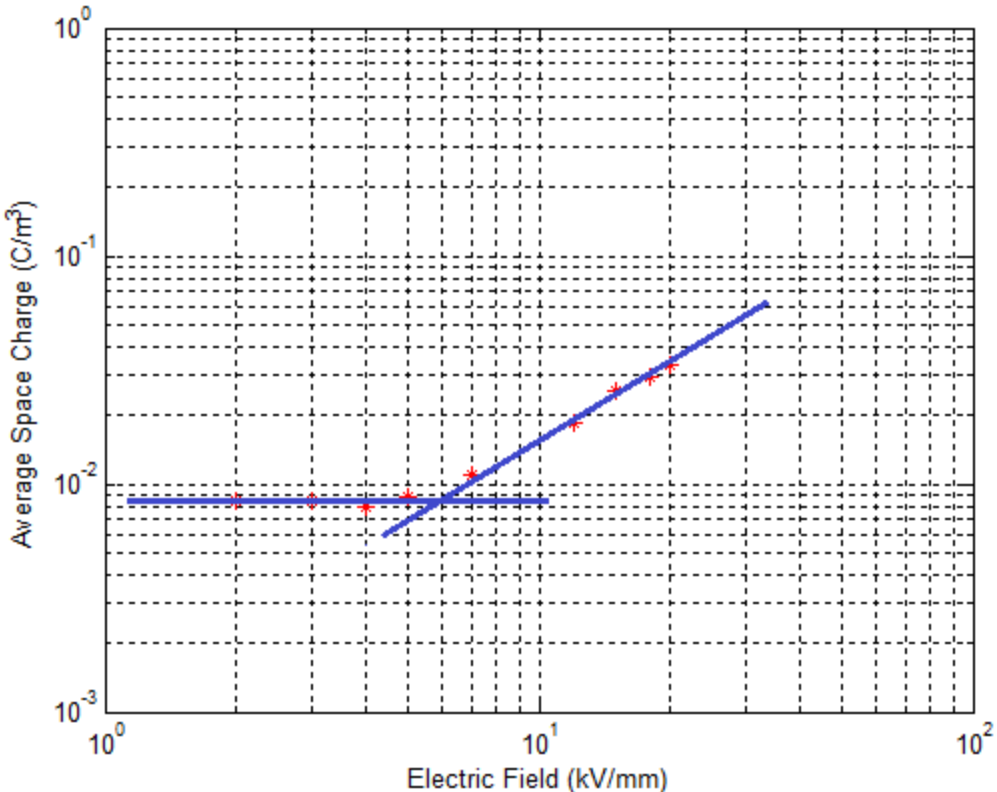


Figure 4.6 - E-ρ characteristic of cable 11544-2 @20°C

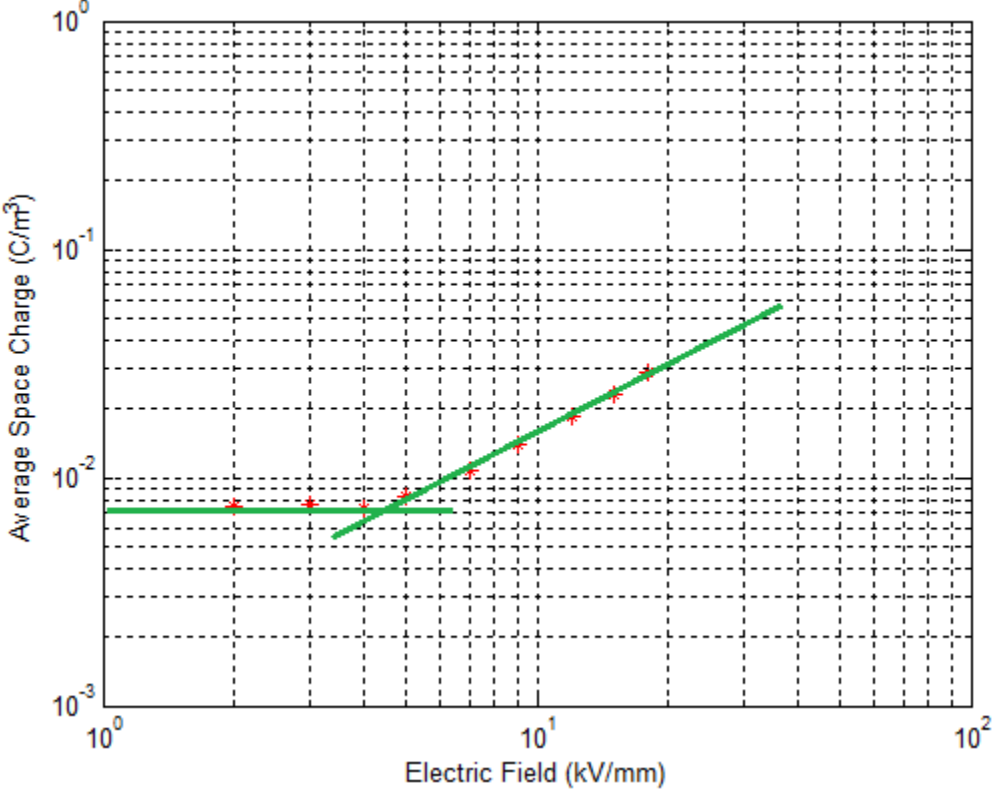


Figure 4.7 - E-ρ characteristic of cable 11544-2 @40°C

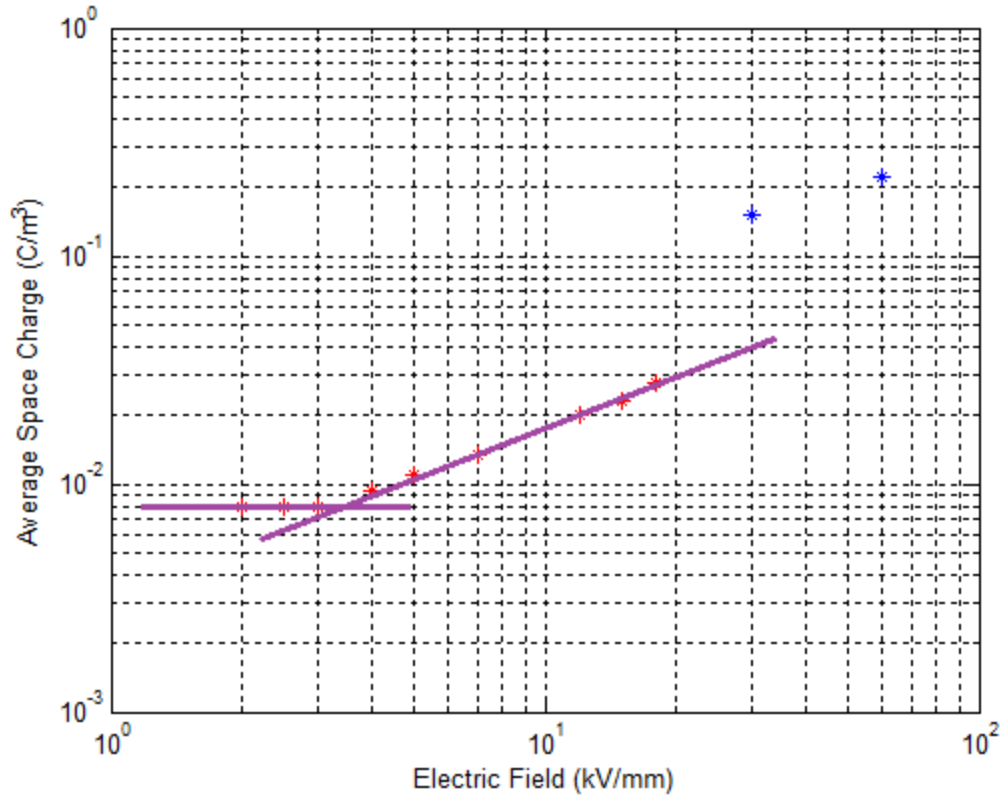


Figure 4.8 - E- ρ characteristic of cable 11544-2 @60°C

Temperature effect on the fitting line slope

In table 4.2, the slopes at the three different temperatures are presented.

Table 4.2 – Fitting line slopes at different temperatures for cable 11544-2

Temperature	20°C	40°C	60°C
Slope	1.09	0.95	0.69
Angle	47.4°	43.6°	34.5°

It can be observed from the above results that also for this cable the fitting line slopes show negative temperature dependence. The possible reason for this phenomenon is discussed in section 4.1.1.

Threshold temperature dependence

The threshold values are the same as for cable 11543-2. Therefore, they can be described by the same exponential relationship (equation 4.1).

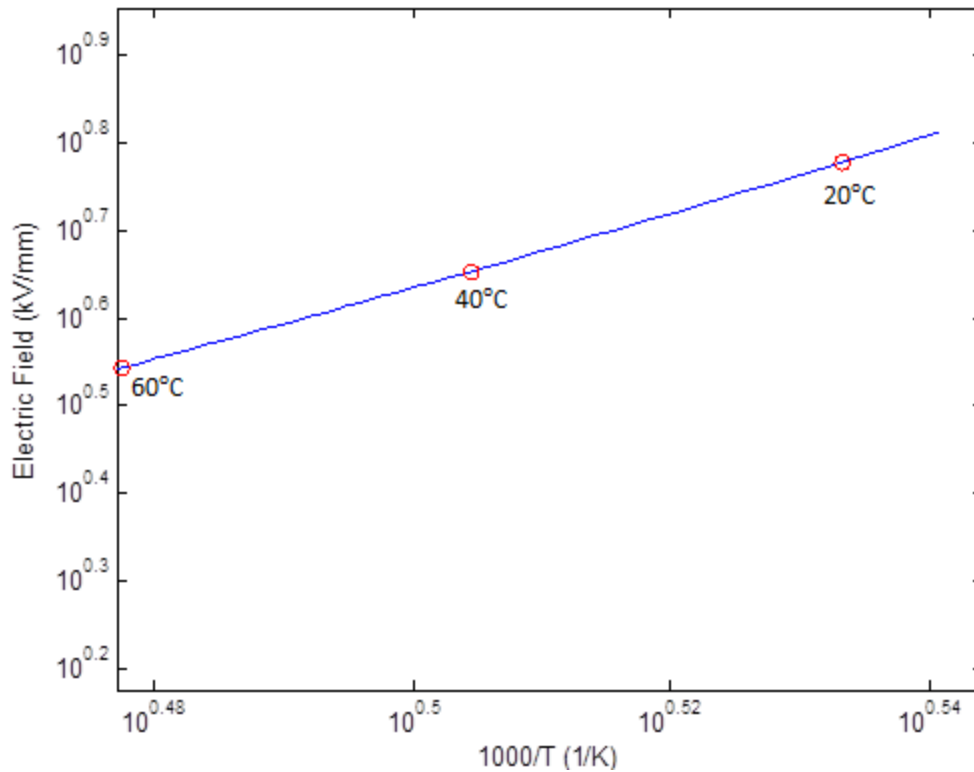


Figure 4.9 – Temperature dependence of electric threshold for cable 11544-2

4.1.3 Cable 11543-1

Space charge accumulation threshold

This cable is composed of insulation type I (cross-linked polyethylene with less than 0.5 wt.% “styrenic” charge trapping agent) and two semicon layers of type F (copolymer blend of reduced polarity, “medium” carbon black loading). The obtained E - ρ characteristics at 20°C, 40°C and 60°C are displayed in figures 4.10, 4.11 and 4.12 respectively.

For this cable, higher electric thresholds were found. At 20°C the threshold is almost 8kV/mm and at 40°C and 60°C the threshold values are 5.5kV/mm and 4kV/mm respectively.

Furthermore, in figure 4.12, it can again be observed that the data points at 30kV/mm and 60kV/mm are out of the fitting line. Therefore, the hypothesis that fast moving charge packets could cause this difference is strengthened.

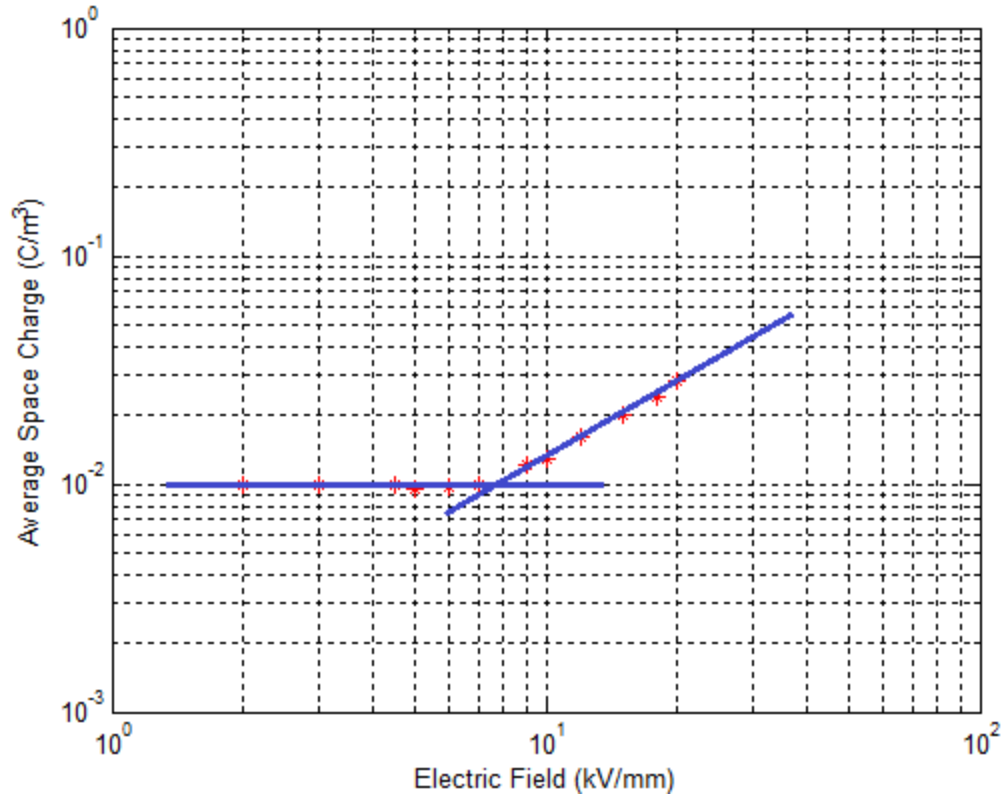


Figure 4.10 – E- ρ characteristic of cable 11543-1 @20°C

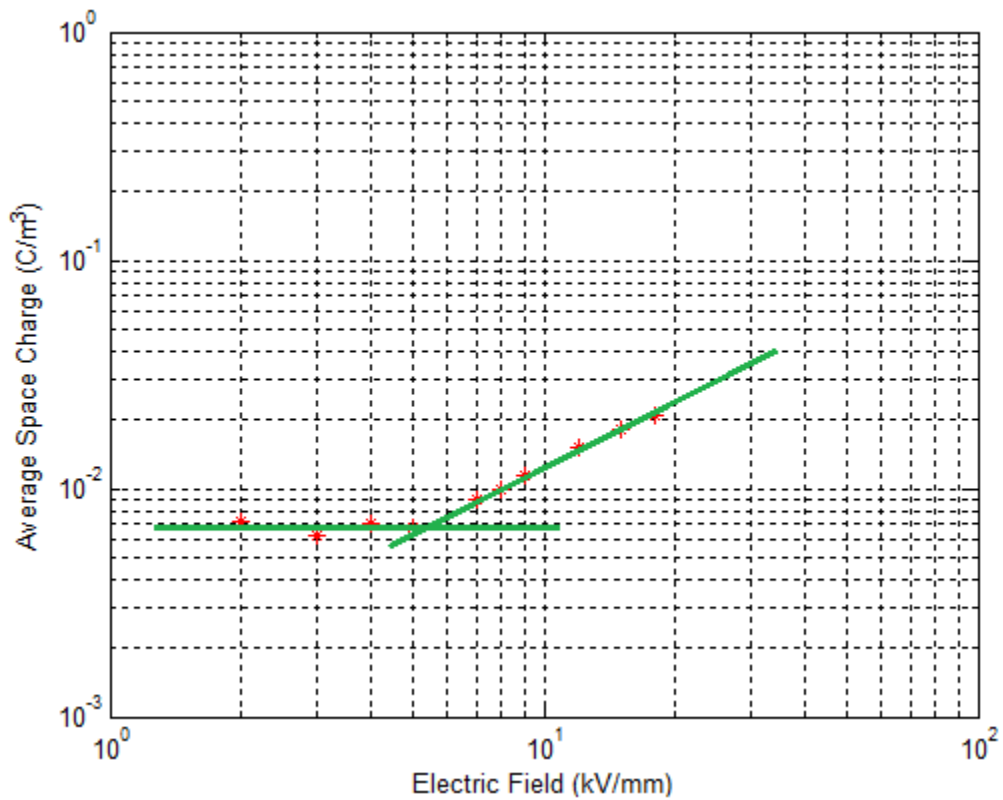


Figure 4.11 – E- ρ characteristic of cable 11543-1 @40°C

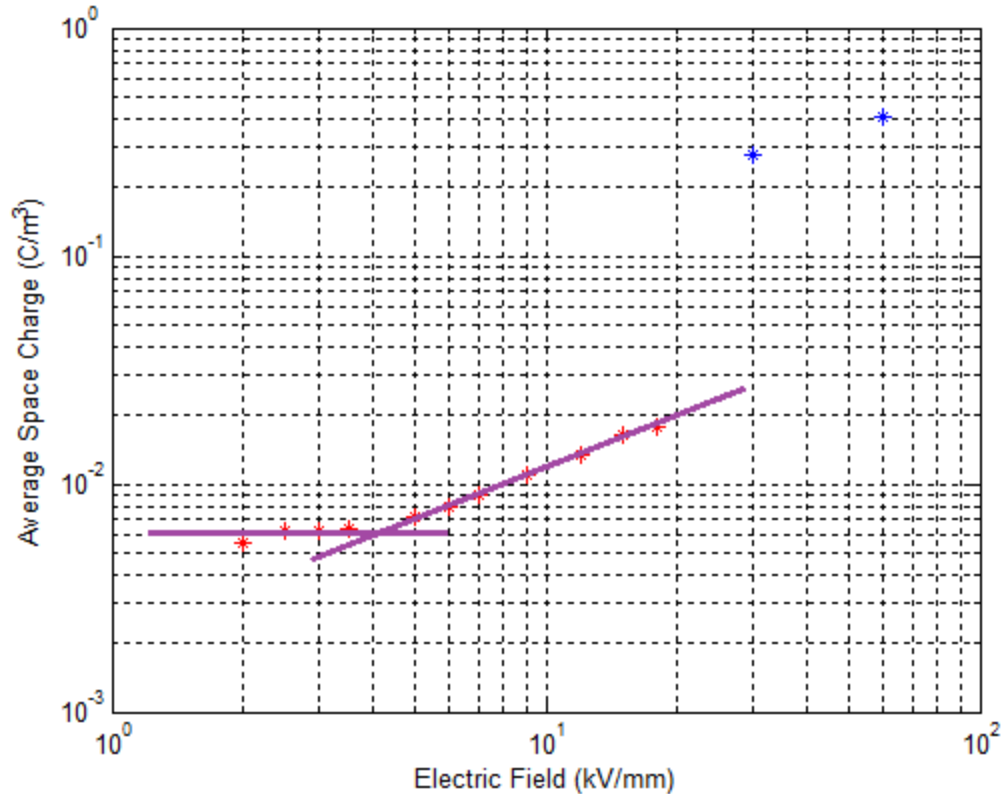


Figure 4.12 – E- ρ characteristic of cable 11543-1 @60°C

Temperature effect on the fitting line slope

The slopes of the fitting lines show the same tendency as in the case of cables 11543-2 and 11544-2. Therefore, the fitting line slope decreases with the temperature increase and the results are presented in table 4.3.

Table 4.3 – Fitting line slopes at different temperatures for cable 11543-1

Temperature	20°C	40°C	60°C
Slope	1.13	1.00	0.70
Angle	48.5°	45.0°	34.9°

Threshold temperature dependence

For this cable the thresholds at different temperatures can again be fitted into a line which is described by an exponential law. The fitting line is presented in figure 4.13.

A larger exponential factor B (1718.1K) is observed (equation 4.2) compared to the value of cables 11543-2 and 11544-2 (equation 4.1). This difference shows a stronger temperature dependence of the threshold for cable 11543-1.

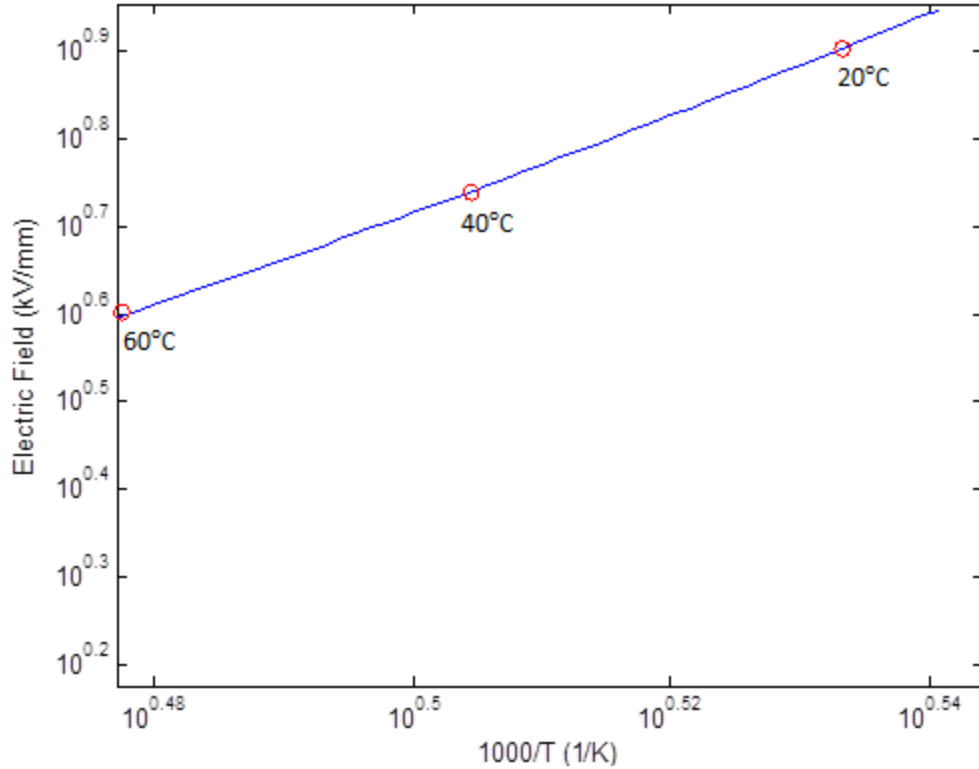


Figure 4.13 – Temperature dependence of electric threshold for cable 11543-1

$$E_{thr} = 0.0227 \exp \left[\frac{1718.1}{T} \right] \quad (4.2)$$

4.1.4 Cable 11544-3

Space charge accumulation threshold

The last cable tested under positive electric field is composed of insulation type II (cross-linked polyethylene with less than 1 wt.% carbon black) and two semicon layers of type F (copolymer blend of reduced polarity, “medium” carbon black loading). The obtained E- ρ characteristics at 20°C, 40°C and 60°C are displayed in figures 4.14, 4.15 and 4.16 respectively.

The thresholds are almost equal to the thresholds of cable 11543-1. At 20°C the threshold is 7.5kV/mm, at 40°C it is 5.5kV/mm and at 60°C the threshold is determined at 4kV/mm.

The fact that the only difference between cables 11543-1 and 11544-3 is the insulation type supports the observation that the semicon type plays a major role in the electric field threshold determination.

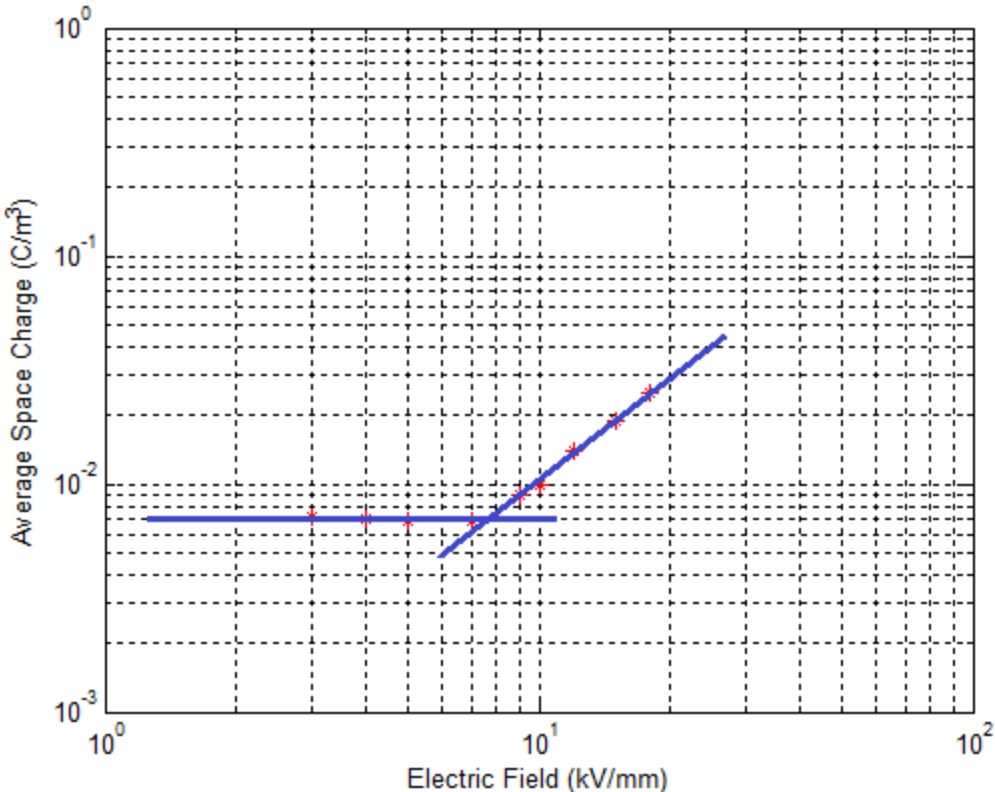


Figure 4.14 – E-ρ characteristic of cable 11544-3 @20°C

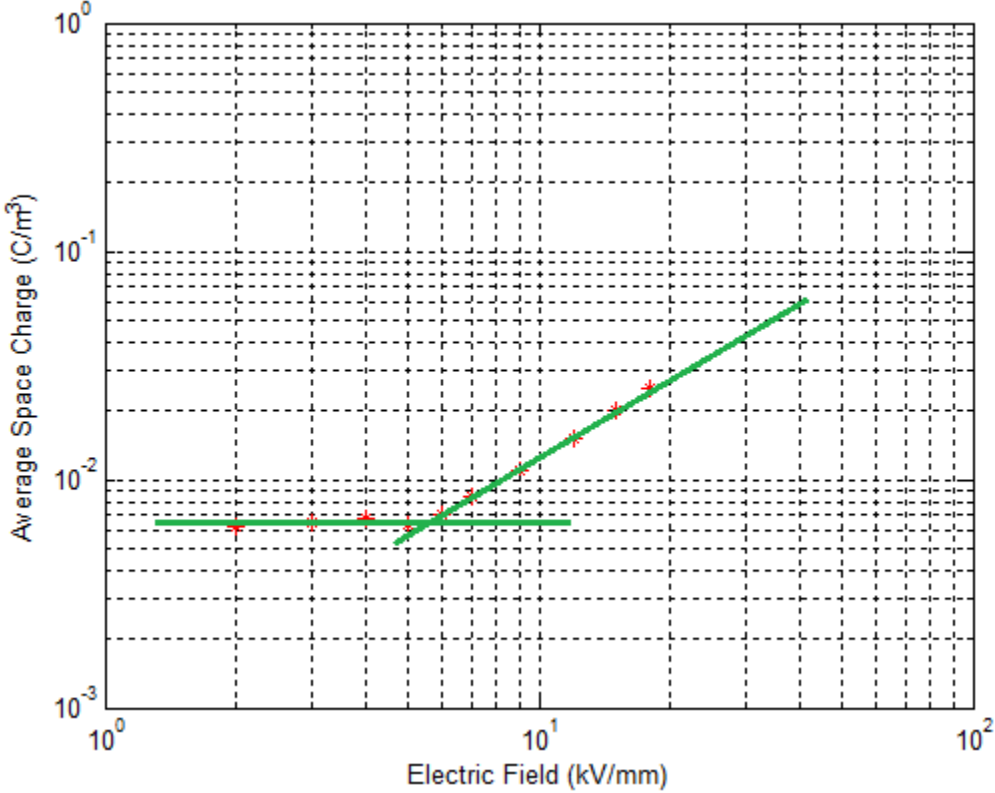


Figure 4.15 – E-ρ characteristic of cable 11544-3 @40°C

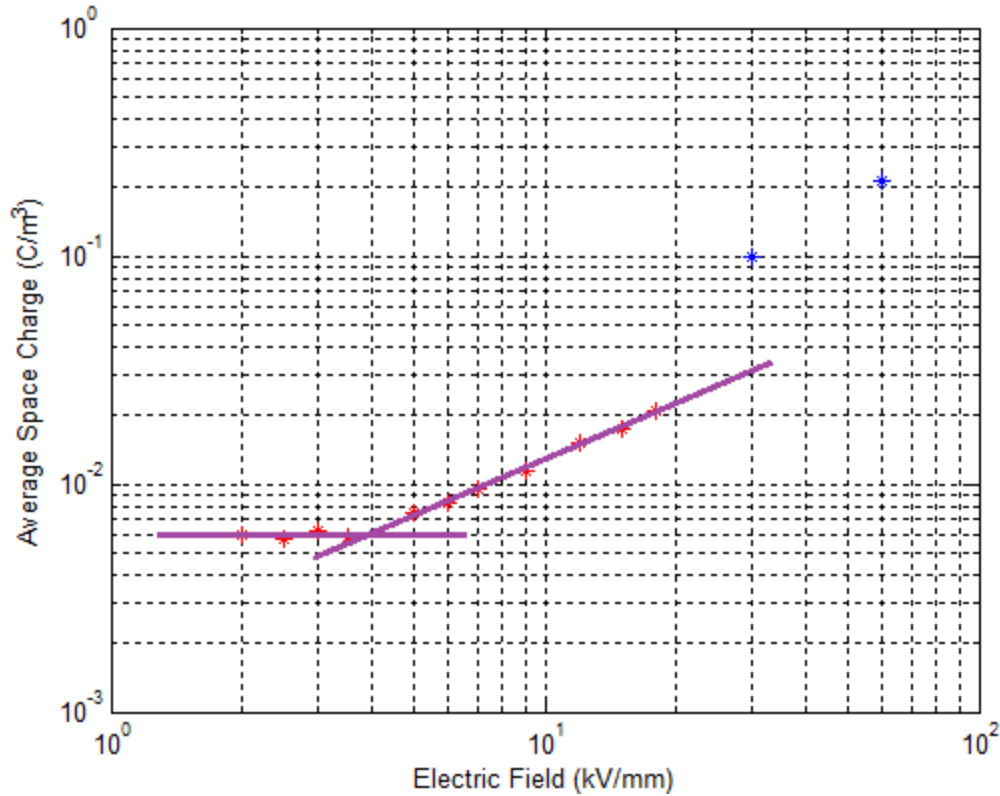


Figure 4.16 – E- ρ characteristic of cable 11544-3 @60°C

Temperature effect on the fitting line slope

The results of the fitting line slopes at different temperatures are displayed in table 4.4. The negative temperature dependence of the fitting line slope can be observed.

Table 4.4 – Fitting line slopes at different temperatures for cable 11544-3

Temperature	20°C	40°C	60°C
Slope	1.56	1.15	0.81
Angle	57.3°	48.9°	39.1°

Threshold temperature dependence

As the threshold values are nearly equal to the values of cable 11543-1, equation 4.3 can describe the threshold temperature dependence. In figure 4.17 the relevant plot is displayed.

For this cable the threshold again shows a stronger temperature dependence compared to cables 11543-2 and 11544-2.

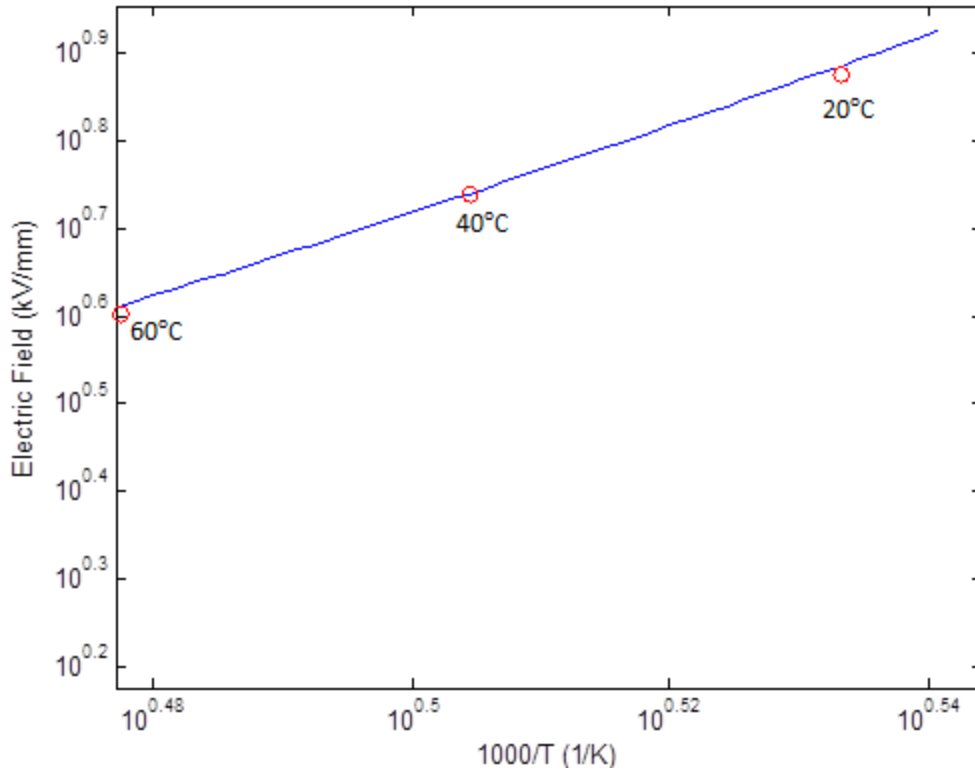


Figure 4.17 – Temperature dependence of electric threshold for cable 11544-3

$$E_{thr} = 0.041 \exp \left[\frac{1533.3}{T} \right] \quad (4.3)$$

4.1.5 Results obtained during an earlier project

The other four cables described in section 3.1.1, were tested by means of the PEA method during an earlier project [7]. The composition of these cables is summarized in table 4.5.

Table 4.5 – Composition of the cables tested in an earlier project [7]

Cable	Insulation	Semicon
11543-3	I	C
11543-4	I	D
11544-1	II	D
11544-4	II	C

The results obtained during the space charge measurements and concerning the electric field thresholds at three different temperatures are presented in table 4.6.

Table 4.6 – Thresholds [kV/mm] of the cables tested in an earlier project [7]

Cable	20°C	40°C	60°C
11543-3	7.3	6	4.5
11543-4	4	3	3
11544-1	4	3	2.3
11544-4	8	6	4.5

4.1.6 Cable comparison & discussion

The electric thresholds of all eight cables at 20°C, 40°C and 60°C are presented in figures 4.18, 4.19 and 4.20 respectively. In these figures, the latin numbers (I,II) refer to the insulation type and the letters (C,E,D,F) to the semicon type.

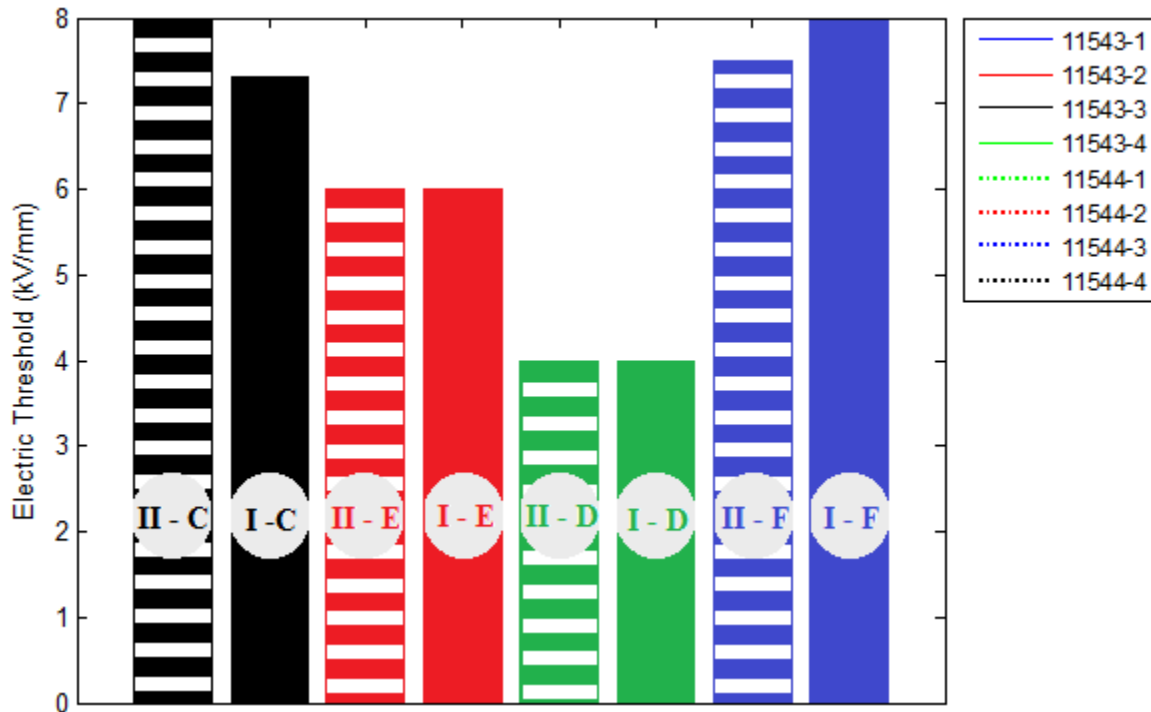


Figure 4.18 – Space charge accumulation thresholds of all the cables @20°C

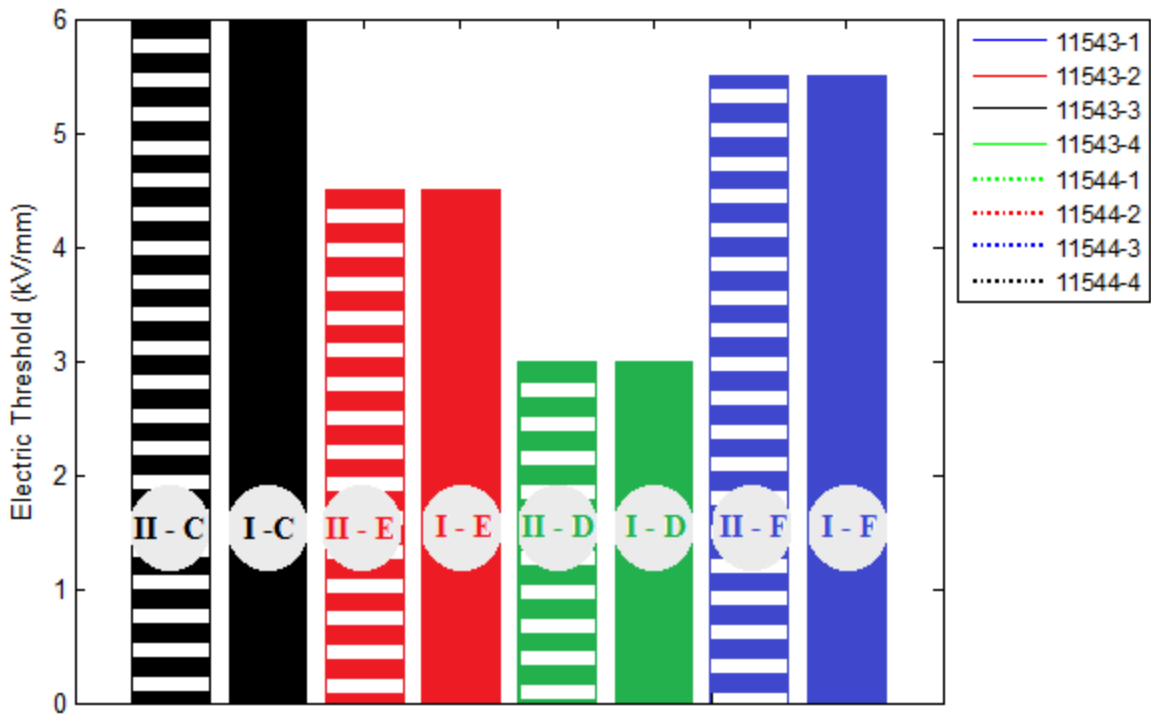


Figure 4.19 – Space charge accumulation thresholds of all the cables @40°C

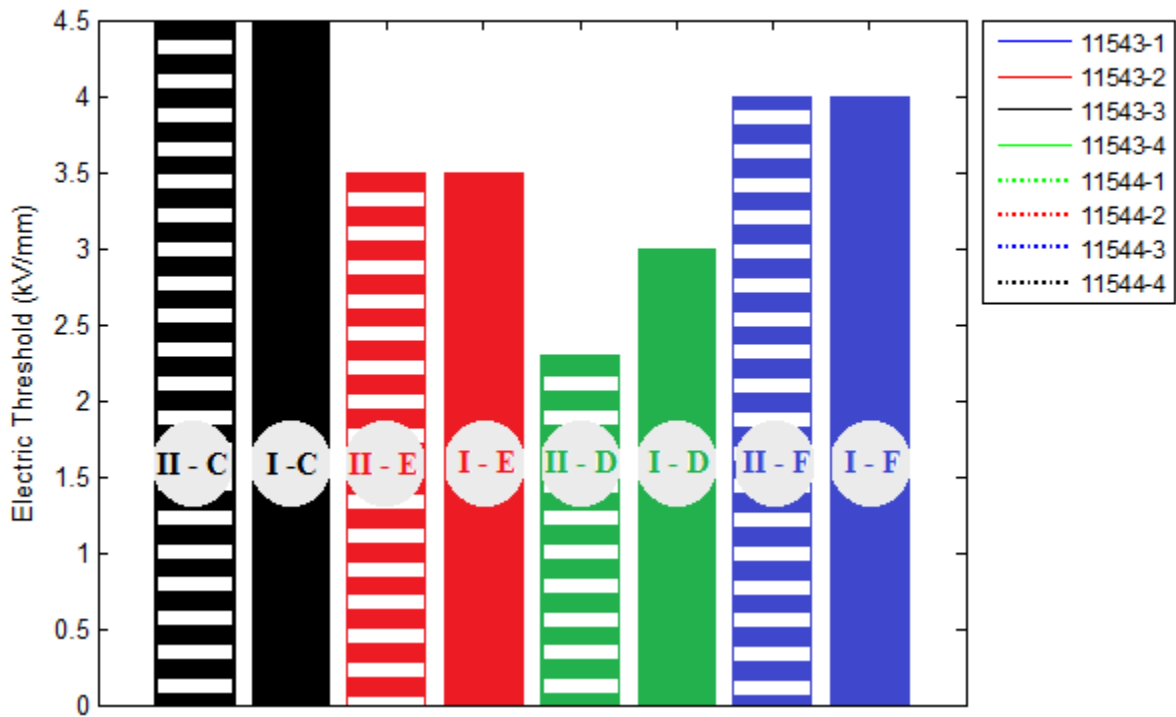


Figure 4.20 – Space charge accumulation thresholds of all the cables @60°C

From the above results, it is clear that the cables made from the same type of semicon and different insulation materials nearly result in the same electric field thresholds. This holds for all three temperatures. This observation suggests that the type of semi-conductive layer plays a significant role in determining the threshold for space charge accumulation. Therefore, it can be claimed that the injection/extraction process at the semicon-insulation interface greatly affects the value of the electric field threshold.

The only difference between the three types of semi-conductive layers C, E and D is the carbon black content. The highest threshold is observed for the cables with semicon C (ethylene copolymer with polar comonomer, “low” carbon black loading). Higher carbon content in the semicon seems to result in a lower electric field threshold for space charge accumulation.

Furthermore, conduction current measurements on semicon plaques were carried out in order for their conductivity to be estimated. The results are presented in section 5.1 and as it was expected, they revealed that higher carbon content results in higher semicon conductivity. Therefore, the threshold for space charge accumulation could also be related to the conductivity of the semicon. Higher semicon conductivity seems to result in a lower electric field threshold and vice versa.

The cables made from semicon F (‘medium’ carbon content) have a threshold close to the cables with semicon of ‘low’ carbon content (semicon C). This observation suggests that a possible decrease in the carbon content of semicon F could lead to an even higher threshold.

The slopes of the fitting lines for all the cables are presented in table 4.7.

Table 4.7 – Fitting line slopes at different temperatures for all eight cables

Cable	20°C	40°C	60°C
11543-1	1.13	1.00	0.70
11543-2	1.37	0.91	0.62
11543-3	1.28	0.52	0.33
11543-4	0.69	0.55	0.61
11544-1	0.80	0.61	0.46
11544-2	1.09	0.95	0.69
11544-3	1.56	1.15	0.81
11544-4	1.47	0.80	0.62

It is clear that the slope of the fitting lines decreases as temperature increases. This observation could be related to the injection/extraction and detrapping processes. All these processes show positive temperature dependence which is explained in detail in section 4.1.1 of this thesis.

The decrease in the fitting line slope could be attributed to the assumption that when temperature increases, the injection rate increases at slower pace than the extraction and charge detrapping rate. However, the injection rate is still higher than the extraction and detrapping rate in order for space charge accumulation to take place inside the insulation.

4.2 Space charge measurements at negative polarity

The cable 11544-4 was examined under negative polarity, thus negative voltage was applied to the conductor of the cable during the tests. The purpose for carrying out these measurements was to investigate the effect of voltage polarity on the space charge accumulation threshold.

This cable consists of insulation type II (cross-linked polyethylene with less than 1 wt.% carbon black) and two semicon layers of type C (ethylene copolymer with polar comonomer, “low” carbon black loading). The obtained E- ρ characteristics at 20°C, 40°C and 60°C are displayed in figures 4.21, 4.22 and 4.23 respectively.

The thresholds are determined at 7kV/mm, 5.5kV/mm and 4.3kV/mm at 20°C, 40 °C and 60 °C respectively. The results obtained under positive polarity for the same cable is presented in table 4.6.

As it can be observed, the results at positive and negative polarity are close to each other. The largest difference occurs at 20°C. However, taking into consideration the fact that the uncertainty in the PEA method is approximately 15% (section 3.2.2) and that the thresholds at 40°C and 60°C are almost equal for positive and negative polarity, then it can be claimed that the voltage polarity does not significantly affect the threshold value.

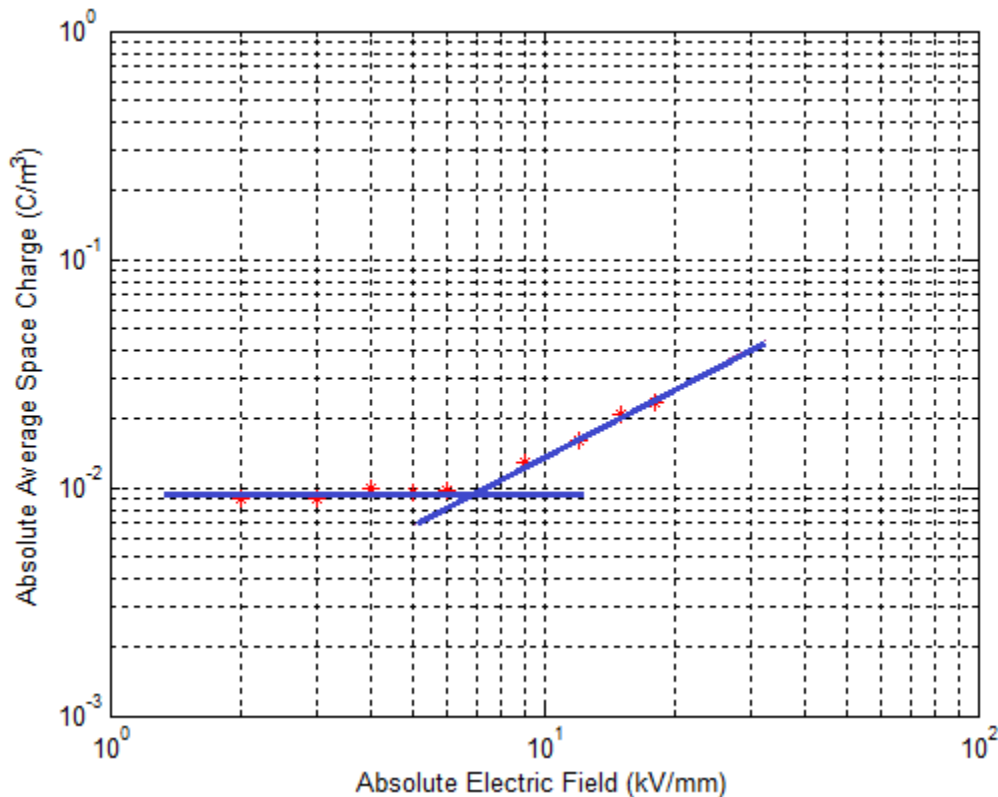


Figure 4.21 – E- ρ characteristic of cable 11544-4 @20°C

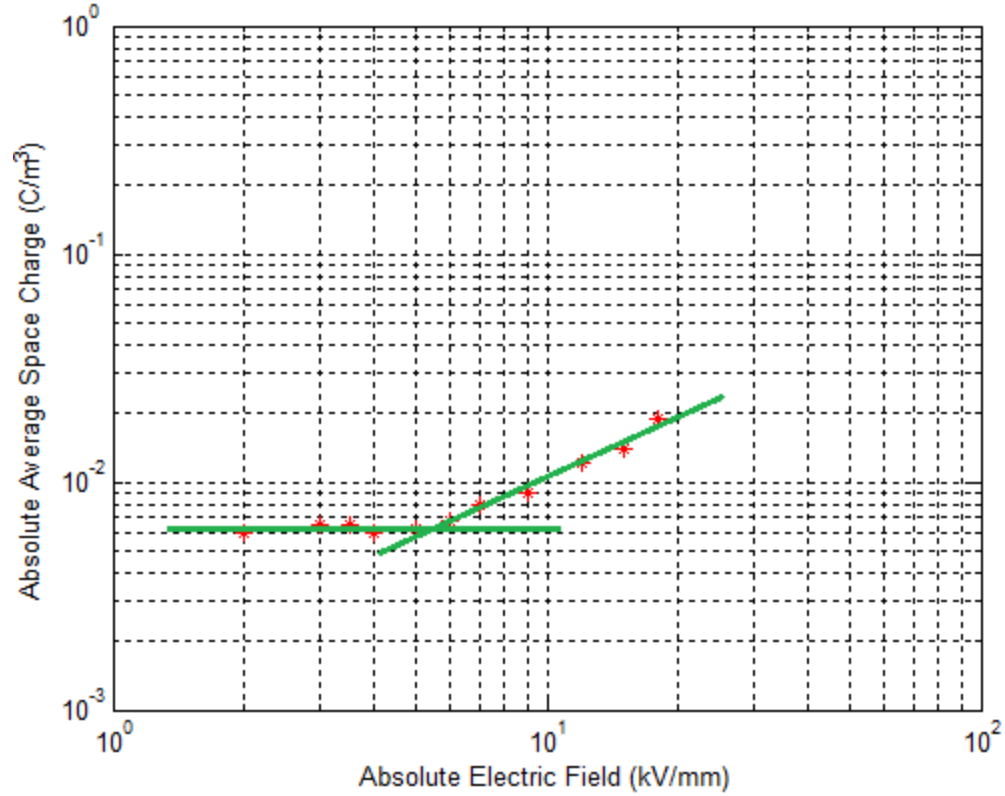


Figure 4.22 – E- ρ characteristic of cable 11544-4 @40°C

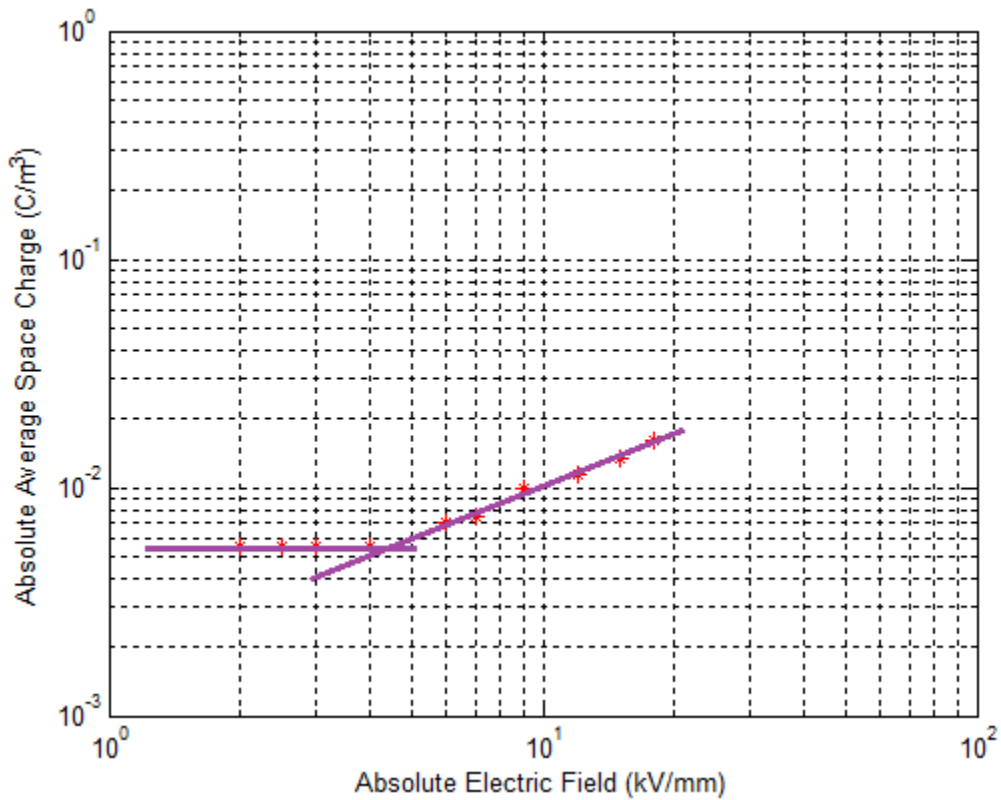


Figure 4.23 – E- ρ characteristic of cable 11544-4 @60°C

Temperature effect on the fitting line slope

The fitting line slopes at different temperatures are displayed in table 4.8. The same tendency occurs even for negative polarity and therefore the fitting line slope decreases as temperature increases. This kind of behavior is discussed in section 4.1.1.

Table 4.8 – Fitting line slopes at different temperatures for cable 11544-4

Temperature	20°C	40°C	60°C
Slope	1.04	0.80	0.71
Angle	46.1 °	38.9 °	35.6 °

Threshold temperature dependence

The thresholds under negative polarity at different temperatures can also fit into an exponential relationship. Equation 4.4 describes the threshold temperature dependence of this cable.

$$E_{thr} = 0.1233 \exp \left[\frac{1188.6}{T} \right] \quad (4.4)$$

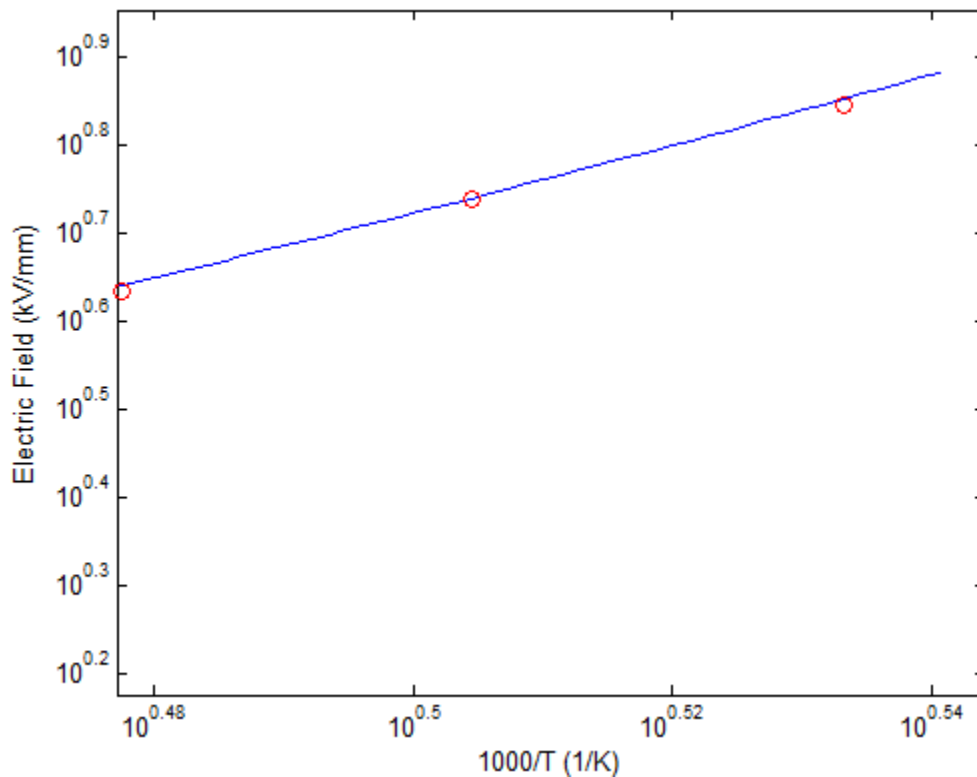


Figure 4.24 – Temperature dependence of electric threshold for cable 11544-4

4.3 Mobility and trap depth estimation

4.3.1 Apparent trap – controlled mobility

The apparent trap-controlled mobilities of all eight cables were derived via their depolarization characteristics. These characteristics obtained at 60kV/mm and at 65°C.

The poling field was chosen to be relatively high in order for a large amount of space charge to remain after the voltage turn-off. At lower poling fields (i.e. 30kV/mm) the accumulated space charge is relatively low and there is no significant decrease within three hours of depolarization. In this case far longer depolarization times are required.

The calculation of the apparent trap-controlled mobility is based as explained in section 2.7, on the use of equation 2.23 and the results of all eight cables under examination are shown in figure 4.25. The results are also summarized in table 4.9.

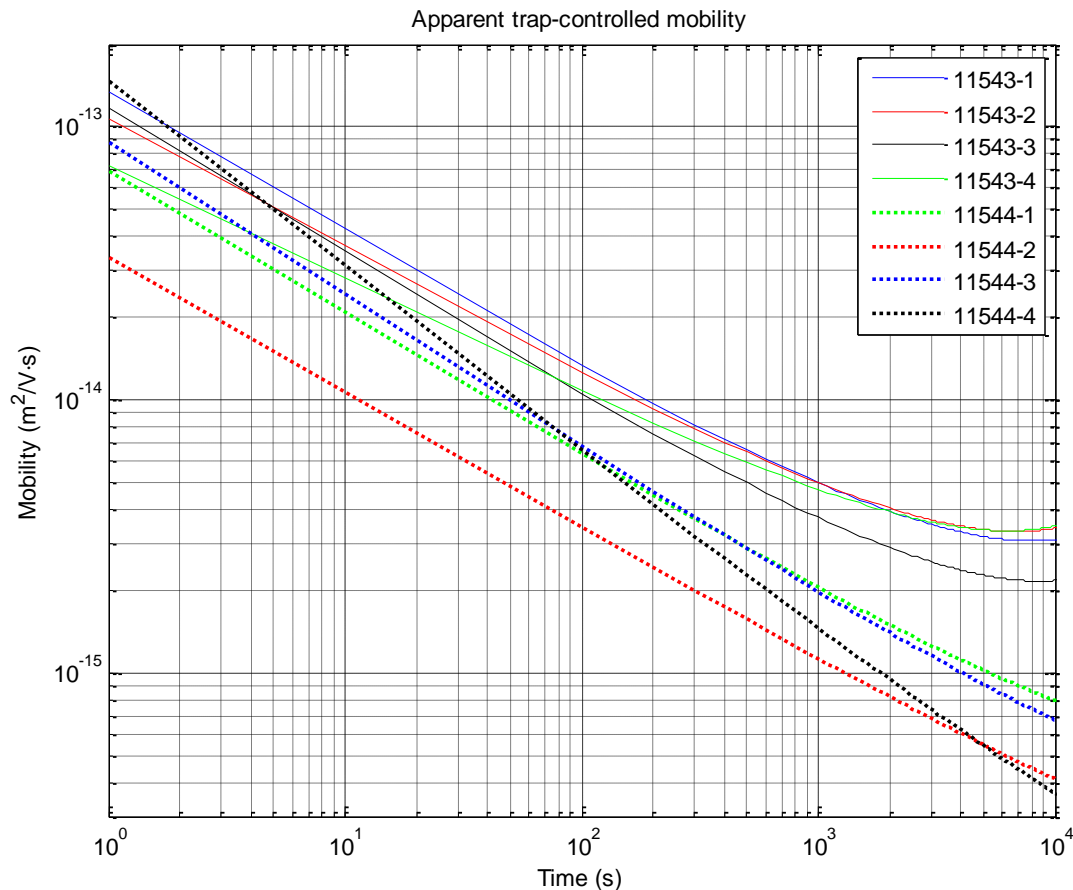


Figure 4.25 – Apparent trap-controlled mobility of all eight cables @65°C

The apparent trap-controlled mobility decreases for all the cables as depolarization time increases. Mobility characteristics vary with time since they are related to progressive emptying of deeper and deeper traps as depolarization elapses. In order to make the comparison of the cables easier, the results of table 4.9 are also presented in figure 4.26.

Table 4.9 - Apparent trap-controlled mobilities after 17 minutes and 3 hours of depolarization

Cable	Apparent trap controlled mobility @65°C after 17 min [$\text{m}^2/\text{V}\cdot\text{s}$]	Apparent trap controlled mobility @65°C after 3 hours [$\text{m}^2/\text{V}\cdot\text{s}$]
11543-1	$4.99 \cdot 10^{-15}$	$3.09 \cdot 10^{-15}$
11543-2	$4.99 \cdot 10^{-15}$	$3.39 \cdot 10^{-15}$
11543-3	$3.72 \cdot 10^{-15}$	$2.19 \cdot 10^{-15}$
11543-4	$4.71 \cdot 10^{-15}$	$3.51 \cdot 10^{-15}$
11544-1	$2.06 \cdot 10^{-15}$	$7.79 \cdot 10^{-16}$
11544-2	$1.13 \cdot 10^{-15}$	$4.06 \cdot 10^{-16}$
11544-3	$1.99 \cdot 10^{-15}$	$6.81 \cdot 10^{-16}$
11544-4	$1.47 \cdot 10^{-15}$	$3.51 \cdot 10^{-16}$

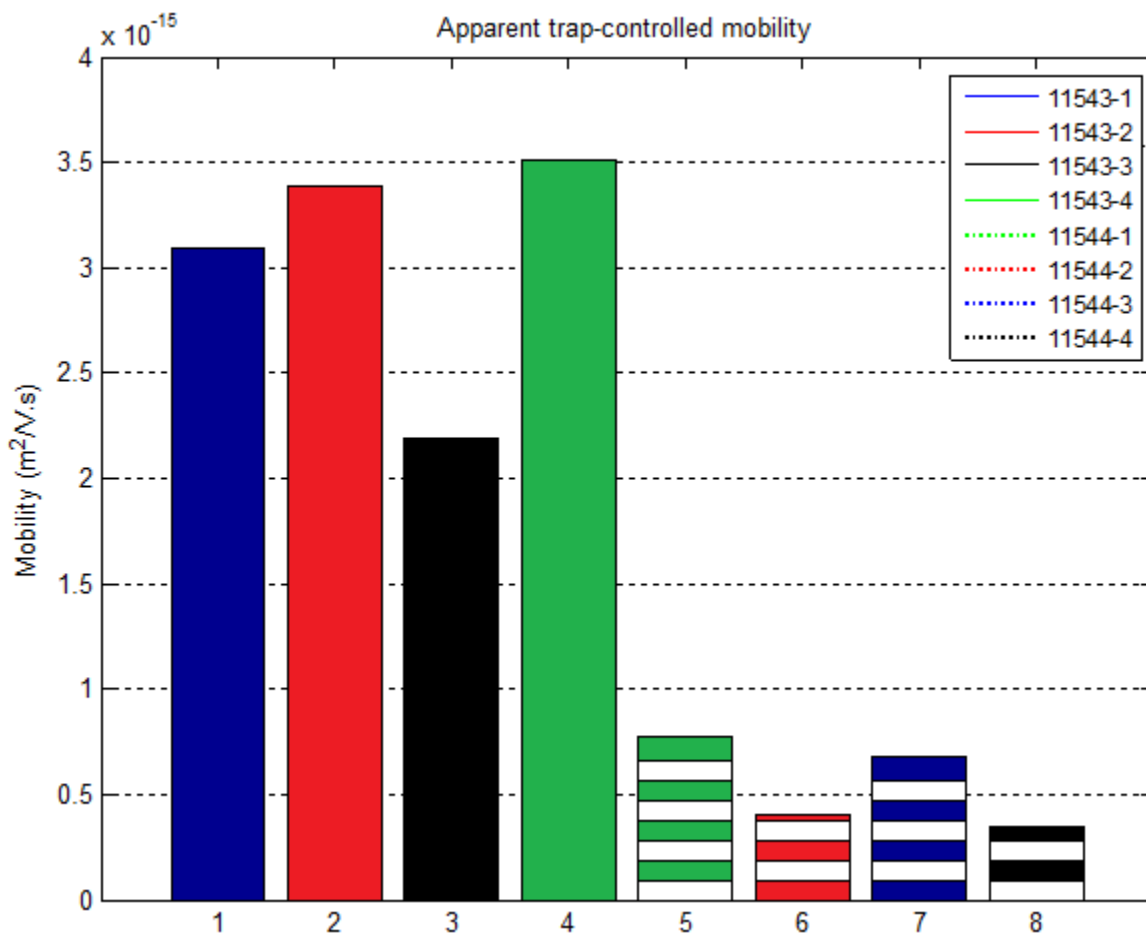


Figure 4.26 – Apparent trap-controlled mobility after 3 hours of depolarization @65°C

From the above results, it is observed that the apparent trap-controlled mobilities of the cables with the same insulation material but with different semi-conductive layers are close to each other. They are of the same order of magnitude, 10^{-15} and 10^{-16} for insulation type I and II respectively. Insulation type I has a faster depletion rate of trapped charge than insulation type II.

The type of insulation seems to play a major role in the determination of the apparent trap-controlled mobility. On the contrary, there is little influence of the semicon type on the apparent trap-controlled mobility. It seems that the apparent trap-controlled mobility is significantly affected by the detrapping process in the insulation rather than the extraction process at the semicon-insulation interfaces.

4.3.2 Trap depth

The apparent trap depths were determined from the same depolarization characteristics used for the determination of the apparent trap-controlled mobilities of the cables. The model used to determine the apparent trap depths is described in section 2.7. Five trap levels were assumed. Therefore, the depolarization characteristic of each cable was divided into five segments. In each segment, the data were fitted into an exponential law and the coefficients a_i and b_i were determined. Finally, the trap depth values were derived from equation 2.27. The increase in number of trap levels does not affect the maximum trap depth values. The apparent trap depths of all eight cables are shown in figure 4.27.

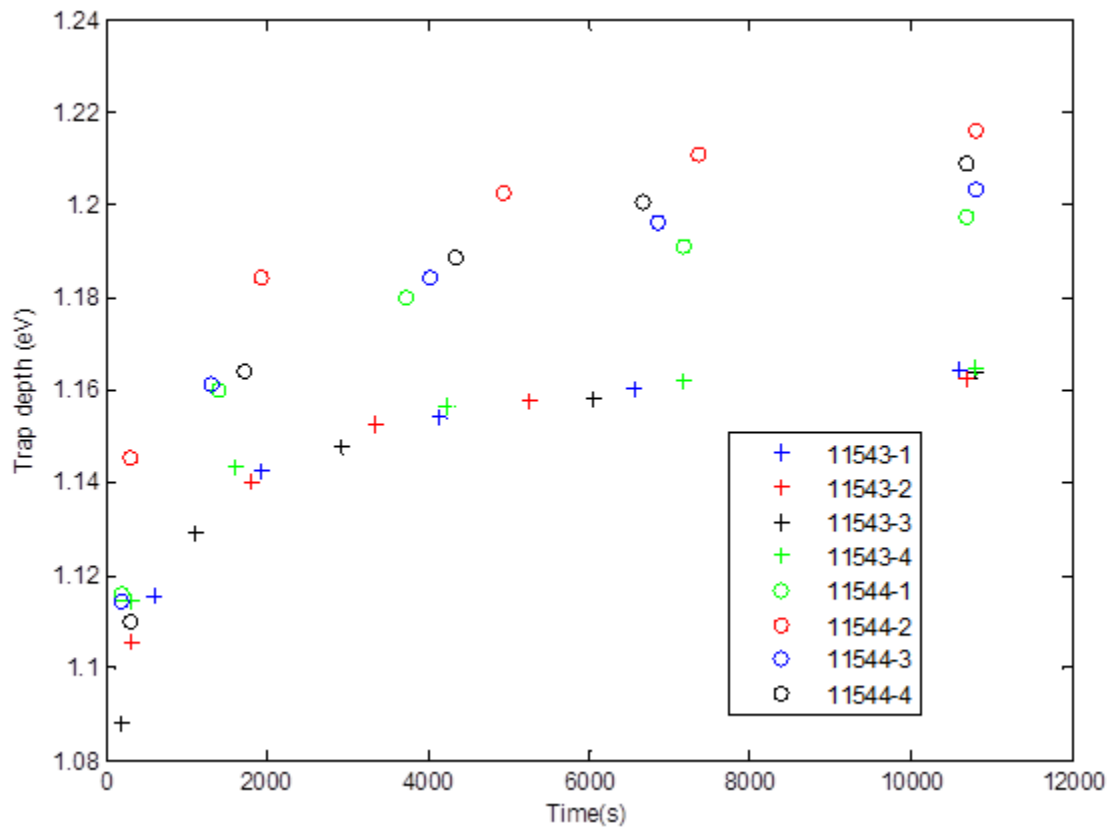


Figure 4.27 – Apparent trap depths of all the cables within 3 hours of depolarization

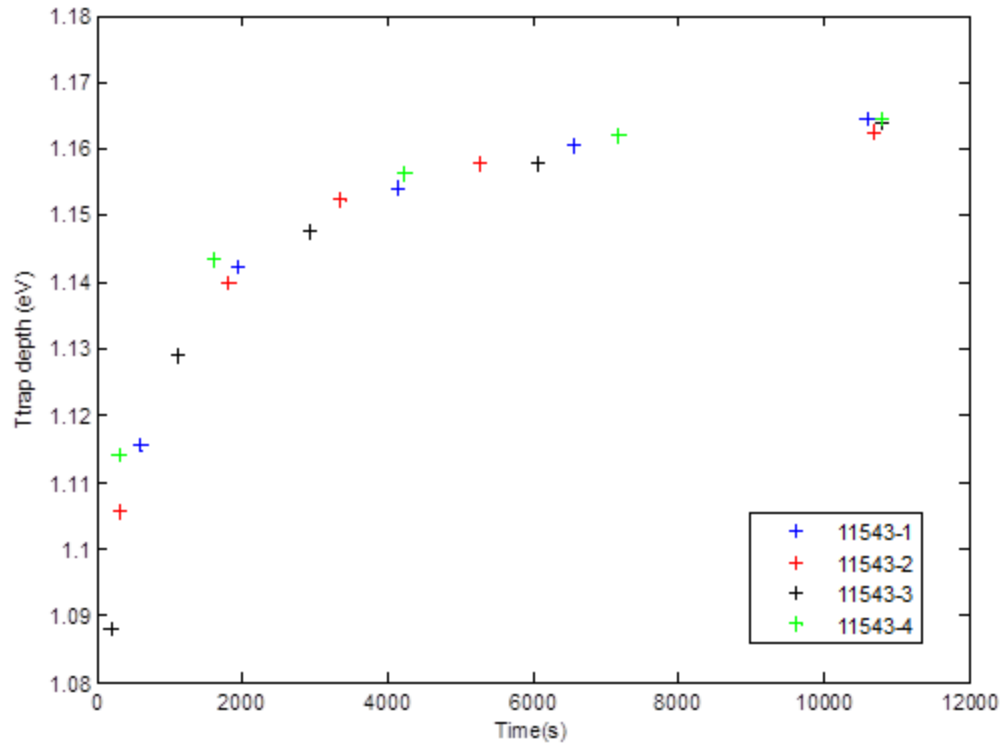


Figure 4.28 – Apparent trap depths of the cables with insulation type I

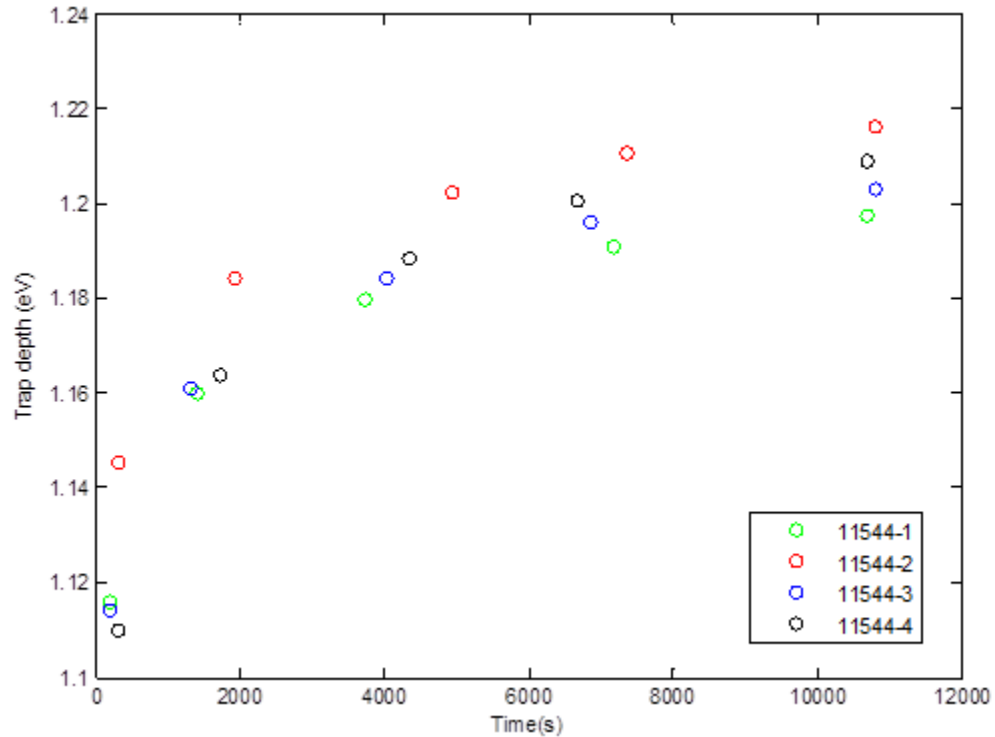


Figure 4.29 – Apparent trap depths of the cables with insulation type II

The trap depth values after 3 hours of depolarization are also shown in table 4.10 and in figure 4.30.

Table 4.10 – Apparent trap depths after 3 hours of depolarization

Cable	Trap depth (eV)
11543-1	1.16
11543-2	1.16
11543-3	1.16
11543-4	1.16
11544-1	1.20
11544-2	1.21
11544-3	1.20
11544-4	1.21

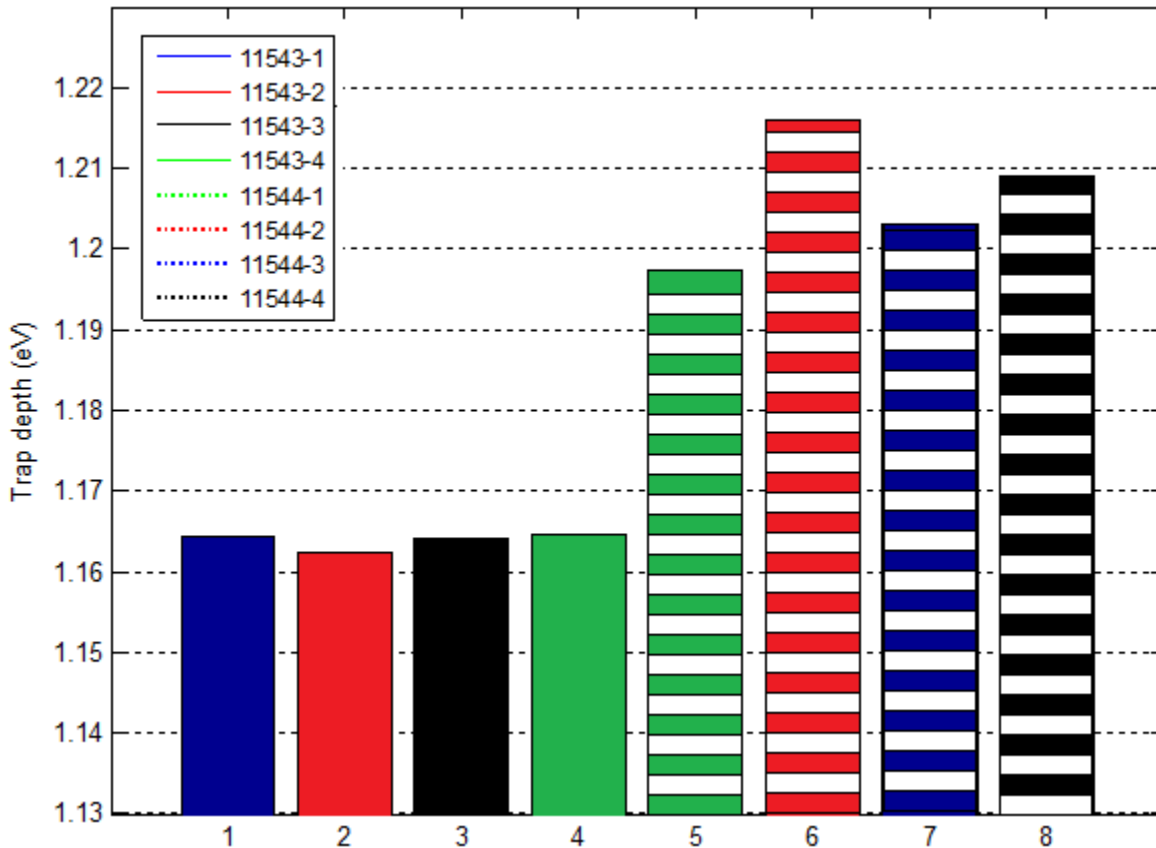


Figure 4.30 – Apparent trap depths of the cables after 3 hours of depolarization

As in the case of apparent trap-controlled mobility, the trap depths are mainly affected by the insulation type rather than the semicon type. The cables made from the same type of insulation have nearly equal trap depths. In insulation type II deeper traps are present than in insulation type I.

The addition of “styrenic” charge trapping agent seems to lead to the creation of shallower traps than carbon black. Insulation type I exhibits a better performance with regard to trap depths. Deeper trap depths result in longer trapping time periods. The distribution of the trapped charge along the trap levels is presented in table 4.11.

Table 4.11 – Space charge distribution along the trap levels

Trap level	Cable : 11543-1	Cable : 11544-3
	Space charge density (C/m ³)	Space charge density (C/m ³)
1	0.0379	0.0147
2	0.0160	0.0072
3	0.0107	0.0054
4	0.0085	0.0046
5	0.4273	0.4757

Trap level	Cable : 11543-2	Cable : 11544-2
	Space charge density (C/m ³)	Space charge density (C/m ³)
1	0.0323	0.008
2	0.0140	0.0041
3	0.0094	0.0032
4	0.0069	0.0030
5	0.4097	0.5097

Trap level	Cable : 11543-3	Cable : 11544-4
	Space charge density (C/m ³)	Space charge density (C/m ³)
1	0.0463	0.0224
2	0.0189	0.0087
3	0.0127	0.0062
4	0.0100	0.0056
5	0.4618	0.5356

Trap level	Cable : 11543-4	Cable : 11544-1
	Space charge density (C/m ³)	Space charge density (C/m ³)
1	0.0226	0.0160
2	0.0099	0.0077
3	0.0069	0.0059
4	0.0050	0.0054
5	0.3861	0.5001

In insulation type I more space charge is trapped at the highest trap levels than in insulation type II. Most of the time, larger amount of space charge is trapped at levels 1 to 4 for insulation type I. On the contrary, in insulation type II more space charge is trapped at the lowest trap level (level 5). This observation coincides with the fact that insulation type I has a higher depletion rate (mobility) than insulation type II as more space charge is trapped at shallower traps where less energy and time are required in order for these charges to be liberated from there.

5. Experimental Results of Conduction Current Measurements

In this chapter the results of the conduction current measurements are presented. Section 5.1 contains the results related to the measurements on semi-conductive plaques. In section 5.2, the results concerning the measurements on three cables are included.

5.1 Conduction current measurements on semicon plaques

Four different types of semi-conductive layers are used in the construction of the cables under examination. Conduction current measurements were performed on semicon plaques in order for their conductivity to be determined. The composition of the different semi-conductive layers is described in table 5.1. The measurements were carried out at 1kV and at room temperature. The results are listed in table 5.2.

Table 5.1 – Composition of semi-conductive plaques

Semicon	Composition
C	Ethylene copolymer with polar comonomer, ‘low’ carbon black loading
D	Ethylene copolymer with polar comonomer, ‘high’ carbon black loading
E	Ethylene copolymer with polar comonomer, ‘medium’ carbon black loading
F	Copolymer blend of reduced polarity, ‘medium’ carbon black loading

Table 5.2 – Conductivity of semi-conductive plaques

Semicon	Thickness [mm]	Applied electric field [kV/mm]	Steady-state current [μ A]	Conductivity [S/m]
C	0.63	1.59	1.52	3.10E-9
D	0.7	1.43	1.52	3.43E-9
E	0.7	1.43	1.48	3.34E-9
F	0.675	1.48	1.50	3.27E-9

As it was expected, the concentration of carbon black determines the semicon conductivity. Higher carbon black concentration results in higher conductivity and vice versa.

5.2 Conduction current measurements on cables

Conduction current measurements were carried out on three mini-cables. The purpose of these measurements was to evaluate their electric field thresholds with the use of a different technique. In this way, the results of the space charge measurements described in chapter 4 can be verified.

The electric field thresholds of the cables were evaluated via the voltage - conduction current (V-I) characteristics, as it is explained in section 2.2. A number of measurements at different voltage levels and at three different temperatures (20°C, 40°C and 60°C) was performed in order to obtain these characteristics.

5.2.1 Cable 11544-4

Space charge accumulation threshold

This cable is composed of insulation type II (cross-linked polyethylene with less than 1 wt.% carbon black) and two semicon layers of type C (ethylene copolymer with polar comonomer, “low” carbon black loading). The obtained V-I characteristics at 20°C, 40°C and 60°C are displayed in figures 5.1, 5.2 and 5.3 respectively.

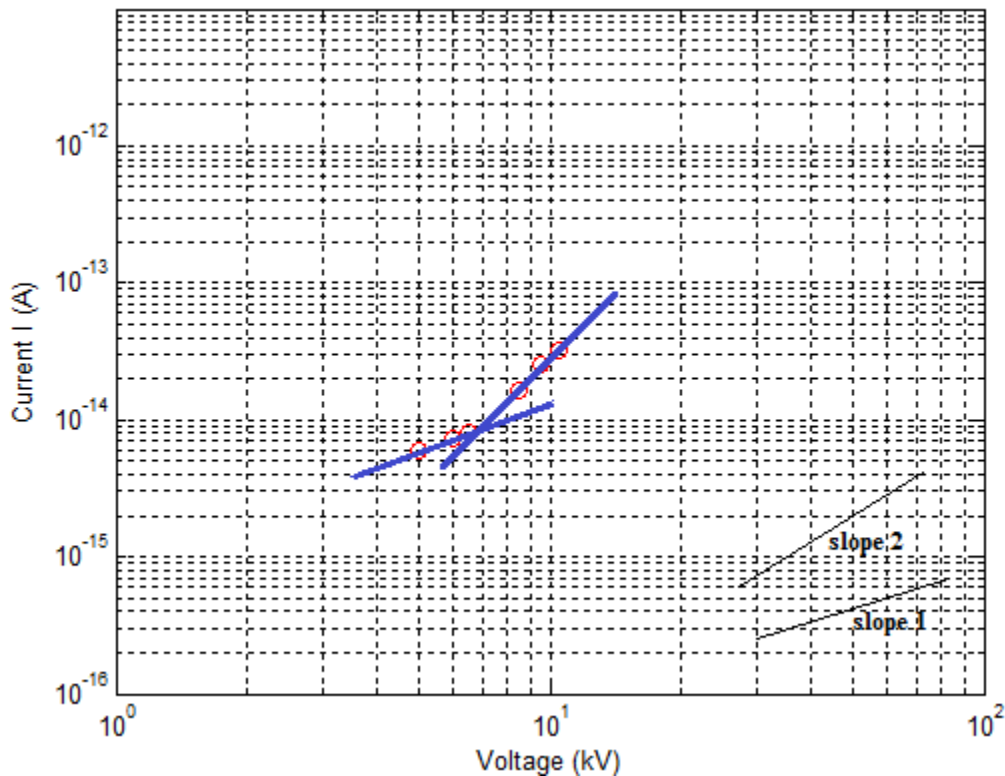


Figure 5.1 – V-I characteristic of cable 11544-4 @20°C

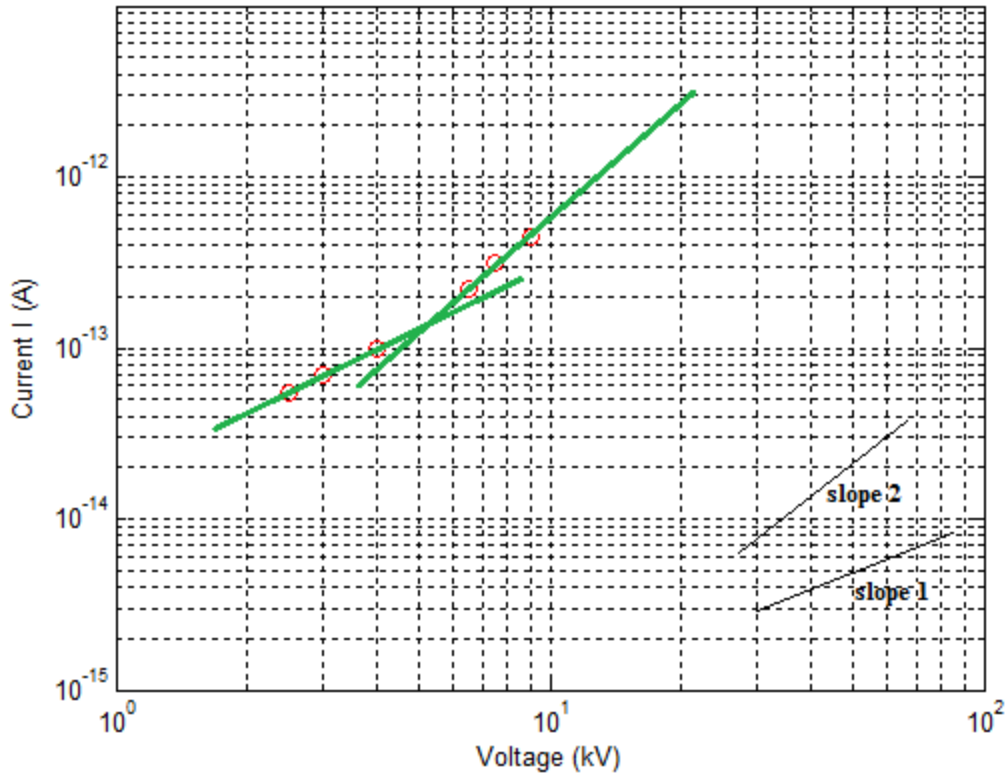


Figure 5.2 – V-I characteristic of cable 11544-4 @40°C

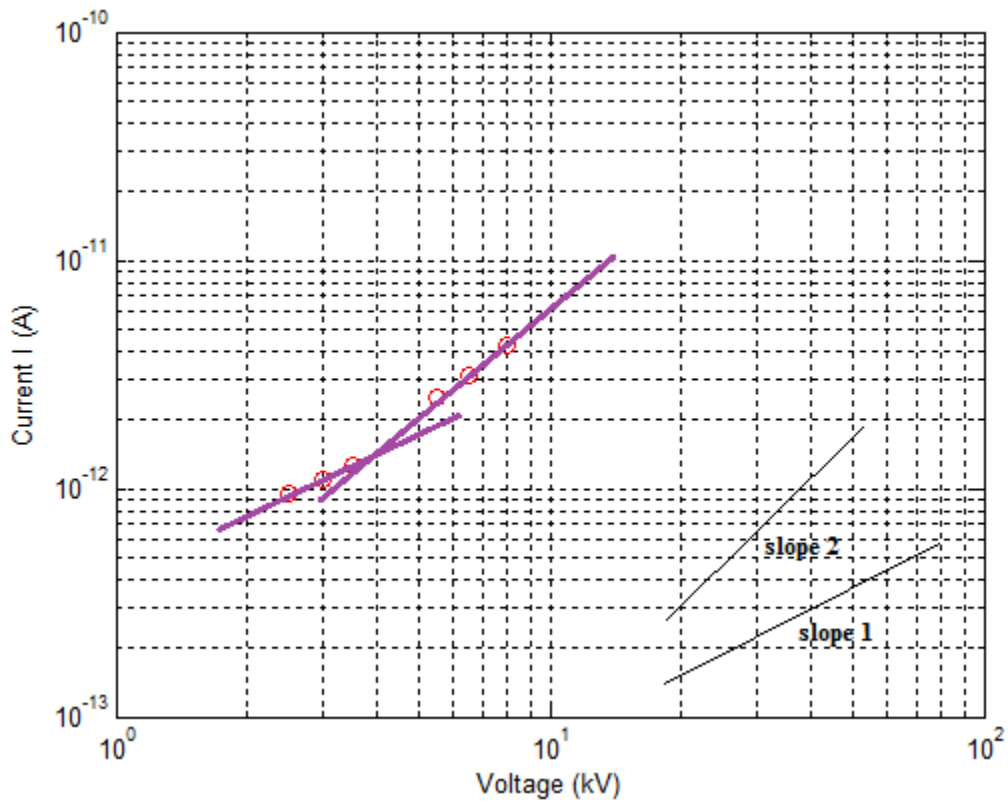


Figure 5.3 – V-I characteristic of cable 11544-4 @60°C

The point at which the slope of the V-I characteristic changes, determines the electric field above which a non-Ohmic behavior occurs. This point coincides with the establishment of steady-trapped charges in the insulation and therefore, with the threshold for space charge accumulation. A power law describes the conduction mechanism above threshold (section 2.2). At 20°C the electric field threshold is found to be at 7kV/mm. At 40°C and 60°C, the thresholds for space charge accumulation are determined at 5.3kV/mm and 4kV/mm respectively. The electric field – conductivity σ characteristics for this cable are presented in figure 5.4.

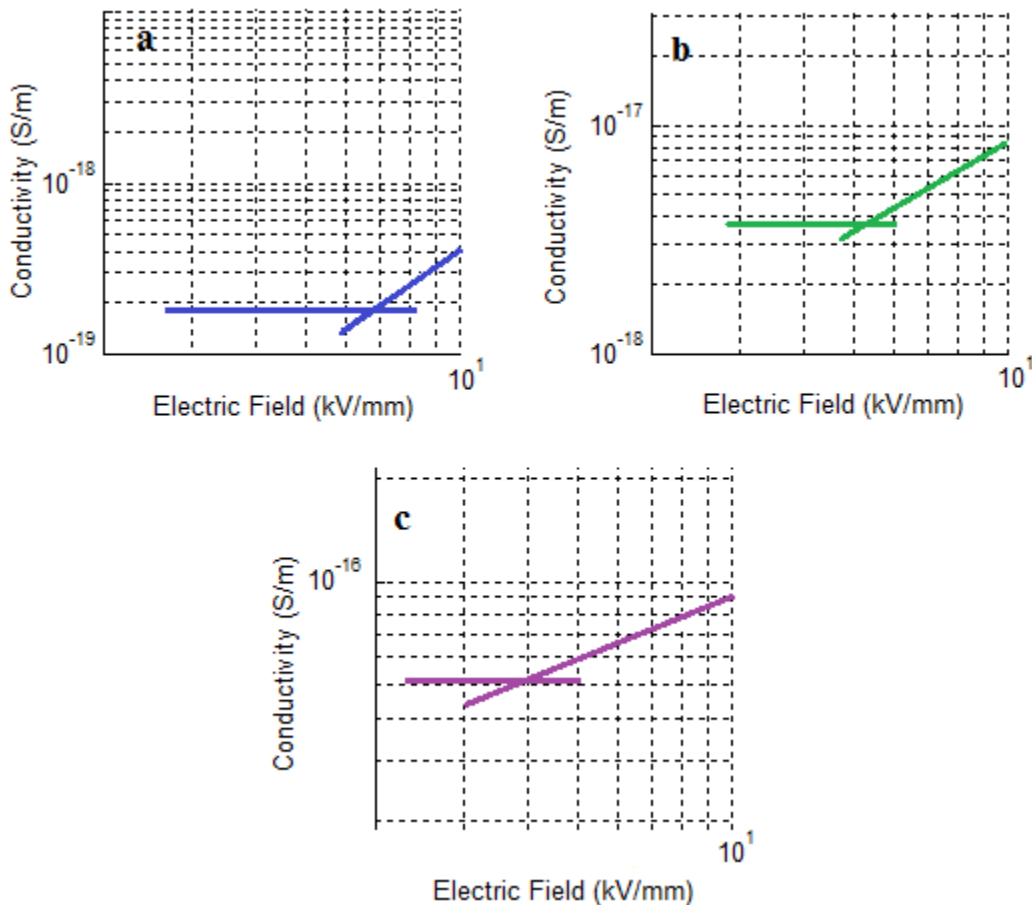


Figure 5.4 – E- σ characteristics of cable 11544-4, a: @20°C, b:@40°C, c: 60°C

As it was expected, the conductivity increases with the temperature increase (section 2.4). The conductivity at a given electric field above threshold and within the range 20°C to 60°C, fits well into an Arrhenius-type relationship which is described by equation 5.1. The relevant plot is given in figure 5.5.

$$\sigma(T) = 110 \exp \left[-\frac{1.196}{kT} \right] \quad (5.1)$$

Where k is the Boltzmann constant and it equals 8.617×10^{-5} eV/K.

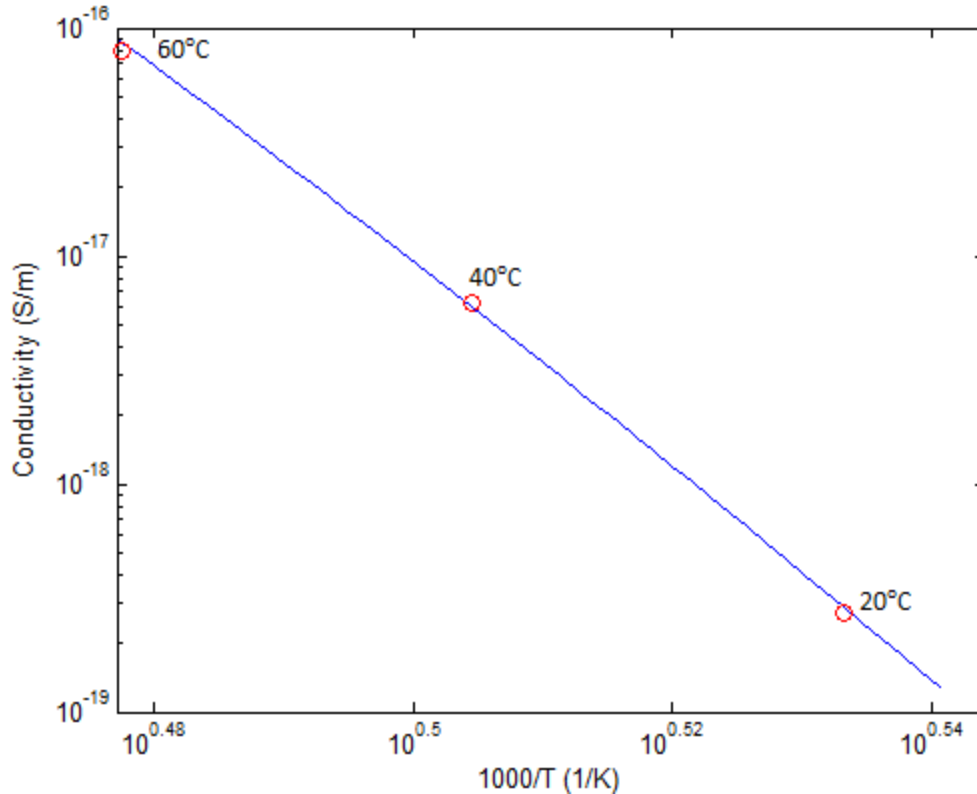


Figure 5.5 – Cable 11544-4, conductivity vs. reciprocal absolute temperature @ 8kV/mm

The trap-limited mobility is believed to be the reason for the Arrhenius-type dependence of the conductivity on temperature [31]. Not all the charge carriers contribute to the conduction due to the presence of trap states within the band gap of the insulation. However, the number of effective charge carriers, which is proportional to the mobility and then to the conductivity, is a function of temperature and an Arrhenius-type model describes the physical phenomenon.

The conductivity increase is a thermally-activated process and for this cable the corresponding activation energy approximately equals 1.20eV.

Electric field threshold comparison

In table 5.3 the results of the space charge and the conduction current measurements on cable 11544-4 are presented.

Table 5.3 – Electric field thresholds of cable 11544-4

	Threshold @20°C [kV/mm]	Threshold @40°C [kV/mm]	Threshold @60°C [kV/mm]
PEA	8	6	4.5
CCM	7	5.3	4

As it can be observed, the space charge measurements by means of the PEA method and the conduction current measurements result almost in the same thresholds. The slight difference between the results can be attributed either to the uncertainty of each measuring technique or/and to their different sensitivity. Also, the physics behind each measuring technique contributes to this slight difference [17].

The accuracy of each measuring technique is discussed in detail in section 3.2.2 for the space charge measurements and in section 3.4 for the conduction current measurements.

However, it can be observed that the thresholds estimated by the conduction current measurements are consistently lower than the values determined by the space charge measurements. This kind of behavior could be attributed to the higher sensitivity of the conduction current measurements. As soon as a small amount of space charge appears in the insulation, an Ohmic behavior cannot hold anymore. Space charge and Ohmic behavior are mutually incompatible. On the other hand, a small amount of accumulated space charge is not always detectable with the use of the PEA method.

5.2.2 Cable 11543-3

Space charge accumulation threshold

This cable is composed of insulation type I (cross-linked polyethylene with less than 0.5 wt.% “styrenic” charge trapping agent) and two semi-conductive layers of type C (ethylene copolymer with polar comonomer, “low” carbon black loading). The obtained V-I characteristics at 20°C, 40°C and 60°C are displayed in figures 5.6, 5.7 and 5.8 respectively.

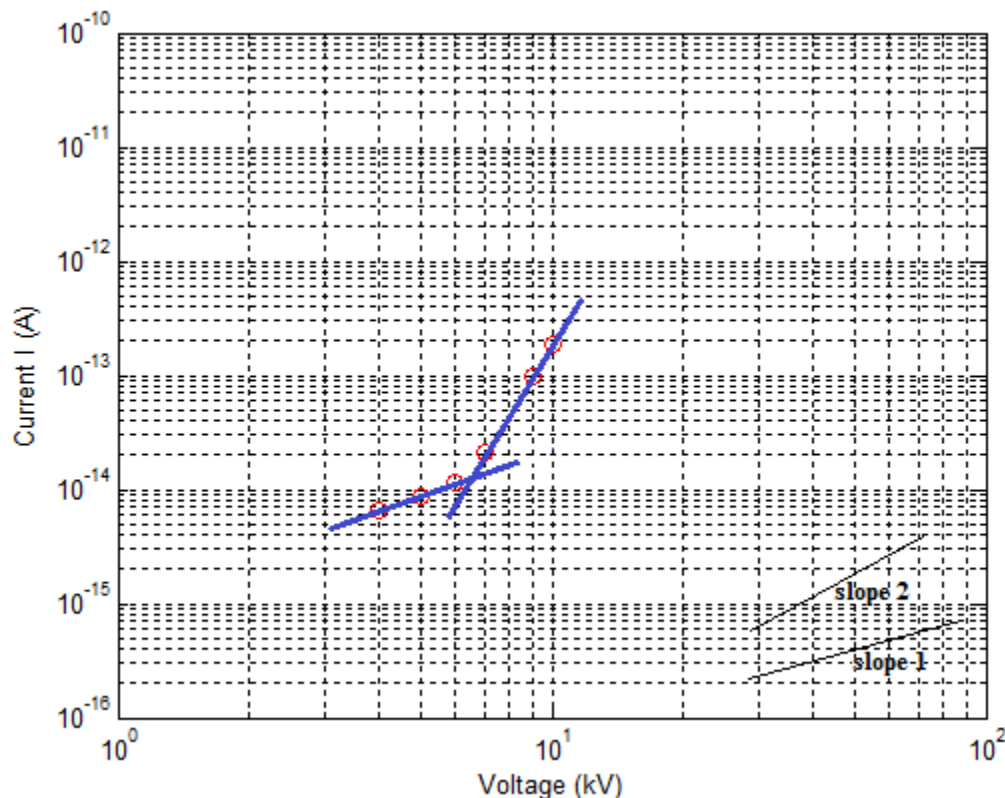


Figure 5.6 – V-I characteristic of cable 11543-3 @20°C

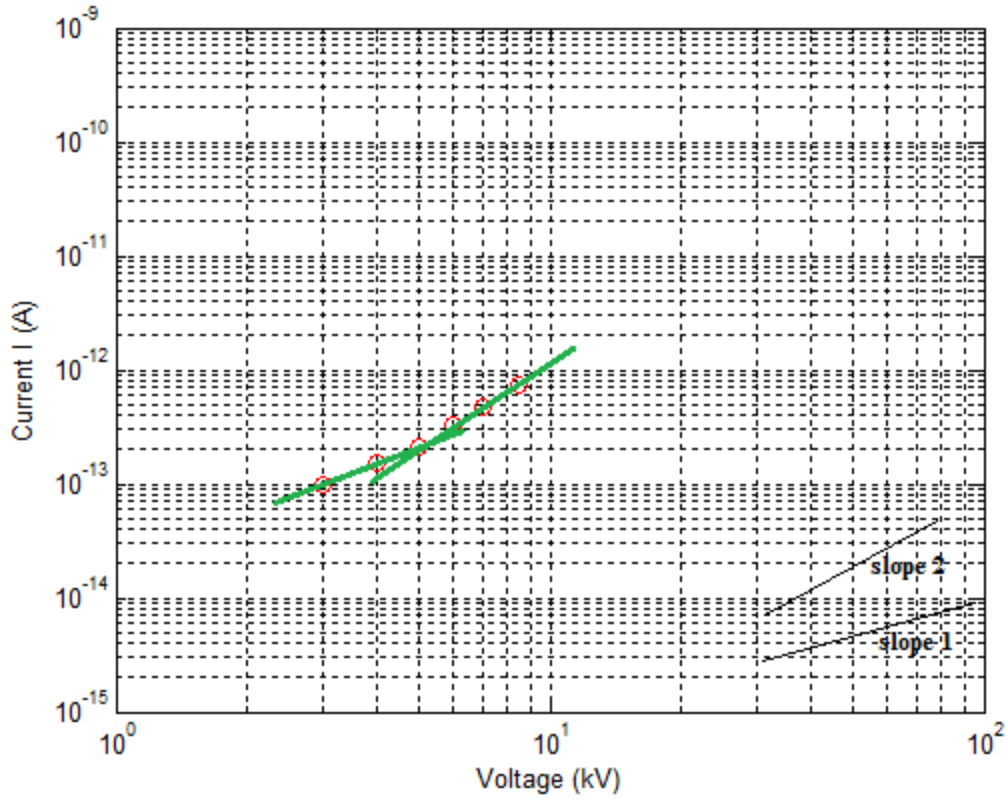


Figure 5.7 – V-I characteristic of cable 11543-3 @40°C

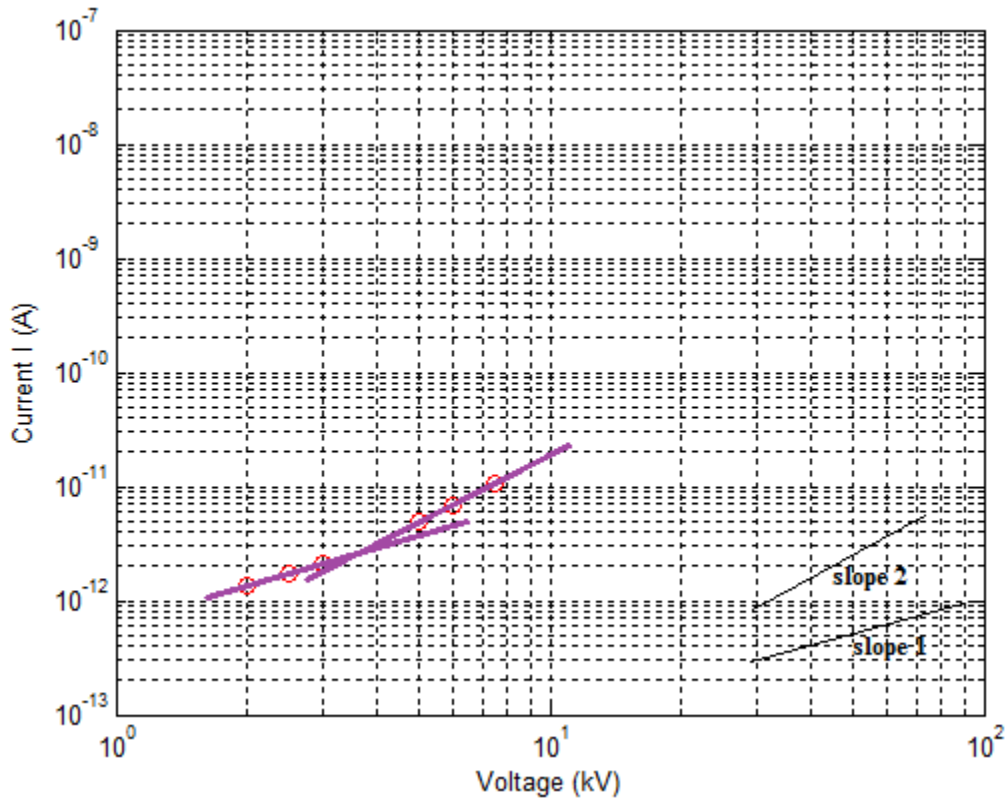


Figure 5.8 – V-I characteristic of cable 11543-3 @60°C

The electric field threshold at 20°C is estimated at 6.5kV/mm. At 40°C and 60°C the thresholds for space charge accumulation are determined at 5.3kV/mm and 3.8kV/mm respectively.

It can be observed that the thresholds for cable 11543-3 are close to the values of cable 11544-4. The only difference between the two cables is the insulation type as they have the same type of semi-conductive layers. This observation supports the results of the space charge measurements.

During the space charge measurements by means of the PEA method, it was suggested that the threshold is determined to a high extent by the semi-conductive layers rather than the insulation type (section 4.1.2). This suggestion is now verified by the conduction current measurements as well.

The electric field vs. the conductivity σ of cable 11543-3 at different temperatures are presented in figure 5.9.

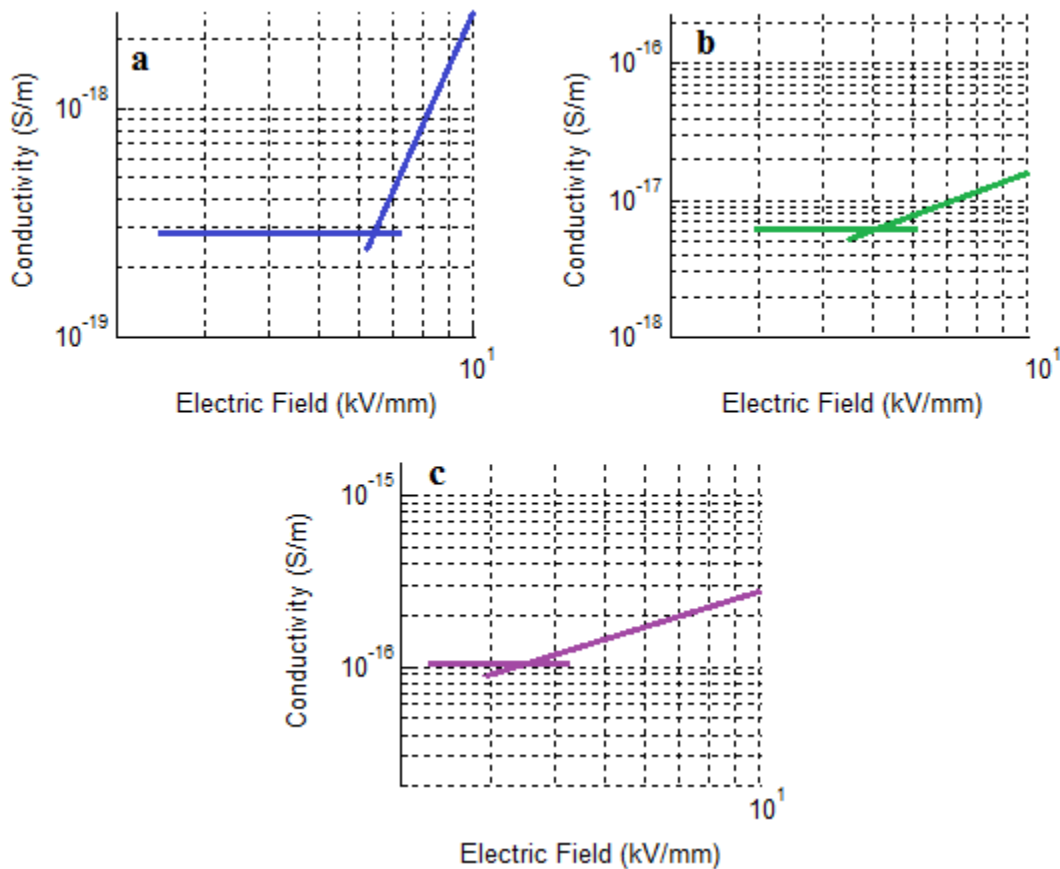


Figure 5.9 – E- σ characteristics of cable 11543-3, a: @20°C, b:@40°C, c: 60°C

The conductivities of this cable at different temperatures show again an Arrhenius-type dependence. Equation 5.2 describes the temperature dependence of the conductivity. The relevant plot is displayed in figure 5.10.

$$\sigma(T) = 146 \exp \left[-\frac{1.181}{kT} \right] \quad (5.2)$$

Where k is the Boltzmann constant and it is equal to 8.617×10^{-5} eV/K.

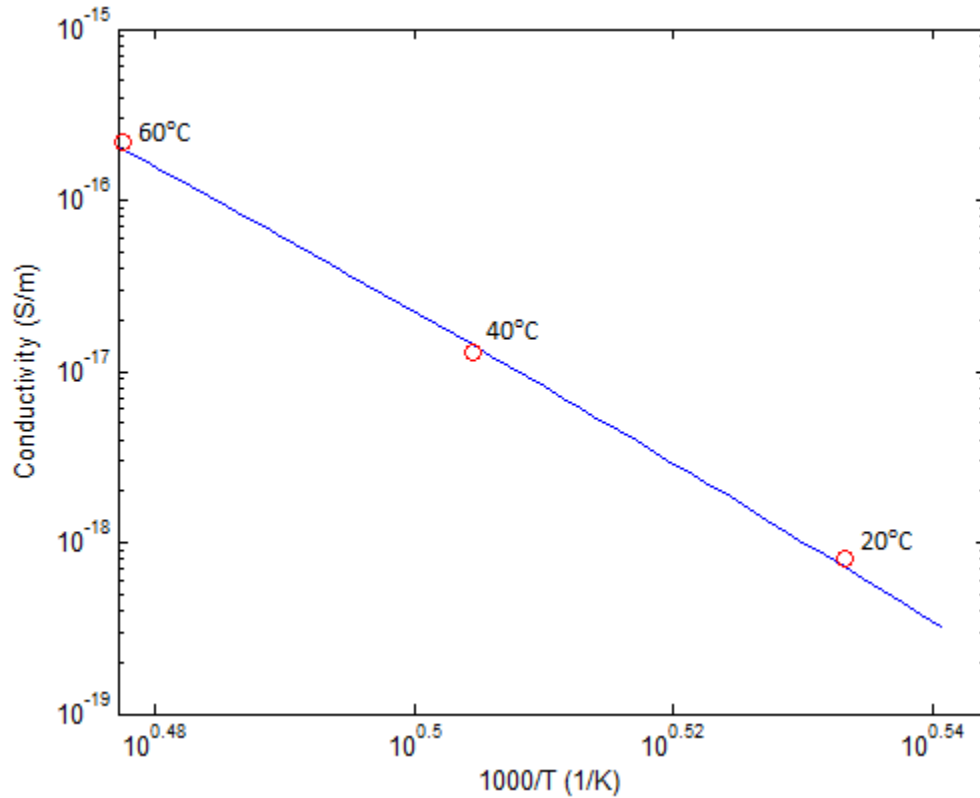


Figure 5.10 – Cable 11543-3, conductivity vs. reciprocal absolute temperature @ 8kV/mm

The reason for which the conductivity follows an Arrhenius-type dependence is discussed in section 5.2.1. The trap-limited mobility is believed to cause this kind of temperature dependence of conductivity. The corresponding activation energy for this cable is 1.18eV.

Electric field threshold comparison

Table 5.4 contains the results of the space charge and the conduction current measurements on cable 11543-3.

Table 5.4 – Electric field thresholds of cable 11543-3

	Threshold @20°C [kV/mm]	Threshold @40°C [kV/mm]	Threshold @60°C [kV/mm]
PEA	7.3	6	4.5
CCM	6.5	5.3	3.8

As it can be observed the results are close to each other. The slight difference between the results of the two techniques is discussed in detail in section 5.2.1. The fact that space charge is detected only above the threshold found by the conduction current measurements is consistently observed in this case as well. The experimental results appear to be in agreement with the theoretical prediction that space charge and Ohmic conduction are mutually exclusive.

5.2.3 Cable 11543-4

Space charge accumulation threshold

This cable consists of insulation type I (cross-linked polyethylene with less than 0.5 wt.% “styrenic” charge trapping agent) and two semi-conductive layers of type D (ethylene copolymer with polar comonomer, “high” carbon black loading). The obtained V-I characteristics at 20°C, 40°C and 60°C are displayed in figures 5.11, 5.12 and 5.13 respectively.

The threshold at 20°C is estimated at 3.6kV/mm. At 40°C and 60°C the electric field threshold is determined at 2.8kV/mm and 1.6kV/mm respectively.

The only difference between cables 11543-3 and 11543-4 is the semicon type. However, there is a significant difference in their electric field thresholds. Cable 11543-4 shows much lower electric field thresholds than cable 11543-3 at all three temperatures. This observation coincides with the results of the space charge measurements where it is suggested that higher carbon black content in the semi-conductive layer results in a lower electric field threshold (section 4.1.4). This suggestion is verified by the conduction current measurements.

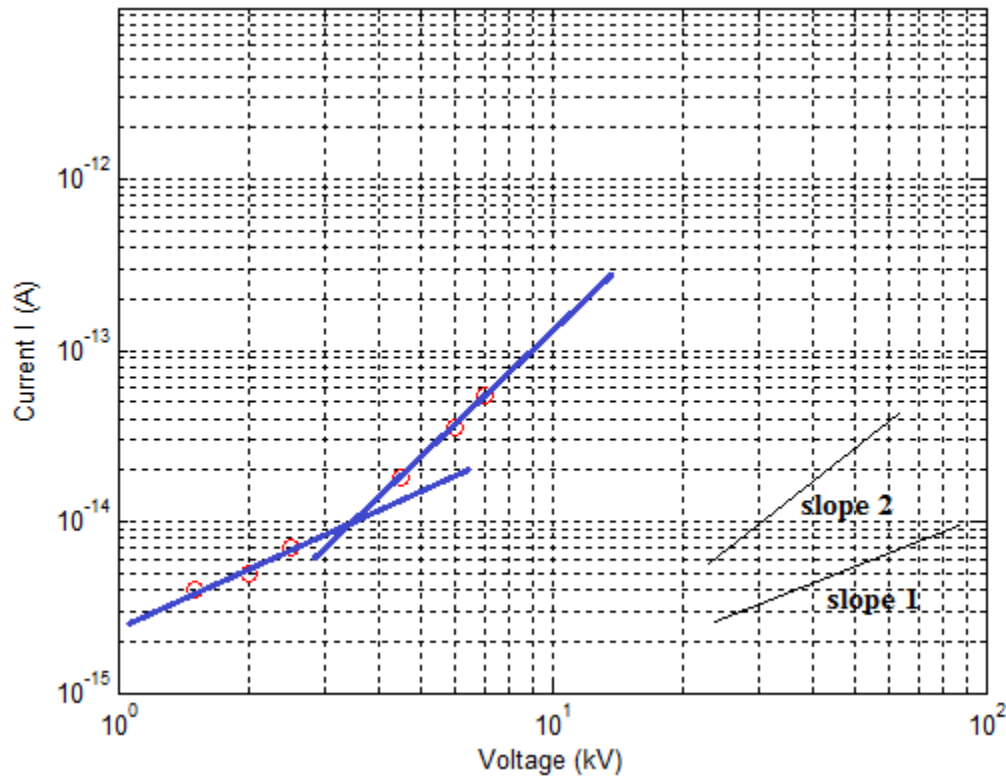


Figure 5.11 – V-I characteristic of cable 11543-4 @20°C

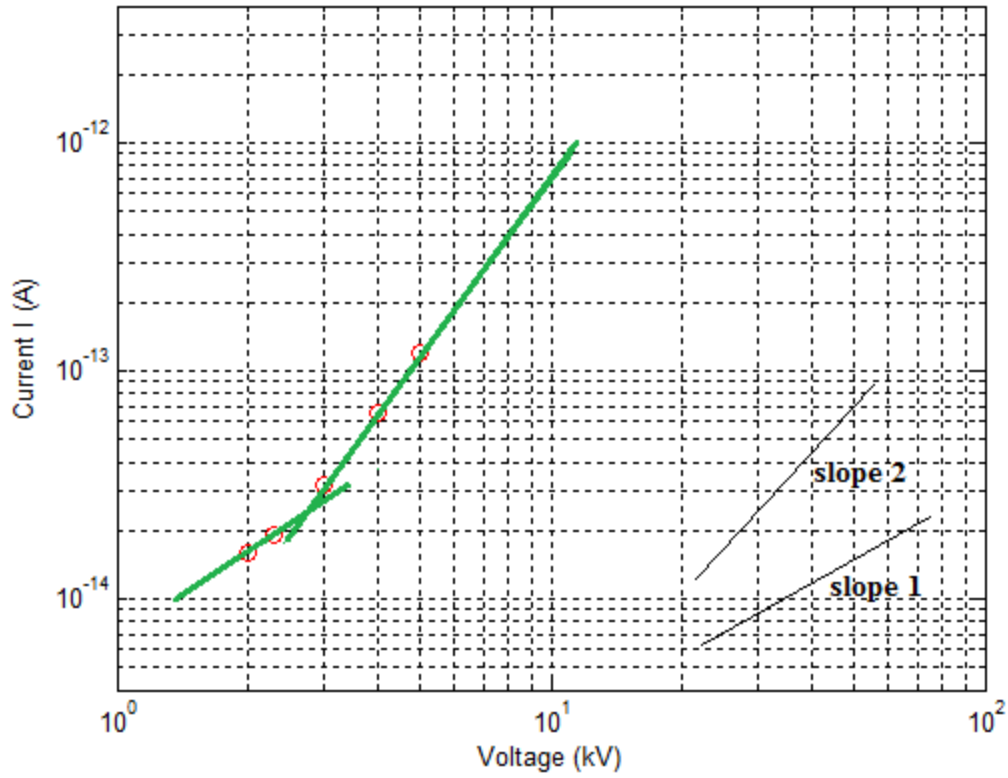


Figure 5.12 – V-I characteristic of cable 11543-4 @40°C

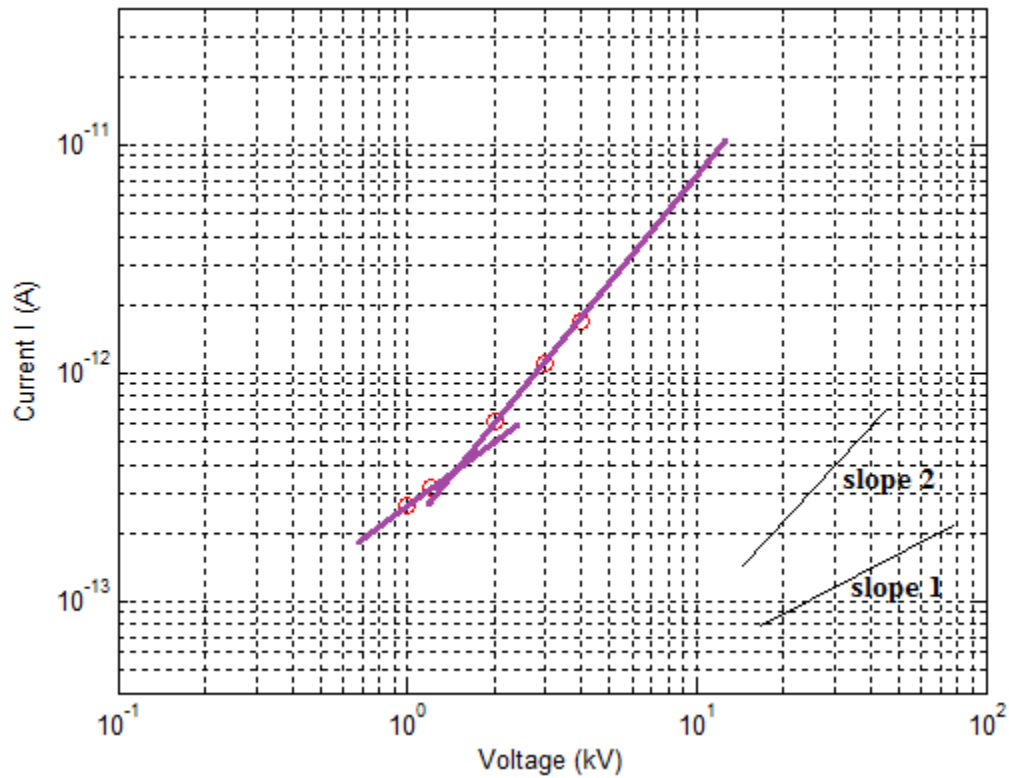


Figure 5.13 – V-I characteristic of cable 11543-4 @60°C

The electric field vs. the conductivity σ of cable 11543-4 at different temperatures are presented in figure 5.14.

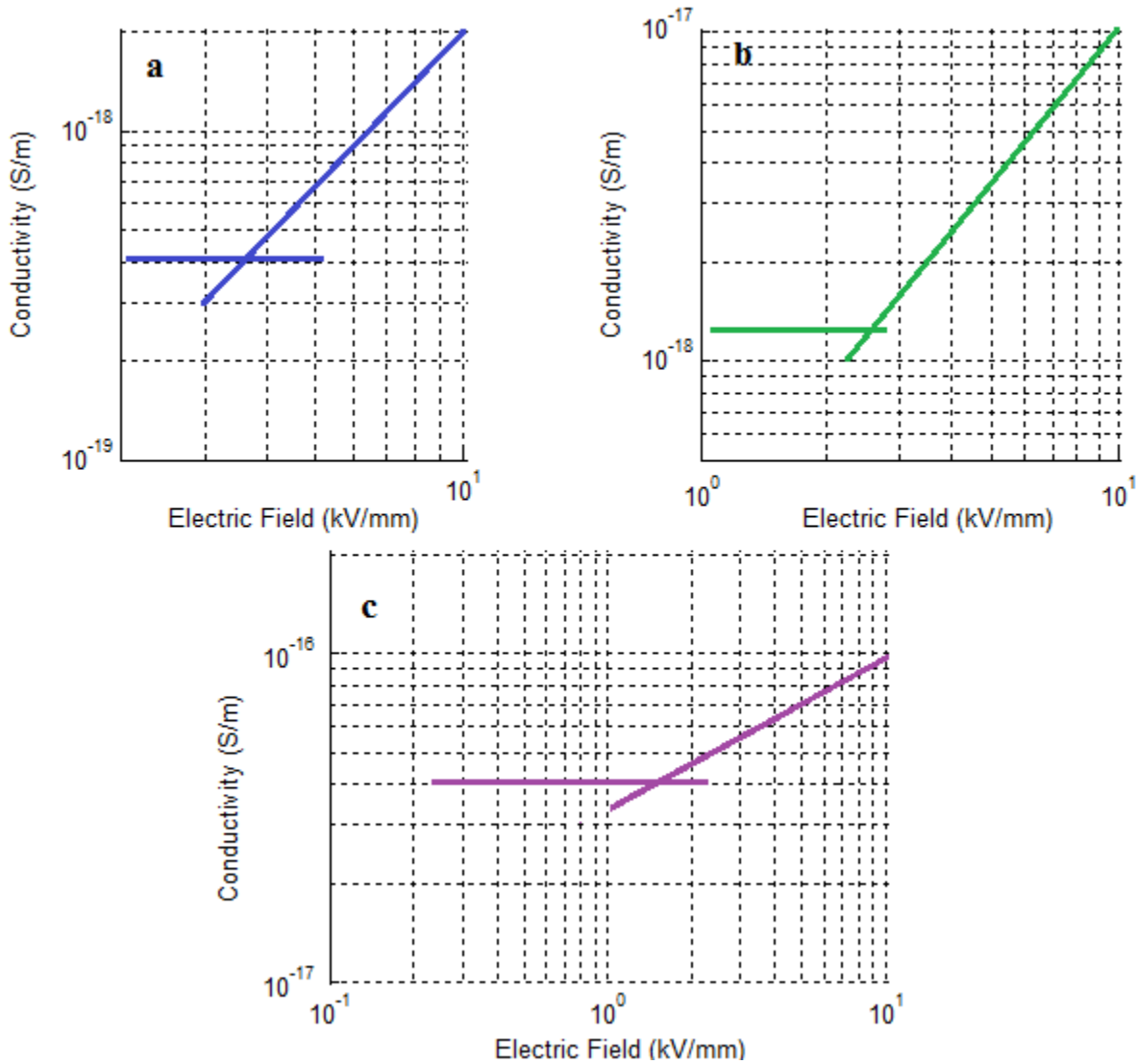


Figure 5.14 – E- σ characteristics of cable 11543-4, a: @20°C, b:@40°C, c: 60°C

The conductivity at a given electric field above threshold and within the range 20°C to 60°C, can fit quite well into an Arrhenius-type relationship which is described by equation 5.3. The corresponding activation energy is equal to 0.88eV and the relevant plot is given in figure 5.15.

$$\sigma(T) = 0.0014 \exp \left[-\frac{0.88}{kT} \right] \quad (5.3)$$

Where k is the Boltzmann constant and it is equal to 8.617×10^{-5} eV/K.

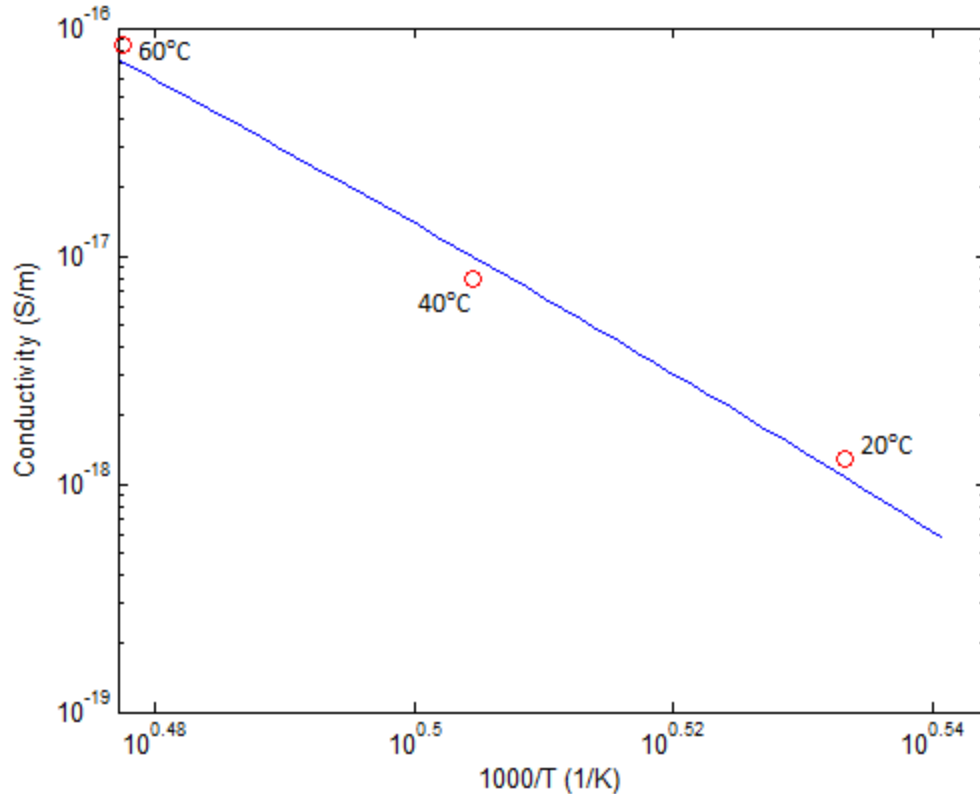


Figure 5.15 – Cable 11543-4, conductivity vs. reciprocal absolute temperature @ 8kV/mm

Electric field threshold comparison

Table 5.4 contains the results of the space charge and the conduction current measurements of cable 11543-3.

Table 5.5 – Electric field thresholds of cable 11543-4

	Threshold @20°C [kV/mm]	Threshold @40°C [kV/mm]	Threshold @60°C [kV/mm]
PEA	4	3	3
CCM	3.6	2.8	1.6

It can be observed that the results of both techniques are close to each other in case of 20°C and 40°C. However, at 60°C there is a significant difference between the results obtained by the space charge and the conduction current measurements. It should be taken into account the fact that the accuracy of the PEA method in this case is restricted by two factors.

The average space charge values at very low field strengths are less accurate because of the fact that the signal is relative small with respect to the distortion [7]. The combination of this with the fact that the average space charge density rises relatively slowly with increasing field strength at 60°C makes the determination of the threshold more difficult [7]. Therefore, the results of the space charge measurements at 60°C for this cable should be handled with caution.

5.3 Discussion

The conduction current measurements on the semicon plaques revealed that the concentration of carbon black determines the conductivity of the semi-conductive layer. Higher carbon black concentration results in higher semicon conductivity.

Combining the results of the space charge measurements (section 4.1.4) and the conduction current measurements on the semicon plaques, the electric field thresholds of the mini-cables could also be related to the conductivity of the semi-conductive layer. According to the space charge measurements, the electric field threshold is significantly affected by the semicon type. Higher carbon black content results in a lower electric field threshold at all three temperatures (20°C, 40°C and 60°C). The results of the conduction current measurements on the semicon plaques suggest that higher semicon conductivity results in a lower electric field threshold.

The conduction current measurements on the three cables coincide with the results of the space charge measurements. Therefore, two important suggestions drawn from the space charge measurements are verified by the conduction current measurements. Firstly, the observation that the type of semicon determines to a high extent the threshold for space charge accumulation. Secondly, the observation that the concentration of carbon black in the semi-conductive layer greatly affects the electric field threshold.

The conduction current measurements verified that the cables made from different insulation materials and the same type of semicon result almost in the same electric field thresholds. Also, they assured that higher carbon content in the semicon results in a lower electric field threshold. These statements hold for all three temperatures.

6. Conclusions & Recommendations

In this chapter, the conclusions drawn from the space charge and the conduction current measurements are presented and discussed in section 6.1. Thus, the results of the electric field thresholds, apparent trap-controlled mobilities and trap depths for all the cables are analyzed. Section 6.2 contains some recommendations for further research into the space charge dynamics of the mini-cables.

6.1 Conclusions

Electric thresholds at positive polarity

The space charge measurements revealed that the electric field thresholds of these mini-cables are mainly dictated by the semi-conductive layers rather than the insulation type. The cables made from different insulation materials and the same type of semicon exhibit close thresholds for space charge accumulation. Therefore, it can be claimed that the insulation material plays no or insignificant role in the determination of the space charge accumulation threshold. This observation suggests that the electric field thresholds of these mini-cables are significantly affected by the injection/extraction processes at the semicon-insulation interfaces.

The fact that the insulation type does not significantly affect the electric field threshold could also be related to the Fermi levels of the insulations used in the construction of the mini-cables. More specifically, both insulation types seem to have nearly equal Fermi levels as the cables made from different insulations and the same semicon result almost in the same thresholds. However, the Fermi levels seem to vary from semicon to semicon. This suggestion is based on the fact that the semicon type plays a significant role in the determination of the electric field threshold. Therefore, injection/extraction of charge carriers at the semicon-insulation interface is of major importance. It can be claimed that semicon C and F result in a higher potential barrier between the semicon – insulation interface compared to that of semicon E and D.

The increase in carbon black concentration in the semi-conductive layers results in lower electric field thresholds. For the six cables made from the semicon composed of ethylene copolymer with polar comonomer, the highest threshold is recorded in the case of “low” carbon black content. The semicon with the lowest concentration of carbon black exhibits the lowest conductivity as well. This observation is verified by the conduction current measurements on the semicon plaques (section 5.1).

On the other hand, the two cables made from semicon F composed of copolymer blend of reduced polarity with “medium” carbon black content, show a threshold close to the cables with semicon C composed of ethylene copolymer with polar comonomer of “low” carbon black content. Therefore, it is likely that a decrease in carbon black concentration of semicon F could lead to an even higher electric field threshold.

The space charge accumulation thresholds of three cables were examined by means of conduction current measurements as well. The results verified that the electric field thresholds are mainly determined by the semi-conductive layers of the cables.

The electric field thresholds of the two cables made from semicon C ('low' carbon content) and different insulation materials were found to be close to each other as in the case of space charge measurements. On the contrary, cable 11543-4 with the semicon of 'high' carbon content has a much lower electric field threshold than the other two cables. This observation verifies the suggestion that higher carbon black content of semicon results in a lower electric field threshold. The thresholds for space charge accumulation estimated by means of the conduction current measurements are close to the results of the space charge measurements.

Electric thresholds at negative polarity

Cable 11544-4 was examined under negative voltage. No significant variation in the electric field thresholds was observed between positive and negative polarity (section 4.2). The slight difference in the results cannot imply a different injection/extraction process; it is more likely to be related to the accuracy of the measurements as there is an uncertainty of approximately 15%.

Fitting line slopes

During the space charge measurements, it was observed that when temperature increases, the slope of the fitting line above the electric field threshold decreases. The fitting line slope expresses the dependence of the space charge density on the applied electric field. At 40°C and 60°C, the fitting line slopes are less steep than the slope at room temperature.

This kind of behavior is believed to be related to the injection/extraction and detrapping processes. In chapter 4, the positive temperature dependence of these processes is discussed in detail. The fact that the fitting line slope decreases as temperature increases could be attributed to the different way in which each process reacts to temperature increase. Therefore, it is believed that when temperature increases the injection rate increases at slower pace than the detrapping and extraction rate. However, the injection rate is still higher than the detrapping and extraction rate in order for space charge accumulation to take place inside the material.

Temperature dependence of electric field thresholds

The space charge measurements on the mini-cables showed that the electric field threshold for space charge accumulation significantly depends on temperature. There is a clear decrease in the threshold for space charge accumulation with temperature increase. This holds for all the cables which were examined.

As it is mentioned above, the semicon mainly determines the electric field threshold. Therefore, the injection/extraction processes at the semicon-insulation interfaces are critical. These processes are thermally activated mechanisms and an increase in temperature causes an increase in the thermal energy of charge carriers. The threshold decrease could be attributed to the higher energy of charge carriers.

The electric field thresholds of all eight cables within the range 20°C to 60°C, fit well into an exponential relationship. The exponential factors of the cables made from the same semicon and different insulation materials are almost equal. This is expected as they have approximately equal thresholds at different temperatures.

However, the cables made from semicon F composed of copolymer blend of reduced polarity exhibit stronger temperature dependence than the cables with semicon E composed of ethylene copolymer with polar comonomer. The different temperature dependence could be related to the different properties of either the semicon-insulation interface or/and the semicon itself.

Temperature Gradient

During the space charge measurements, a temperature gradient was present in the cable insulation. At 40°C the difference between the inner and outer semicon was 5 °C. In the case of 60 °C, the temperature gradient was almost 10 °C. However, the conduction current measurements were performed under isothermal conditions.

The results of the conduction current measurements showed that the temperature gradient does not seem to influence the electric field thresholds of the cables. In spite of the fact that the conduction current measurements were carried out under isothermal conditions, the estimated space charge accumulation thresholds are approximately equal to the results of the space charge measurements. The slight difference between the results of the two techniques is discussed in detail in section 5.2.1 and it could not be related to the temperature gradient.

Apparent trap-controlled mobility and trap depths

It is found that the mobilities of these mini-cables are mainly determined by the insulation material. The role of the semi-conductive layers is insignificant compared to that of the insulation. The fact that the apparent trap-controlled mobility is mainly driven by the insulation type implies that the detrapping process is the prevailing factor with respect to the depletion rate of the accumulated space charge.

The cables made from insulation type I (crosslinked polyethylene *PE* with less than 0.5 wt.% styrenic charge trapping agent) show a higher mobility than those made from insulation type II (crosslinked polyethylene *PE* with less than 1 wt.% carbon black) within three hours of depolarization. Insulation type I exhibits a more favorable behavior with regard to the depletion rate of accumulated space charge than insulation type II.

As far as the trap depth values are concerned, shallower traps are formed in insulation type I. This can be attributed to the addition of styrenic charge trapping agent. The role of this additive is to create more shallow traps and not deep traps.

Finally, the distribution along the trap levels exhibits a different behavior between the two types of insulation. In insulation type I more space charge is accumulated at the higher energy levels. On the contrary, in insulation type II most of the space charge is accumulated at the level with the lowest potential energy. Therefore, in a shorter period of time more space charge is depleted from insulation I than insulation II. The latter statement coincides with the fact that insulation type I shows a higher apparent trap-controlled mobility than type II.

Cable Conductivities

The conductivity of the cables at a given electric field above threshold and within the range 20°C to 60°C, fits well into an Arrhenius-type relationship. This observation holds for all three cables which were examined by means of conduction current measurements.

The trap-limited mobility is believed to be the reason for the Arrhenius-type dependence of the conductivity on temperature. Only a number of charge carriers contribute to the conduction due to the presence of trap states within the band gap of the insulation. However, the number of effective charge carriers, which is proportional to the mobility and then to the conductivity, is function of temperature which is described by an Arrhenius-type relationship.

6.2 Recommendations

Charge packets

The observation that the average space charge densities at 30kV/mm and 60kV/mm (at 60°C) are higher than expected according to the fitting line is consistent for all the cables tested during the space charge measurements (sections 4.1.1 - 4.1.4). Fast moving charge packets could cause this effect.

Further investigation is recommended with the use of a fast acquisition system in order to verify the hypothesis of fast moving charge packets. If this assumption holds, a thorough investigation is required. The inception electric field for the generation of charge packets, their temperature dependence and their mobility should be included in the investigation.

Depolarization characteristics

If a fast acquisition system for space charge measurements is available, new depolarization characteristics at high poling fields are recommended to be obtained. In this way, the first part of the depolarization process is not omitted as it is mentioned in section 2.7. Therefore, the shallowest traps in the insulations can be detected.

It should be mentioned that the polarization process should be long enough in order to reach a steady-state situation in which no more space charge is accumulated in the insulation. As far as the depolarization process is concerned, it should be longer than the polarization duration in order for the accumulated space charge to be depleted to a high extent. A longer depolarization duration is recommended as most of the time, there is an unsymmetrical space charge distribution in the insulation. Consequently, depletion of space charge will take more time than accumulation because a part of the accumulated charge will be driven out and a part will be forced into the bulk of the insulation.

Fitting line slopes

As it is explained in section 4.1, the slope of the fitting line above threshold decreases with temperature increase. The assumption that when temperature increases, the injection rate increases at slower pace than the extraction and charge detrapping rate can be further investigated by carrying out simultaneous space charge and conduction current measurements.

A new setup is required which will be able not only to record the accumulated amount of space charge but also the injection and extraction current density.

Production of new mini-cables

It is mentioned in section 4.1.6 that the cables made from semicon F ('medium' carbon content) have a threshold close to the cables with semicon C ('low' carbon content). Therefore, a new mini-cable composed of insulation type I or II and a new type of semicon which has the same composition as semicon F but with lower carbon black concentration is expected to result in a higher electric field threshold.

Furthermore, the possibility of decreasing the conductivity of semicon C could be investigated. A new semicon type can be produced which will have the same composition as semicon C but with even lower carbon black concentration. If this further decrease in carbon black content is possible, higher electric field thresholds are expected for a cable composed of insulation type I or II and this new semicon type.

Production of a MV-size cable

As it is explained in chapter 4, the highest electric field threshold is observed for the cables made from semicon F or C. Furthermore, insulation type I exhibits a better performance with regard to apparent trap-controlled mobility and trap depths. It has a higher depletion rate (mobility) and shallower trap sites.

An MV-size cable composed of insulation type I and semicon C or F can be produced and tested in order to investigate the effect of the larger volume (larger electrodes and insulation thickness) on the electric field thresholds, apparent trap-controlled mobility and trap depths.

Appendix I - Signal Processing

Deconvolution

The electrical signal is not a correct representation of the space charge profile as the amplifier acts as a high pass filter which distorts the original pressure signal. According to convolution theorem, once the signal response of a linear system is known, the relation between the input and output of that circuit can be calculated. So, the system response H can give the relationship between the detected signal at the oscilloscope $U_{det}(t)$ and the original signal $U_{orig}(t)$. If the system response is known, it is possible to compute the original signal by using the inverse system response H^{-1} . Therefore, in the frequency domain equation I.1 holds.

$$U_{det}(f) = H(f)U_{orig}(f) \quad (I.1)$$

In the time domain the original signal $U_{orig}(t)$ is given by equation I.2.

$$U_{orig}(t) = \mathcal{F}^{-1}\left\{\frac{U_{det}(f)}{H(f)}\right\} \quad (I.2)$$

It is worth noting that the deconvoluted signal $U_{decon}(t)$ is never identical to the original signal $U_{orig}(t)$. Thus, the deconvoluted signal is designated. The deconvolution process is explained with the aid of figure I.1.

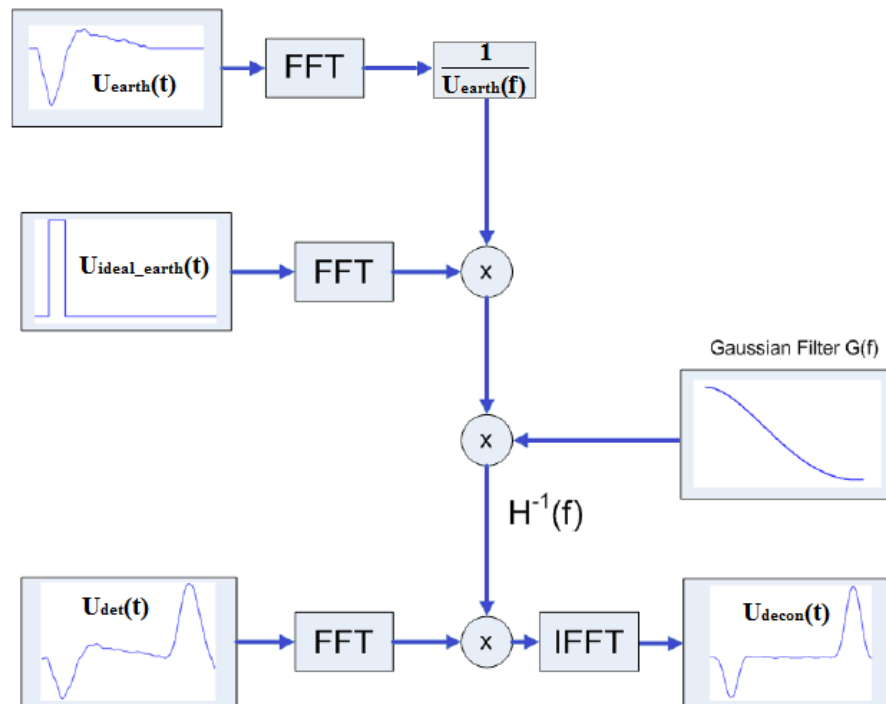


Figure I.1 – Schematic representation of the deconvolution technique

As the system response is not known, equation I.2 cannot be applied directly. The system response is determined by using the signal $U_{earth}(t)$ which represents the earth electrode and the bulk of the material which is part of the detected signal $U_{det}(t)$. Usually, the earth electrode is chosen because the acoustic signal of this charge does not experience any attenuation and dispersion by the sample material.

Also, the ideal signal $U_{ideal_earth}(t)$ from the electrode charge is used. So, it is a signal without the response of the sensor and the amplifier. This ideal signal is represented by a pulse which has approximately the same width as the earth electrode in the detected signal $U_{det}(t)$ and has a height of one. This height is usually much larger than the height of the electrode signal in the detected signal.

The ideal signal $U_{ideal_earth}(t)$ and the measured signal $U_{earth}(t)$ are converted into the frequency domain. Then the former is divided by the latter and the inverse response function $H^{-1}(f)$ can be calculated. However, the presence of high frequency components can affect the final deconvoluted signal $U_{decon}(t)$. In order to eliminate or attenuate these high frequency components a low pass Gaussian filter with transfer function $G(f)$ is used.

However, the deconvoluted signal is still an approximation as the height of the ideal signal is one and the resulting deconvoluted signal does not have the correct value. Therefore, a correction factor K_{cor} is required. This factor can be obtained by dividing the maximum value of the deconvoluted signal by the maximum value of the detected signal according to equation I.3.

$$K_{cor} = \left| \frac{\max(U_{decon}(t))}{\max(U_{det}(t))} \right| \quad (I.3)$$

So, the final deconvoluted signal $U_{f_decon}(t)$ is obtained by using equation I.4.

$$U_{f_decon}(t) = \frac{U_{decon}(t)}{K_{cor}} \quad (I.4)$$

The deconvolution process is performed correctly only when the signal is free of space charge. Otherwise, the signal $U_{earth}(t)$ cannot be flat outside the charge region.

Divergence

The electric field distribution E_{pulse} due to the applied pulse U_p is given by equation I.5.

$$E_{pulse}(r) = \frac{U_p}{r \ln\left(\frac{r_{out}}{r_{in}}\right)} \quad (I.5)$$

Where r is the cable radius.

Therefore, it is clear that the pulsed field distribution is not homogeneous and it depends on the radial position r . As the magnitude of the pressure wave generated at the space charge location is proportional to the pulsed field at this location, the space charge distribution will be position dependent. In order to correct the detected signal from the divergence of the pulsed field, a correction factor K_{g_pulse} is defined according to equation I.6.

$$K_{g_pulse} = \frac{p(r_{out})}{p(r)} = \frac{E_{pulse}(r_{out})}{E_{pulse}(r)} = \frac{r}{r_{out}} \quad (I.6)$$

Where $p(r_{out})$ is the magnitude of a pressure wave which corresponds to a given amount of charge at the outer radius and $p(r)$ is the magnitude of a pressure wave associated to the same amount of charge at an arbitrary radius r .

The magnitude of an acoustic wave decreases while travelling from the inner part of the cable towards the sensor.

$$v^2 \nabla^2 p - \frac{\partial^2 p}{\partial t^2} = 0 \quad (I.7)$$

Where v is the acoustic wave velocity inside the insulation.

Assuming that the length of the cable is much larger than its thickness and the insulation material is homogeneous in the axial direction, then the analysis can be limited to the radial dimension only. Equation I.7 can be written in cylindrical coordinates.

$$v^2 \left[\frac{\partial}{\partial r} \left(r \frac{\partial p}{\partial r} \right) \right] - \frac{\partial^2 p}{\partial t^2} \quad (I.8)$$

The solution of the above partial differential equation is given by equation I.9.

$$p(r, t) = \frac{A}{\sqrt{r}} \exp \left(\frac{i\omega}{v} (r - vt) \right) \quad (I.9)$$

Where ω is the angular frequency of the acoustic wave and A is a constant determined by the boundary conditions.

It is clear from equation I.9 that the amplitude of a cylindrical acoustic wave which travels in the radial direction decreases with the squared root of the radius. Therefore, the amplitude of an acoustic wave detected at the sensor is smaller than the amplitude of the wave at the space charge location. The detected signal is corrected with the use of a correction factor K_{g_wave} defined according to equation I.10.

$$K_{g_wave} = \frac{p(r, t)}{p(r_{out}, t - \tau)} = \frac{p(r, t)}{p(r, t) \sqrt{\frac{r}{r_{out}}}} = \sqrt{\frac{r_{out}}{r}} \quad (I.10)$$

Where $p(r, t)$ is the magnitude of a pressure wave generated at an arbitrary radius r , whereas $p(r_{out}, t - \tau)$ is the magnitude of the same pressure wave after having traveled for a time τ from the radius r to the outer radius r_{out} .

Finally, a correction factor which combines both effects can be defined. It is called geometrical factor K_g and it is given by equation I.11.

$$K_g = K_{g_pulse} K_{g_wave} = \sqrt{\frac{r}{r_{out}}} \quad (I.11)$$

Then, the corrected signal is given by equation I.12.

$$U_{div}(t) = K_g U_{f_decon}(t) \quad (\text{I.12})$$

Attenuation and dispersion

A general expression for a planar acoustic wave $p(x,t)$ travelling through an ideal medium can be described in the frequency domain by equation I.13.

$$p(x, \omega) = P_0(\omega) \exp(-i\beta\omega) \quad (\text{I.13})$$

Where $P_0(\omega)$ represents the magnitude of the pressure wave with angular frequency ω at zero location ($P_0(0,\omega)$). This wave propagates without attenuation and its velocity v is related to the phase coefficient β according to equation I.14.

$$\beta = \frac{v}{\omega} \quad (\text{I.14})$$

An acoustic wave $p(x,t)$ travelling through a lossy and dispersive medium can be described in the frequency domain by equation I.15.

$$p(x, \omega) = P_0(\omega) \exp(-\alpha(\omega)x) \exp(-i\beta(\omega)x) \quad (\text{I.15})$$

Where $\alpha(\omega)$ is the frequency-dependent attenuation factor and $\beta(\omega)$ is the frequency-dependent phase factor. The former takes into account that the wave magnitude decreases as the wave travels through the medium and the latter takes into account the frequency dependence of the speed of sound in the medium.

$$G(x, \omega) = \frac{p(x, \omega)}{p(0, \omega)} = \exp(-\alpha(\omega)x) \exp(-i\beta(\omega)x) \quad (\text{I.16})$$

The coefficients $\alpha(\omega)$ and $\beta(\omega)$ are calculated with the use of two acoustic waves at two different locations in the sample. The acoustic wave generated at the HV electrode $p(d,\omega)$ and the corresponding acoustic wave detected at the sensor $p(0,\omega)$ are used. Therefore, equation I.17 holds.

$$G(d, \omega) = \frac{p(d, \omega)}{p(0, \omega)} = \exp(-\alpha(\omega)d) \exp(-i\beta(\omega)d) \quad (\text{I.17})$$

When the function $G(d,\omega)$ is defined, the coefficients $\alpha(\omega)$ and $\beta(\omega)$ can be calculated. In this way the function $G(x,\omega)$ can be determined and the pressure distribution $p(x,t)$ inside the sample can be derived according to equation I.18. The initial acoustic wave at any location is determined by the acoustic wave detected at the sensor.

$$p(x, t) = \mathcal{F}^{-1}\{p(0, \omega)G(x, \omega)\} \quad (\text{I.18})$$

The pressure distribution $p(x,0)$ corresponds to the acoustic wave at its initial location where it is generated and the pressure distribution $p(0,t)$ corresponds to the acoustic wave at the sensor location after travelling through the sample.

In order to implement the procedure described above, the original signal at the HV electrode which corresponds to the acoustic wave $p(d,\omega)$ is required. If the sample is space charge free, the recovered signal at the HV electrode represents the electrode charge only. This charge can be calculated when a known voltage is applied across the sample. It is worth noting that the recovered signal does not exactly correspond to the original signal as some of the higher frequencies of the original signal may be totally attenuated.

The calculation of the coefficients $\alpha(\omega)$ and $\beta(\omega)$ with the use of the function $G(d,\omega)$ includes some difficulties. Firstly, the function $G(d,\omega)$ is defined as the ratio of two other functions. So, if the denominator contains zeros, the division cannot be performed. Secondly, during the mathematical procedure high frequencies of the signal are amplified more than the low frequencies. Thus, if noise is present in the detected signal, it is amplified as well. These two problems can be tackled with defining two approximating equations for the calculation of the coefficients $\alpha(\omega)$ and $\beta(\omega)$.

$$\alpha(\omega) = A + a\omega^2 \quad (\text{I.19})$$

$$\beta(\omega) = b\omega \quad (\text{I.20})$$

Equations I.19 and I.20 are valid under the assumption that the original waveform $y_1(t)$ and the detected waveform $y_2(t)$ are Gaussian functions according to equations I.21 and I.22.

$$y_1(t) = A_1 \exp(-a_1(t - \tau_1)^2) \quad (\text{I.21})$$

$$y_2(t) = A_2 \exp(-a_2(t - \tau_2)^2) \quad (\text{I.22})$$

In the frequency domain equations I.21 and I.22 can be written according to equations I.23 and I.24.

$$Y_1(\omega) = A_1 \sqrt{\frac{\pi}{a_1}} \exp\left(-i\tau_1\omega - \frac{\omega^2}{4a_1}\right) \quad (\text{I.23})$$

$$Y_2(\omega) = A_2 \sqrt{\frac{\pi}{a_2}} \exp\left(-i\tau_2\omega - \frac{\omega^2}{4a_2}\right) \quad (\text{I.24})$$

As a result, the function $G(d,\omega)$ can be written according to equation I.25.

$$\begin{aligned} G(d,\omega) &= \frac{Y_1}{Y_2} = \frac{A_1}{A_2} \sqrt{\frac{a_2}{a_1}} \exp\left(-i\omega(\tau_1 - \tau_2) - \frac{\omega^2}{4}\left(\frac{1}{a_1} - \frac{1}{a_2}\right)\right) \\ &= \exp(-d(A + a\omega^2)) \exp(-ib\omega d) \end{aligned} \quad (\text{I.25})$$

Where the terms A , a and b are determined from equations I.26, I.27 and I.28 respectively.

$$A = -\frac{1}{d} \ln \left(\frac{A_1}{A_2} \sqrt{\frac{a_2}{a_1}} \right) \quad (\text{I.26})$$

$$a = \frac{1}{4d} \left(\frac{1}{a_1} - \frac{1}{a_2} \right) \quad (\text{I.27})$$

$$b = \frac{1}{d} (\tau_1 - \tau_2) \quad (\text{I.28})$$

The values of the above parameters depend on the type of the medium and approximate values are used. Therefore, the coefficients $\alpha(\omega)$ and $\beta(\omega)$ can be determined according to equations I.19 and I.20 respectively.

The corrected signal for divergence $U_{div}(t)$ is subjected to attenuation and dispersion correction according to equation I.29.

$$U_{atten}(t) = \mathcal{F}^{-1}\{G(\omega)U_{div}(\omega)\} \quad (\text{I.29})$$

Where the function $G(\omega)$ is calculated with the use of the parameters α and β according to equation I.30.

$$G(\omega) = \exp(-\alpha(\omega)\tau) \exp(-i\beta(\omega)\tau) \quad (\text{I.30})$$

Where τ is the time difference between the peak of the earth electrode and the peak of the HV electrode in the signal. This time interval corresponds to the distance between the electrodes and thus, to the thickness of the sample.

Calibration

As it is mentioned in section 3.2.1, a calibration factor is required in order to convert the non-calibrated signal in mV into a calibrated signal in C/m^3 . The calibration procedure is the same as in the case of flat specimens and it is based on a known charge at the earth electrode when a known voltage V is applied. Therefore, equation 3.1 can be applied here as well. The surface charge density σ_e at the earth electrode is calculated according to equation I.31.

$$\sigma_e = \varepsilon_0 \varepsilon_r E_e \quad (\text{I.31})$$

Where ε_r is the relative permittivity of the sample and E_e is the electric field at the outer radius r_{out} of the cable where the earth electrode is located and it is calculated according to equation I.32.

$$E_e = \frac{V}{r_{out} \ln\left(\frac{r_{out}}{r_{in}}\right)} \quad (I.32)$$

Then the calibration factor K_{cal} is calculated with the use of equation I.33.

$$K_{cal} = \frac{\int_{x_1}^{x_2} U_{atten}(x) dx}{\sigma_e} \quad (I.33)$$

Where x_1 and x_2 denote the starting and the ending point of the earth electrode respectively.

Finally, the space charge profile can be determined.

$$\rho(r) = \frac{U_{atten}(r)}{K_{cal}} \quad (I.34)$$

Once the radial space charge distribution $\rho(r)$ is known, the accuracy of the calibration procedure can be checked as in the case of flat specimens. The electric field distribution is calculated from equation I.35.

$$E(r) = \frac{1}{r \epsilon_0 \epsilon_r} \int_{r_{in}}^{r_{out}} r \rho(r) dr \quad (I.35)$$

Then, the voltage distribution is given by equation I.36.

$$V(r) = - \int_{r_{in}}^{r_{out}} E(r) dr \quad (I.36)$$

The voltage across the sample should be the same as the applied voltage at the HV electrode and zero at the earth electrode. Therefore, the sample should be initially free of space charge.

Appendix II

Technical Specifications of the PEA Setup

Table II.1 – HVDC generator


	Type	Sorensen 1101
	Input	230 V
		50 Hz
		4 A
	Output	100 kV
		1.5 mA

Table II.2 – Pulse generator

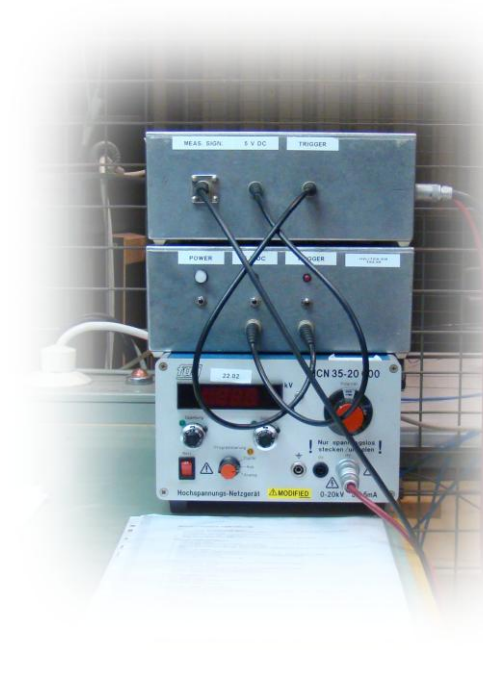
	HVDC generator	Type	Fug HCN 35-20000
		Input	230V \pm 10% 47-63Hz
		Output	20 kV 1.5 mA
Switch Box	Built up by Riccardo Bodega (TU Delft)		
	Amplitude	0 - 4 kV	
	Pulse width	80 ns	
	Pulse rise time	10 ns	

Table II.3 – Pulse electrode


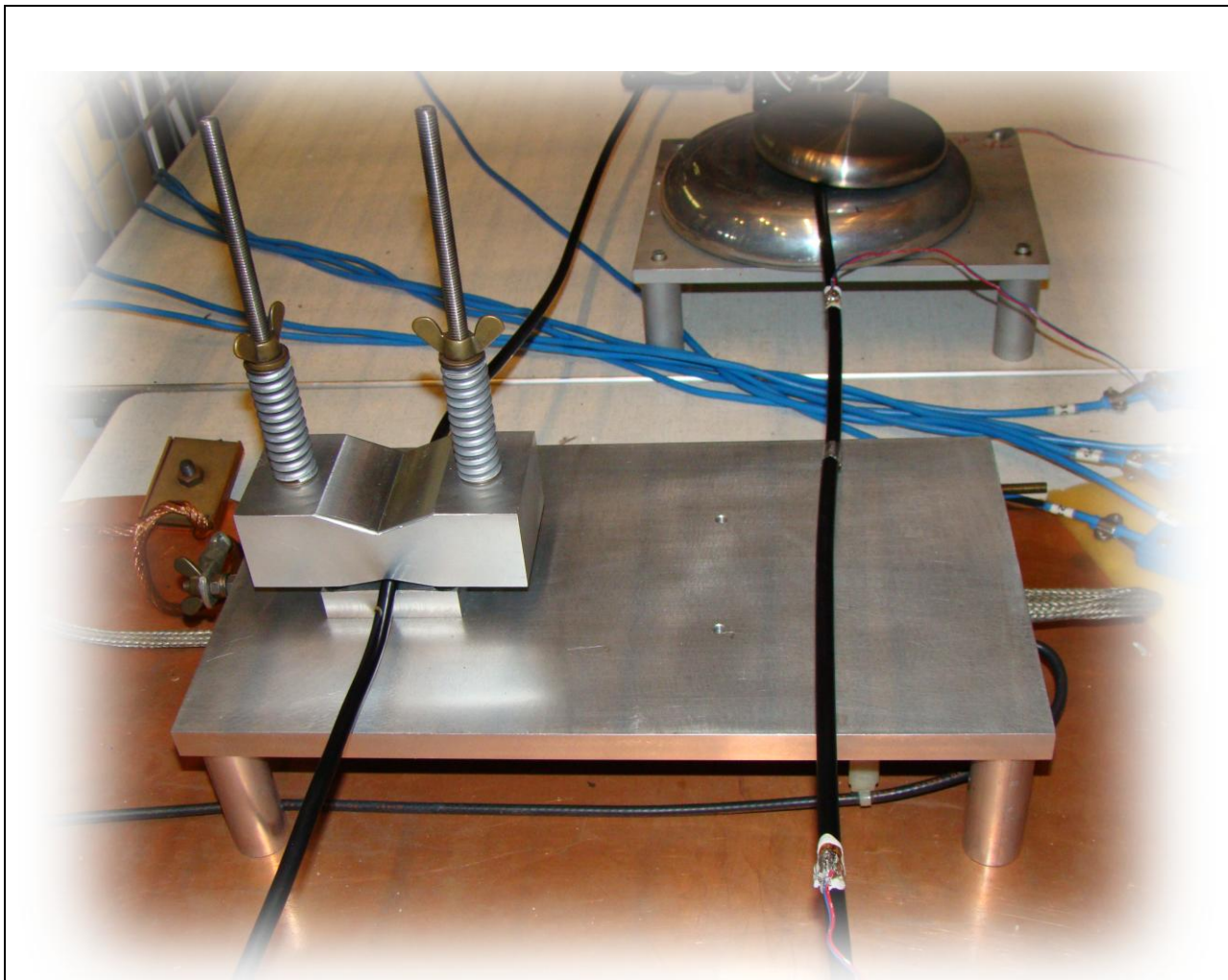
	
$R_{\text{pulse}} = 50 \Omega$	$R_d = 155 \Omega$

Table II.4 – PEA cell



Sensor	PVDF	25 μm	
Amplifier	Gain	70 dB	
	Input impedance	1.5 k Ω	
	Bandwidth	0.1-100 MHz	
	Max. temperature	70°C	

Table II.5 – Oscilloscope


	Lecroy Waverunner 6050A	
	Sample rate	5 GS/sec
	RIS	200 GS/sec
	Bandwidth	500 MHz
	Averaging	Up to 1 million sweeps

Table II.6 – Current induction transformer


	Manufacturer	De Drie electronics B.V. EDE Nederland	
	Primary	2*280 V	50 Hz
	Secondary	6 V	

Table II.7 – Autotransformer


	General radio company		
	Type	W20HM	
	Line	240 V	50 – 60 Hz
	load	0-280 V	8 A

Table II.8 – Current transformer


	Manufacturer	AEG
	Primary	15 – 800 A
	Secondary	5 A

Table II.9 – Ammeter


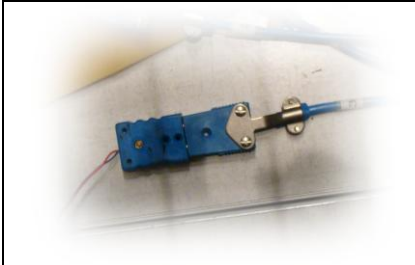

	Manufacturer	Goerz Electro Ges
	Type	Unigor 3p

Table II.10 – Temperature measurement

	Thermocouple	
	Type	T
	Temperature indicator	
	Type	RS 1314

Appendix III

Technical Specifications of the CCM Setup for Plaques

Table III.1 – HVDC generator


	Type	Fug HCN 350-35000
	Input	230V ±10% 47-63Hz
	Output	35 kV 10 mA

Table III.2 – Electrometer


	Manufacturer	Keithley
	Model	617
	Measuring range	0.1 fA – 20 mA

Table III.3 – Electrodes

HV electrode diameter	28 mm	
Measuring electrode diameter	35 mm	
Guard electrode diameter	40 – 350 mm	
Max. temperature	80°C	
Max. voltage	±30 kV	

Appendix IV

Technical Specifications of the CCM Setup for Cables

Table IV.1 – HVDC generator


	Type	Fug HCN 35-35000
	Input	220V \pm 10% 50Hz
	Output	35 kV 1 mA

Table IV.2 – Electrometer


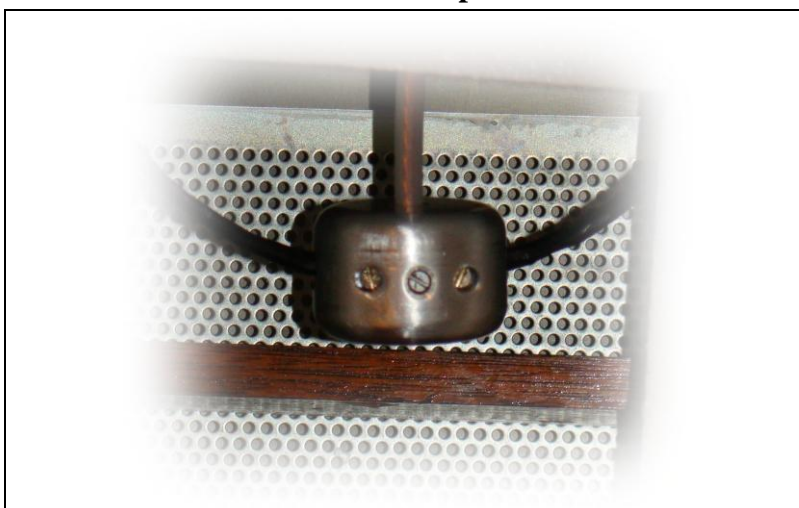
	Manufacturer	Keithley
	Model	617
	Measuring range	0.1 fA – 20 mA

Table IV.3 – Furnace

Manufacturer	Salvis	
Type	LSE37	
Max. temperature	250°C	

Table IV.4 – Aluminum spherical electrode

Bibliography

- [1] L.A. Dissado and J.C. Fothergill , *Electrical Degradation and Breakdown in Polymers*, Peter Peregrinus Ltd. / 1992
- [2] A.K. Jonscher, *Dielectric Relaxation in Solids*, Chelsea Dielectric Press, 1983
- [3] J.J O’Dwyer, *The Theory of Electrical Conduction and Breakdown in Solid Dielectrics*, Clarendon press, Oxford 1973
- [4] F.H Kreuger, *Industrial High DC Voltage*, Delft university press / 1995
- [5] P.H.F. Morshuis, *Lecture Notes of High Voltage DC*, Delft university of technology / 2010
- [6] R. Bodega, *Space Charge Accumulation in Polymeric High Voltage DC Cable Systems*, Ph.D. dissertation, Delft university of technology / 2006
- [7] D. van der Born, *Investigation of space charge injection, conduction and trapping mechanisms in polymeric HVDC mini-cables*, Master thesis, Delft university of technology / 2011
- [8] T. L. Hanley, R. P. Burford, R. J. Fleming, K. W. Barber, *A General Review of Polymeric Insulation for Use in HVDC Cables*, 0883-7554/03 IEEE
- [9] M. Jeroense, *Charges and Discharges in HVDC Cables*, Ph.D. dissertation, Delft university of technology / 1997
- [10] L.A.Dissado, *The Origin and Nature of ‘Charge Packets’: A Short Review*, 978-1-4244-7944-3/10 IEEE
- [11] D. Fabiani, G.C. Montanari, L.A. Dissado, C.Laurent, G. Teyssedre, *Fast and Slow Charge Packets in Polymeric Materials under DC Stress*, 1070-9878/09, 2009 IEEE
- [12] B. Alijagic - Jonuz, *Dielectric Properties and Space Charge Dynamics of Polymeric High Voltage DC Insulating Materials*, Ph.D. dissertation, Delft university of technology / 2007
- [13] G. Mauanti, G. C. Montanari, J. M. Alison, *A Space-Charge Based Method for the Estimation of Apparent Mobility and Trap Depth as Markers for Insulation Degradation-Theoretical Basis and Experimental Validation*, 1070-9878/1, 2003 IEEE
- [14] G.C. Montanari, G. Mazzanti, E Palmieri, G. Perego, S. Serra, *Dependence Of Space Charge Trapping Threshold On Temperature In Polymeric DC Cables*, 0-7803-6352-3, 2001 IEEE
- [15] L.A. Dissado, S.Zadeh, J.C.Fothergill, A. See, *Temperature Dependence of Charge Packet Velocity in XLPE Cable Peelings*, 1-4244-1482-2/07, 2007 IEEE

- [16] G C Montanari, G Mazzanti, F Palmieri, A Motori, G Perego and S Serra, *Space Charge Trapping and Conduction in LDPE, HDPE and XLPE*, 0022-3727/01/182902, 2001 IOP
- [17] L.A. Dissado, C. Laurent, G. C. Montanari, P. H. F. Morshuis, *Demonstrating a Threshold for Trapped Space Charge Accumulation in Solid Dielectrics under dc Field*, 1070-9878/05 IEEE
- [18] D. Fabiani, G.C. Montanari, C. Laurent, G. Teysedre, P. H. F. Morshuis, R. Bodega, *HVDC Cable Design and Space Charge Accumulation. Part 3:Effect of Temperature Gradient*, 0883-7554/07, 2008 IEEE
- [19] G.C. Montanari, *Bringing an Insulation to Failure: The Role of Space Charge*, 978-1-4244-9470-5/10 IEEE
- [20] G. Mazzantia, G. C. Montanari, F. Palmieri, J. Alison, *Apparent Trap-Controlled Mobility Evaluation in Insulating Polymers Through Depolarization Characteristics Derived by Space Charge Measurements*, 0021-8979/2003/94(9)/5997/8, 2003 American Institute of Physics
- [21] S. Delpino, D. Fabiani , G.C. Montanari , L. A. Dissado, C. Laurent, G. Teysedre, *Fast Charge Packet Dynamics in XLPE Insulated Cable Models*, 1-4244-1482-2/07 IEEE
- [22] G.C. Montanari, P.H.F. Morshuis, *Space Charge Phenomenology in Polymeric Insulating Materials*, 1070-9878/05, 2005 IEEE
- [24] D. Fabiani and G. C Montanari, C. Laurent and G. Teysedre, P. H. F. Morshuis, R. Bodega, L. A. Dissado, A. Campus and U. H. Nilsson, *Polymeric HVDC Cable Design and Space Charge Accumulation. Part 1: Insulation/Semicon Interface*, 0883-7554/07 IEEE
- [25] M. P. Bahrman, *HVDC Transmission Overview*, 978-1-4244-1904-3/08 IEEE
- [26] I. Mattson, A. Ericsson, B.D. Railing, J.J. Miller, B. Williams, G. Moreau, C. D. Clarke, Murraylink, *The Longest Underground HVDC Cable in The World*, B4-103 / 2004 Cigre
- [27] B. D. Railing, J. J. Miller, P. Steckley, G. Moreau, P. Bard, L. Ronstrom, J. Lindberg, *Cross Sound Cable Project Second Generation VSC Technology for HVDC* , B4-102 / 2004 Cigre
- [28] G.C. Montanari, *The Electrical Degradation Threshold of Polyethylene Investigated by Space Charge and Conduction Current Measurements*, 1070-9878/0, 2000 IEEE
- [29] G.C. Montanari, I. Ghinello, F. Peruzzotti, M. Albertini, *Behavior of Voltage-Current Characteristics and Threshold Indications for XLPE-Based Materials*, 0-7803-5035-9/98, 1998 IEEE.
- [30] Y. Li, M. ka Yasuda, T. Takada, *Pulsed Electroacoustic Method Measurement of Charge for Accumulation in Solid Dielectrics*, 1070-9878/94, 1994 IEEE
- [31] R. Bodega, G.C. Montanari, P.H.F. Morshuis, *Conduction Current Measurements on XLPE and EPR Insulation*, 0-7803-6584-5/04, 2004 IEEE
- [32] Walter S. Zaengl, *Dielectric Spectroscopy in Time and Frequency Domain for HV Power Equipment, Part I: Theoretical Considerations*, 0883-7554/03, 2003IEEE
- [33] K. S. Suh, C. R. Lee, J. S. Noh, J. Tanaka, and D. H. Damon, *Electrical Conduction in Polyethylene with Semiconductive Electrodes*, 1070-9878/94 ,1994 IEEE

Acknowledgments

Apart from my own efforts, many people contributed to the success of this thesis research. I would like to express my gratitude to all of them.

Firstly, I would like to express my appreciation to Dr. ir. Peter H.F. Morshuis for giving me the opportunity to participate in such an interesting project. I cannot say thanks enough for his important help and support. Every time after our weekly meetings I felt motivated and encouraged.

I would like to gratefully acknowledge the enthusiastic supervision of Ir. Dennis van der Born during this work. His guidance, especially in the beginning of the project, helped me to get familiar with the PEA method. Furthermore, he was always eager to help me with any unexpected problems and the interpretation of the results.

Also, I wish to acknowledge the help provided by the staff of the high voltage lab. Ing. Paul van Nes and Mr. Wim Termorshuizen were always available in order to help me. Their contribution to the construction of the conduction current setup for cables was significant.

Finally, I would like to thank my family who inspired, encouraged and fully supported me in every aspect of my life. I thank them for giving me not just financial but moral and spiritual support as well.